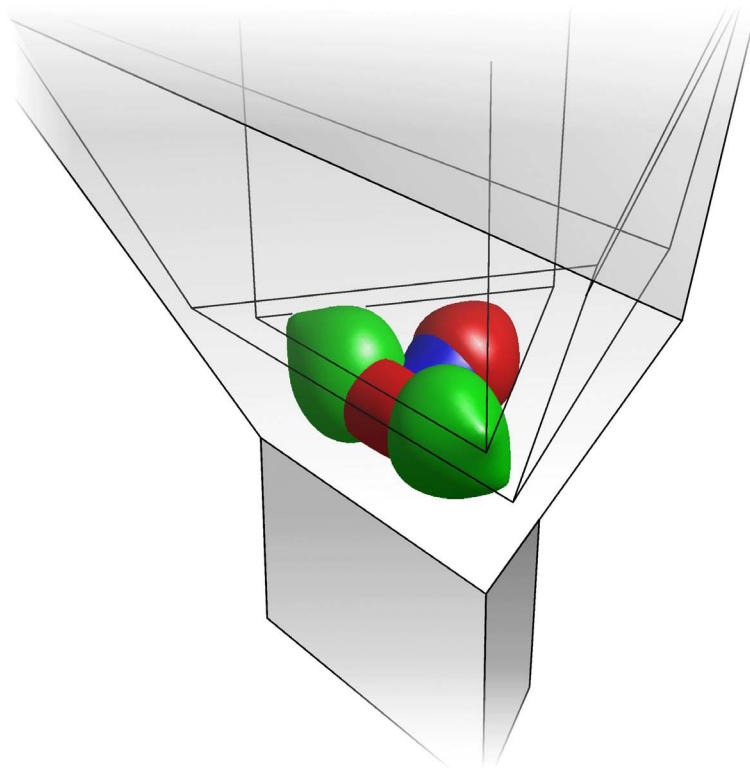# Theory of Polaron States in Pyramidal

GaAs/AlGaAs Quantum Dots

Master Thesis presented by

DANAIL OBRESCHKOW

February 2005

Institut de Photonique et d'Electronique Quantiques (IPEQ)

Faculté des Sciences de Base (FSB)

Ecole Polytechnique Fédérale de Lausanne (EPFL)

Thesis directors: Dr. Fabienne Michelini, Dr. Marc-André Dupertuis

Abstract

We address the subject of strong electron-phonon coupling in pyramidal quantum dots and pursue detailed physical, analytical and numerical investigations. The strong coupling polaron states in a pyramidal GaAs/AlGaAs quantum dot are computed numerically with an enhanced matrix diagonalization method that accounts for the particular structure of the Hamiltonian and uses an irregular reciprocal space discretization. Electron-electron interactions and multiple phonon interactions are neglected. We study quantum dots with either three or four confined electron states associated with two or three electron levels, respectively. Further, we develop a set of analytical tools to predict and interpret the polaron states of a more general model of quantum dots. Applying these tools to the particular case allows a complete classification of the polaron states and reveals new physical insight.

Front image

Isosurfaces of the "vibrational density functions" of a strong coupling polaron state in a pyramidal GaAs/AlGaAs quantum dot. Those functions are the Fourier transforms of the respective "normal mode distribution functions". Detailed explications are given in chapter 5 of this report.

The model of the pyramidal quantum dot has been developed at EPFL by Fabienne Michelini [1, 2].

Table of contents

1   Introduction

1.1   Underlying motivation

Quantum dots are point-like nanoscale heterostructures with an attractive potential for charge carriers. Their physical interest relies on yet undiscovered physical properties and promising technological applications.

First, specific theoretical and experimental investigations of the interactions inside quantum dots offer a key tool for fundamental quantum research. Namely, interactions between electrons, phonons and photons reveal some essence of quantum behavior, since superpositions and entanglement lead to observable consequences.

Second, several potential technological applications based on quantum dots were proposed. For example, we mention the application of quantum logic in a hypothetical new generation of computers referred to as "quantum computers" [3]. Their fundamental information units are discrete energy states, which can form superpositions, unlike the classical "zero-one" information. For a physical system to be an appropriate representation of quantum information, it needs to satisfy the DiVincenzo's criteria [4]. Explicitly, one should dispose of suitable tools to prepare the system in a given initial state, to apply universal quantum operations and to perform appropriate measurements, all keeping the environmental decoherence low. Many researchers affirm that localized electrons in quantum dots could exhibit an appropriate representation of quantum information [e.g. 5].

Another promising application of quantum dots, which is somewhat more concrete, relies on their particular optical properties. Certain quantum dots reveal the capacity to efficiently emit single photons or pairs of correlated photons. The feasibility of such controlled photon emitters has been shown theoretically [6, 7] as well as experimentally in the case of CdSe quantum dots [8], InAs quantum dots [9] and GaAs quantum dots [10]. The latter cases have been investigated at EPFL [11, 12] using the pyramidal heterostructures presented in this report (see section 4.1).

1.2   State of the art

Up to the late eighties of the past century, quantum dots were mainly theoretical objects, their systematic production being impossible. Thereafter, significant progress in the in the micro fabrication technology of heterostructures allowed the physical realization of different small confinement structures, such as quantum wires and quantum dots. This achievement enabled reproducible experimental investigations and induced an intensive research on quantum dots.

Preliminary theoretical studies led to the prediction that electron relaxation in quantum dots is inefficient [13, 14], meaning that the typical mechanical relaxation times prevail the photon emission times. This prediction was based on the widely spaced energy spectrum of the electron states in quantum dots and the narrow dispersion of the longitudinal optical (LO) phonon spectrum. Unless an electron energy separation is accidentally found in the vicinity of the LO-phonon energy, the relaxation through LO-phonon emission was considered impossible by virtue of Fermi's golden rule. This concept was referred to as "phonon bottleneck". It led to consider another relaxation channel through interactions with longitudinal-acoustic (LA) phonons. Those interactions are nevertheless negligibly weak for electronic energy separations above a few meV. Consequently, the phonon bottleneck should prevent excited electrons (or excitons) in quantum dots from relaxing to their ground state.

First experimental investigations of relatively large quantum dots (~1000Å) showed in deed poor luminescence from electron-hole ground state recombination [15] and proved evidence of luminescence associated with excited energies [16, 17, 18]. Those results seemed to confirm the concept of phonon bottleneck.

Yet, many later experimental attempts to confirm this concept with smaller quantum dots failed [e.g. 19, 20]. Instead of confirming the phonon bottleneck, the electron-hole pairs were observed to relax efficiently to their ground states and to recombine radiatively. Some effort was made to explain this unexpected feature, keeping the bottleneck concept unchanged. For example, partial explanations resulted from the inclusion of multi-phonon processes involving LO+LA decay [21] and Auger relaxation processes [22].

The deep theoretical impact, however, came about the millennium change with the affirmation that electrons in quantum dots are subject to strong coupling with certain superpositions of phonon states [30, 31, 32, 33]. Thus, the prevailing observable entity is the polaron rather than the electron. A major manifestation of this strong coupling feature is the multiplication of optical transition possibilities. In addition, the polaron concept offers a new way of electron relaxation: In the entangled superpositions of electron and phonon states, phonon-phonon interactions translating the crystal anharmonicity imply changes in the electronic part [33, 23].

Many subsequent theoretical investigations [e.g. 24] and direct observations of strong electron-phonon coupling [25, 26] have confirmed the new concept of "strong coupling polarons". Together with the unexplained observations of the efficient electron relaxation, this strong-coupling evidence brought the community to reject the concept of "phonon-bottleneck" in favor of the "strong coupling polaron" concept. Recently, some dots with large electron confinement have nevertheless revealed inefficient energy relaxation [27, 28].

In consequence of the strong coupling concept, the perturbation theory no longer presents an acceptable approach to the relaxation process. In particular, the irreversible treatment of electron-phonon interactions through Fermi's golden rule is no longer applicable.

1.3   Objectives and main results

Quantum dots are subject to experimental and theoretical research activities at EPFL. Recently, the envelope functions of electron states confined to a pyramidal quantum dot have been computed [1]. Similar computations have been performed with an enhanced quantum dot model including a vertical quantum wire [2, 29]. A long-term objective is the description of the electron capture from the quantum wire and the subsequent relaxation inside the quantum dot. As mentioned in section 1.2, the relaxation process is subject to regimes of strong electron-phonon coupling [30, 31, 32, 33] and thus we consider the polarons as the crucial physical entities.

Our goal is to compute the strong coupling polaron states in a pyramidal GaAs/AlGaAs quantum dot with three or four confined electron states. A particularly important point in such a complex problem is to find theoretical tools that allow to predict the physical results and to provide physical interpretation.

Our main results can be summarized as follows:

1) Physics: We compute the polaron states of quantum dots with three or four electron states and classify them with respect to their energy shift, degeneracies and mutual coupling. In particular, the states are grouped in nearly independent subsets, each of which is associated to a physical image of coupled crystal vibrations.

2) Analysis: We develop a set of analytical tools that allows to predict and to interpret the polaron spectrum of a more general quantum dot model. This leads us to introduce a "natural basis" of polaron states with a suitable analytical expression and physical sense.

3) Numerics: We represent the crystal dynamics by normal modes, which are irregularly distributed in the reciprocal space. This irregular discretization is generated adaptively in function of the particular electronic wave functions. For this application, the Fröhlich Hamiltonian is transcribed to an irregular, finite reciprocal space discretization. The resulting numerical method leads us to fast convergence and short computation times.

4) Computing: The developed program code allows to study a large set of quantum dots with an arbitrary number of discrete energy levels.

1.4   About this text

Even though the presented research is somewhat an entangled mixture of physical insight, analytical developments and numerical methods, we address the physical side in the first instance. Thus, analytical and numerical parts are mainly developed in appendix, whereas the principal part focuses on physical aspects.

We first present an introduction to the dynamics of electrons and nuclei in chapter 2. Particular importance is assigned to the conceptual basis, physical assumptions and mathematical representations. Using these fundamentals, we introduce the interaction between electrons and phonons, first in a general configuration of atoms, then in a general crystal and finally in a polar diatomic crystal. This naturally leads to the Fröhlich interaction, which we discuss physically. A reader familiar with those notions is invited to skip this chapter and step on to chapter 3. There, we define a general model of a polar quantum dot and develop analytical tools for the prediction and physical interpretation of the polaron states. Those tools will be used later to interpret the computational results. From the general model we are led to chapter 4, which describes the particular physical system of a pyramidal GaAs/AlGaAs quantum dot. Important aspects about the numerical implementation of this system are exposed briefly. In chapter 5 we present the computational results obtained for quantum dots with three or four confined electron states. The strong coupling polaron states are classified and physically interpreted. Thereafter we critically review the employed mathematical tools as well as the physical results with respect to the state of the art (chapter 6). We conclude with an overview and some windows to future research in chapter 7.

Separated from the main part by a blue page, chapter 8 constitutes an extended appendix – quite as long as the rest of the report. Therein we show analytical developments and demonstrations, numerical methods, details about the program code, additional results and original historical sources. The references are listed in chapter 9.

2   Conceptual basics of nuclei–electron dynamics

This chapter resumes generalities about nuclei-electron dynamics with a particular focus on phonon-electron interactions. The reader familiar with those general concepts is invited to continue with chapter 3, p. 33.

A generally accepted scheme of treating the dynamics of a large number of atoms such as found in molecules and crystals is exposed in section 2.1. The underlying physical assumptions are step wisely introduced and widely discussed: "Adiabatic approximation", "Born-Oppenheimer approximation", "Harmonic approximation", "Hartree approximation".

On this conceptual basis, we focus on the interaction between phonon and electrons. Section 2.2 exposes a general theory of electron-phonon interaction. This theory is then applied to the particular case of periodic crystals in section 2.3. Finally the case of polar crystals is regarded in great detail in section 2.4. In this framework the Fröhlich Hamiltonian is developed and its physical meaning is carefully discussed.

The whole chapter focuses on physical assumptions and interpretations. Mathematical developments are exposed briefly or even skipped. They are all given in the extended developments of appendix 8.1.

Source remark:

The sections 2.1 and 2.2 are mostly based on chapter 9 of François Reuse's carefully composed notes on quantum electrodynamics [34]. Chapter 2.3 is equally inspired by chapter 3.7 of F. Reuse and chapter 4 of F. Mila's lecture notes on the subject of superconductivity [35]. Chapter 2.4 is composed on the basis of a chapter from R. Evrard in the textbook "Polarons in Ionic Crystals and Polar Semiconductors" [36] and a text from J. Devreese published in the Encyclopedia of Applied Physics [37].

2.1   Basic schemes of electron-nuclei dynamics

This section gives a general description of the dynamics of a system of charged particles, which we call a "general molecule". It includes macroscopic systems such as crystals. The main intention is to clarify the underlying physical assumptions and to shine light on the structure of the mathematical representations.

The physical model and the theory describing its evolution are introduced. They are mathematically represented by a Hilbert space and a Hamiltonian operator acting inside this space. Then, the dynamical variables of the system are decoupled in three sections: electron-nuclei decoupling through the Born-Oppenheimer approximation,

nuclei-nuclei decoupling through harmonic normal modes, electron-electron decoupling through the mean field approximation. An overview and a discussion of the final Hamiltonian conclude this section.

2.1.1   Physical model of a "general molecule"

We consider a set of N nuclei μ with positive charge $+eZ_\mu$ and mass M_μ and n electrons ν with negative charge $-e$ and mass m_e. Those particles move in vacuum without external fields. Electromagnetic radiation between the particles are neglected as well as the particle spins. The spins only appear by the mean of Pauli's exclusion principle. The so described model is treated in a non-relativistic quantum mechanical scheme.

Electrons are identical fermions. In order to account for their exchange antisymmetry a completely antisymmetric space is chosen. The nuclei are considered distinguishable and are described in a symmetric space.

$$\mathcal{H}_{molecule} = \mathcal{H}_{electrons} \otimes \mathcal{H}_{nuclei} = \mathcal{A}\left(\mathcal{H}_{electron}^{\otimes n}\right) \otimes \mathcal{S}\left(\mathcal{H}_{nucleus}^{\otimes N}\right)$$

$\mathcal{A}$ is the orthogonal projector on the completely antisymmetric subspace. $\mathcal{S}$ is the orthogonal projector on the completely symmetric subspace. In this way any arbitrary vector of $\mathcal{H}_{molecule}$ represents a physical state.

The dynamics of the system is given by a Hamiltonian operator containing all kinetic terms and all Coulomb interaction terms,

$$H_{molecule} = H_{electrons} \otimes 1_{nuclei} + 1_{electrons} \otimes H_{nuclei} + V_{e^- - nuclei}$$

where $\quad H_{electrons} = \displaystyle\sum_{\nu=1}^{n} \frac{\vec{p}_\nu^2}{2m_e} + \frac{e^2}{8\pi\varepsilon_0} \sum_{\nu \neq \nu'} \frac{1}{\left|\vec{r}_\nu - \vec{r}_{\nu'}\right|}$

$$H_{nuclei} = \sum_{\mu=1}^{N} \frac{\vec{P}_\mu^2}{2M_\mu} + \frac{e^2}{8\pi\varepsilon_0} \sum_{\mu \neq \mu'} \frac{Z_\mu}{\left|\vec{R}_\mu - \vec{R}_{\mu'}\right|}$$

$$V_{e^- - nuclei} = -\frac{e^2}{4\pi\varepsilon_0} \sum_{\mu=1}^{N} \sum_{\nu=1}^{n} \frac{Z_\mu}{\left|\vec{r}_\nu \otimes 1_{nuclei} - 1_{electrons} \otimes \vec{R}_\mu\right|}$$

$\vec{r}_\nu$ and $\vec{p}_\nu$ are the position and momentum operators of the electrons. $\vec{R}_\mu$ and $\vec{P}_\mu$ are the positions and momentum operators of the nuclei. They satisfy the standard commutations relations,

$$\left[\vec{r}_\nu, \vec{p}_{\nu'}\right] = i\hbar\,\delta_{\nu\nu'} \cdot 1_{electrons} \qquad \left[\vec{r}_\nu, \vec{r}_{\nu'}\right] = 0 \qquad \left[\vec{p}_\nu, \vec{p}_{\nu'}\right] = 0$$

$$\left[\vec{R}_\mu, \vec{P}_{\mu'}\right] = i\hbar\,\delta_{\mu\mu'} \cdot 1_{nuclei} \qquad \left[\vec{R}_\mu, \vec{R}_{\mu'}\right] = 0 \qquad \left[\vec{P}_\mu, \vec{P}_{\mu'}\right] = 0$$

We note that operators belonging to different particles naturally commute because they act on different parts of a product space. This is not related to the exchange symmetries of identical particles. However, due to those exchange symmetries, there is no physical eigenstate of a given operator $\vec{r}_\nu$ or $\vec{p}_\nu$ if there is more than one electron.

All potential energy terms of $H_{molecule}$ relate to 2-body interactions. There is no free evolution term so far. The plan over the next three sections is to decouple step by step all the 2-body interactions.

2.1.2 Decoupling of the two body interactions

Nuclei-electron decoupling: "Born-Oppenheimer approximation"

(An extended version of this section is found in appendix 8.1.1.)

Inside the reduced space $\mathcal{H}_{electrons}$, the Hamiltonian $H_{electrons}$ describes an unstable dynamic of negative particles that all repel each other. In the same way H_{nuclei} describes an unstable system of positive particles in the space $\mathcal{H}_{nuclei}$. In this section, we shall include the mean effect of the nuclei in the electron Hamiltonian $H_{electrons}$ and the mean effect of the of the electrons in the nuclei Hamiltonian H_{nuclei}. Finally, the electron and the nuclei dynamics yield stable solutions, which are close to the solution of the full Hamiltonian. This approximate decoupling of the electronic and nuclear motion is globally referred to as the "Born-Oppenheimer approximation".

The mean influence of the electrons on the nuclei is treated in the "adiabatic approximation". It considers the electrons as slaves without inertia. They follow instantaneously the relatively slow nuclear motion. Mathematically, the rapid variable are decoupled from the slow ones and the electrons are considered to be always in the ground state around the instantaneous nuclear configuration. The electrons only contribute to the nuclear dynamics by the mean of a potential $E_0\left(\vec{R}.\right)$, which is the electronic ground state energy of the instantaneous nuclear configuration. Adding this contribution to the nuclei Hamiltonian, the latter becomes

$$H_{nuclei}^{adia} = \sum_{\mu=1}^{N} \frac{\vec{P}_\mu^2}{2M_\mu} + \frac{e^2}{8\pi\varepsilon_0} \sum_{\mu\neq\mu'} \frac{Z_\mu}{\left|\vec{R}_\mu - \vec{R}_{\mu'}\right|} + \left[E_0\left(\vec{R}.\right) - E_0\left(\vec{R}.^{(0)}\right)\right].$$

To keep the electrons' contribution small their energy $E_0\left(\vec{R}.^{(0)}\right)$ in the crystals equilibrium configuration $\vec{R}.^{(0)}$ has been subtracted.

In a second step, we look for an approximate electronic Hamiltonian in the subspace $\mathcal{H}_{electrons}$, which accounts for the mean influence of the nuclei. This is generally done by assuming that the nuclei are classical charges retained in the equilibrium positions $\vec{R}.^{(0)}$. They act on the electrons by Coulomb interaction, such that

$$H_{electrons}^{equil} = \sum_{v=1}^{n} \frac{\vec{p}_v^2}{2m_e} + \frac{e^2}{8\pi\varepsilon_0} \sum_{v \neq v'} \frac{1}{|\vec{r}_v - \vec{r}_{v'}|} - \frac{e^2}{4\pi\varepsilon_0} \sum_{\mu=1}^{N} \sum_{v=1}^{n} \frac{Z_\mu}{|\vec{r}_v - \vec{R}_\mu^{(0)} \cdot 1_{electrons}|}$$

We have thus found an approximate Hamiltonian that separates the electronic and nuclear dynamics from one another:

$$H^{Born-Oppenheimer} = H_{electrons}^{equil} \otimes 1_{nuclei} + 1_{electrons} \otimes H_{nuclei}^{adia}$$

The two components of this Hamiltonian yield stable configurations of the electrons and nuclei. At low temperatures this configurations are close to the true crystal configuration. The Hamiltonian differs from the full Hamiltonian $H_{molecule}$ by a residual term

$$V_{e^- - nuclei}^{res} = -\frac{e^2}{4\pi\varepsilon_0} \sum_{\mu=1}^{N} \sum_{v=1}^{n} \left[\frac{Z_\mu}{|\vec{r}_v \otimes 1_{nuclei} - 1_{electrons} \otimes \vec{R}_\mu|} - \frac{Z_\mu}{|\vec{r}_v - \vec{R}_\mu^{(0)} \cdot 1_{electrons}|} \otimes 1_{nuclei} \right]$$
$$- 1_{electrons} \otimes \left[E_0\left(\vec{R}.\right) - E_0\left(\vec{R}.^{(0)}\right) \cdot 1_{nuclei} \right]$$

Nuclei-nuclei interaction: "Harmonic normal modes"

(An extended version of this section is found in appendix 8.1.1.)

The next step is to decouple the nuclear coordinates from one another inside the reduced space $\mathcal{H}_{nuclei}$. The standard method consists in neglecting the anharmonic part of the potential energy around the equilibrium configuration and to perform a canonical transformation giving rise to independent normal modes. The energy quanta of each such mode are referred to as "phonons".

Explicitly, the nuclei potential admits the following development around the equilibrium configuration,

$$V_{nuclei}^{adia} = \underbrace{\frac{e^2}{8\pi\varepsilon_0} \sum_{\mu \neq \mu'} \frac{Z_\mu}{|\vec{R}_\mu^{(0)} - \vec{R}_{\mu'}^{(0)}|}}_{V_{nuclei}^{adia,(0)}} + \underbrace{\frac{1}{2!} \sum_{(\mu,i),(\mu',j)} \left.\frac{\partial V_{nuclei}^{adia}\left(\vec{Q}.\right)}{\partial Q_\mu^i \partial Q_{\mu'}^j}\right|_{\vec{Q}.=0} Q_\mu^i Q_{\mu'}^j}_{V_{nuclei}^{adia,harm}} + \underbrace{O(3)}_{V_{nuclei}^{adia,res}}$$

There is no linear term, since the equilibrium configuration corresponds to a minimum of the potential energy. The last term contains all the anharmonic contribu-

tions. Neglecting this term yields the "harmonic approximation" or "harmonic normal mode approximation". The nuclei Hamiltonian under this approximation writes

$$H_{nuclei}^{adia,harm} = \sum_{\mu=1}^{N} \frac{\vec{P}_{\mu}^2}{2M_{\mu}} + V_{nuclei}^{adia,harm}\left(\vec{Q}.\right).$$

In a first step the dynamical variables $\left(\vec{Q}_{\mu}, \vec{P}_{\mu}\right)$ are considered classical variables. It always exists is a particular set of canonically conjugate coordinates, in which the Hamiltonian $H_{nuclei}^{adia,harm}$ becomes decoupled (see appendix). In those coordinates the Hamiltonian looks like

$$H_{nuclei}^{adia,harm} = \sum_{\alpha}\left(P_{\alpha}^2 + \omega_{\alpha}^2 Q_{\alpha}^2\right),$$

where ω_{α}^2 are the eigenvalues of the dynamical matrix (see appendix). Each couple $\left(Q_{\alpha}, P_{\alpha}\right)$ describes an independent harmonic oscillator with angular frequency ω_{α}. Since the ionic displacements depend linearly on Q_{α}, each couple $\left(Q_{\alpha}, P_{\alpha}\right)$ describes a collective harmonic oscillation of all the nuclei at one same frequency. Therefore the new coordinates are called "normal mode coordinates". There are $3N$ modes: 3 global translations, 3 global rotations and $3N-6$ vibrations. The set of all those modes is called $\mathcal{A}$.

The harmonic notation is now transcribed to quantum mechanics. The $3N$ modes are independent properties of motion of the nuclei system. Therefore, each mode α can be assigned a restricted orthogonal subspace $\mathcal{H}_{mode\,\alpha}$ of the full space $\mathcal{H}_{nuclei}$. The full space is isomorphic to the product space $\mathcal{F}_{modes}$ defined by

$$\mathcal{H}_{nuclei} \quad \sim \quad \mathcal{F}_{modes} \equiv \bigotimes_{\alpha \in \mathcal{A}} \mathcal{H}_{mode\,\alpha}$$

This space is called "Fock space of normal modes".

Q_{α} and P_{α} are considered as quantum mechanical operators acting in this space. The commutation relations of the nuclei coordinates transform to

$$\left[Q_{\alpha}, P_{\beta}\right] = i\hbar\delta_{\alpha\beta} \cdot \mathbb{1}_{modes} \qquad \left[Q_{\alpha}, Q_{\beta}\right] = 0 \qquad \left[P_{\alpha}, P_{\beta}\right] = 0$$

We remind, that operators belonging to different normal modes naturally commute because they act on different parts of the product space. This is not related to exchange symmetries of identical particles.

The dynamics of the nuclei system is given by the Hamiltonian operator

$$H_{modes}^{adia,harm} = \sum_{\alpha \in \mathcal{A}}\left(P_{\alpha}^2 + \omega_{\alpha}^2 Q_{\alpha}^2\right) = \sum_{\alpha \in \mathcal{A}} H_{mode\,\alpha}$$

The operator $H_{mode\,\alpha}$ describes a quantum mechanical harmonic oscillator in the space $\mathcal{H}_{mode\,\alpha}$ and acts trivially on all other modes. The standard way to solve the dynamics described by $H_{mode\,\alpha}$ is to introduce the "annihilation operator" d_α and "creation operator" $d_\alpha^\dagger$ of one energy quanta,

$$H_{mode\,\alpha} = \hbar\omega_\alpha d_\alpha^\dagger d_\alpha$$

The operator $N_\alpha = d_\alpha^\dagger d_\alpha$ is hermitian and its spectrum can be shown to contain all non-negative integers. Therefore, the energy eigenstates of each mode α correspond to equally-spaced discrete energies, separated by $\hbar\omega_\alpha$. Further, the spectrum is non-degenerate. Thus a complete set of commuting observables is given by $\{N_\alpha\}$. The corresponding orthogonal basis is noted

$$\left\{ \left| n_\alpha, n_\beta, n_\gamma, ... \right\rangle : n_\alpha, n_\beta, ... \in \{0, 1, 2, 3, ...\} \right\}$$

Physically, the vector $\left| n_\alpha, n_\beta, n_\gamma, ... \right\rangle$ represents a state, where the mode α is $n_\alpha - times$ excited, i.e. it has an energy $n_\alpha \hbar\omega_\alpha$, and so on. The annihilation and creation operators act on the basis vectors as follows

$$d_\alpha \left| .., n_\alpha, .. \right\rangle = \sqrt{n_\alpha} \left| .., n_{\alpha-1}, .. \right\rangle \qquad \text{and} \qquad d_\alpha^\dagger \left| .., n_\alpha, .. \right\rangle = \sqrt{n_\alpha + 1} \left| .., n_{\alpha+1}, .. \right\rangle$$

which justifies their names. This is precisely the mathematical structure of a system of identical bosons. Thus we are led to consider the nuclei vibrations as composed by bosonic particles, called "phonons", which can occupy any of the modes $\alpha \in \mathcal{A}$.

The full dynamic beyond the harmonic approximation is described by the Hamiltonian

$$H_{modes}^{adia} = \sum_{\alpha \in \mathcal{A}} \left(P_\alpha^2 + \omega_\alpha^2 Q_\alpha^2 \right) + V_{modes}^{adia,res}$$

where $V_{modes}^{adia,res} = V_{nuclei}^{adia,res}(Q.)$ contains the anharmonic part of the potential. This term is not diagonal and therefore yields interactions between different normal modes or "phonon-phonon-interactions".

Electron-electron decoupling: "Hartree approximation"

In opposition to the nuclei dynamics, there is no standard way of solving the Hamiltonian $H_{electrons}^{equil}$ inside the reduced space $\mathcal{H}_{electrons}$. One possible approach is the "Hartree approximation" also called "self-consistent field approximation" or "mean field approximation". It considers the electrons to evolve in a time independent potential $V^{sc}(\vec{r})$ representing the Coulomb interaction with all the nuclei in their equilibrium

positions and all the electrons in their collective ground state. In this approximation the Hamiltonian takes the decoupled form

$$H_{electrons}^{equil, sc} = \sum_{v=1}^{n} \left(\frac{p_v^2}{2m_e} + V^{sc}\left(\vec{r}_v\right) \right)$$

where the potential $V^{sc}\left(\vec{r}\right)$ is found by solving the following equations simultaneously:

1) $$\left(\frac{\vec{p}^2}{2m_e} + V^{sc}\left(\vec{r}\right) \right)\left|\varphi_\tau\right\rangle = \varepsilon_\tau \left|\varphi_\tau\right\rangle$$

2) $$V^{sc}\left(\vec{x}\right) = \frac{e^2}{4\pi\varepsilon_0} \left[\int_{\mathbb{R}^3} d^3y \frac{\rho_0\left(\vec{y}\right)}{\left|\vec{x}-\vec{y}\right|} - \sum_{\mu=1}^{N} \frac{Z_\mu}{\left|\vec{x}-\vec{R}_\mu^{(0)}\right|} \right] \quad \text{where} \quad \rho_0\left(\vec{y}\right) \equiv \sum_{\tau=1}^{n} \int_{\mathbb{R}^3} d^3y \left|\left\langle\vec{y}\,\middle|\,\varphi_\tau\right\rangle\right|^2$$

The solution $V^{sc}\left(\vec{r}\right)$ yields electronic states which themselves create this potential. $V^{sc}\left(\vec{r}\right)$ is therefore called "consistent with itself" or "self-consistent". It can be found by iterative methods and is supposed to be unique.

Different one-electron energy eigenstates are distinguished by an index τ. This index also contains the spin part of the electron state. Since equation (1) only covers the spatial part of the state, each energy eigenstate $\left|\varphi_\tau\right\rangle$ has to be doubled to account for the two-fold spin degeneracy, $\varepsilon_\tau \rightarrow \left|\varphi_{\tau+}\right\rangle, \left|\varphi_{\tau-}\right\rangle$.

$H_{electrons}^{equil, sc}$ differs from the full electronic term $H_{electrons}^{equil}$ by a residual term $V_{electrons}^{equil, res}$ such that

$$H_{electrons}^{equil} = H_{electrons}^{equil, sc} + V_{electrons}^{equil, res}$$

where $\quad H_{electrons}^{equil, sc} = \sum_{v=1}^{n} \left(\frac{p_v^2}{2m_e} + V^{sc}\left(\vec{r}_v\right) \right)$

$$V_{electrons}^{equil, res} = \frac{e^2}{4\pi\varepsilon_0} \left[\frac{1}{2} \sum_{v' \neq v} \frac{1}{\left|\vec{r}_v - \vec{r}_{v'}\right|} - \sum_{v=1}^{n} \int_{\mathbb{R}^3} d^3y \frac{\rho_0\left(\vec{y}\right)}{\left|\vec{r}_v - \vec{y} \cdot 1_{electrons}\right|} \right]$$

Physically, the residual potential accounts for the facts that the electrons are eventually not in their ground state and that an electron doesn't interact with itself.

2.1.3   Overview and discussion

The accessible states of the system are represented in the Hilbert space

$$\mathcal{H}_{molecule} = \mathcal{H}_{electrons} \otimes \mathcal{F}_{modes} = \mathcal{A}\left(\mathcal{H}_{electron}^{\otimes n}\right) \otimes \left(\bigotimes_{\alpha \in \mathcal{A}} \mathcal{H}_{mode\,\alpha} \right)$$

The evolution of the system derives from the Hamiltonian operator

$$
\begin{aligned}
H_{molecule} \;=\; & H_{electrons}^{equil,sc} \otimes 1_{modes} \;+\; 1_{electrons} \otimes H_{modes}^{adia,harm} && \left. \vphantom{\int} \right\} H_{molecule}^{free} \\
+\; & V_{electrons}^{equil,res} \otimes 1_{modes} \;+\; 1_{electrons} \otimes V_{modes}^{adia,res} \;+\; V_{e^- - modes}^{res} && \left. \vphantom{\int} \right\} H_{molecule}^{int}
\end{aligned}
$$

$$
\underbrace{H_{electrons}^{equil}} \qquad\qquad \underbrace{H_{modes}^{adia}}
$$

where $\quad H_{electrons}^{equil,sc} = \sum_{\nu=1}^{n}\left(\dfrac{p_\nu^2}{2m_e} + V^{sc}\left(\vec{r}_\nu\right) \right)$

$$
H_{modes}^{adia,harm} = \sum_{\alpha\in\mathcal{A}} P_\alpha^2 + \omega_\alpha^2 Q_\alpha^2
$$

$$
V_{electrons}^{equil,res} = \frac{e^2}{4\pi\varepsilon_0}\sum_{\nu=1}^{n}\left[\frac{1}{2}\sum_{\substack{\nu'=1 \\ \nu'\neq\nu}}^{n}\frac{1}{\left|\vec{r}_\nu - \vec{r}_{\nu'}\right|} - \int_{\mathbb{R}^3} d^3y\,\frac{\rho_0\left(\vec{y}\right)}{\left|\vec{r}_\nu - \vec{y}\cdot 1_{electrons}\right|} \right]
$$

(residual interaction between electron and electron)

$$
V_{modes}^{adia,res} = V_{nuclei}^{adia,res}\left(Q_\cdot\right)
$$

(interaction between normal mode and normal mode)

$$
\begin{aligned}
V_{e^- - modes}^{res} = -\frac{e^2}{4\pi\varepsilon_0}\sum_{\mu=1}^{N}\sum_{\nu=1}^{n} & \left[\frac{Z_\mu}{\left|\vec{r}_\nu \otimes 1_{modes} - 1_{electrons}\otimes\vec{R}_\mu\left(Q_\cdot\right)\right|} - \frac{Z_\mu}{\left|\vec{r}_\nu - \vec{R}_\mu^{(0)}\cdot 1_{electrons}\right|} \otimes 1_{modes} \right] \\
& - 1_{electrons}\otimes\left[E_0\left(\vec{R}_\cdot\left(Q_\cdot\right)\right) - E_0\left(\vec{R}_\cdot^{(0)}\right)\cdot 1_{modes} \right]
\end{aligned}
$$

(residual interaction between electron and normal mode)

There are two useful decompositions. First, a particle nature based decomposition in electrons, normal modes and mutual interaction,

$$
H_{molecule} = H_{electrons}^{equil}\otimes 1_{modes} + 1_{electrons}\otimes H_{modes}^{adia} + V_{e^- - modes}^{res}
$$

It directly results from the Born-Oppenheimer approximation. Second, there is an interaction-based decomposition in free evolution and 2-body interaction,

$$
H_{molecule} = H_{molecule}^{free} + H_{molecule}^{res}
$$

$H_{molecule}^{free}$ only contains potential energy terms acting on a single electron or a single mode. It describes the free evolution of the electrons and normal modes in the framework of the introduced approximations, which were the Born-Oppenheimer approximation, the harmonic approximation and the self-consistent field approximation.

2.2 Electron-phonon interaction in general molecules

In this chapter, we investigate the residual interaction term $V^{res}_{e^- - modes}$ between electrons and normal modes.

The developments being purely mathematical they are presented in all detail the appendix (8.1.2). Here, the ideas of the development are summarized and the results are discussed from a physical viewpoint.

2.2.1 Overview of the mathematical development

It can be shown (see appendix), that the interaction term $V^{res}_{e^- - modes}$ admits the following development, similar to a Taylor series:

$$V^{res}_{e^- - modes} = \underbrace{\sum_{\alpha \in \mathcal{A}} F_\alpha^{(1)}(\vec{r}.) \otimes Q_\alpha}_{V^{res(1)}_{e^- - modes}} + \underbrace{\sum_{\alpha, \beta \in \mathcal{A}} F_{\alpha, \beta}^{(2)}(\vec{r}.) \otimes Q_\alpha Q_\beta}_{V^{res(2)}_{e^- - modes}} + \dots$$

with $\quad F_\alpha^{(1)}(\vec{r}.) = \left. \frac{\partial W}{\partial Q_\alpha} \right|_{Q.=0} \quad, \quad F_{\alpha\beta}^{(2)}(\vec{r}.) = \frac{1}{2!} \left. \frac{\partial W}{\partial Q_\alpha \partial Q_\beta} \right|_{Q.=0} \quad, \quad$ etc.

and $\quad W = -\frac{e^2}{4\pi\varepsilon_0} \sum_{\mu=1}^{N} \sum_{\nu=1}^{n} \left[\frac{Z_\mu}{\left| \vec{r}_\nu - \vec{R}_\mu^{(0)} \cdot 1_{electrons} \right|} \right] - E_0\left(\vec{R}.^{(0)}\right) \cdot 1_{electrons}$

The operators W, F and $V^{res}_{e^- - modes}$ are transcribed to second quantization, which leads to a compact form of the interaction term with physical meaning. In appendix 8.1.2 the methods of second quantization for bosonic and fermionic particles are introduced carefully. The respective annihilation and creation operators are noted as follows:

d_α : *"annihilation operator of one phonon in the normal mode α"*

$d_\alpha^\dagger$: *"creation operator of one phonon in the normal mode α"*

a_τ : *"annihilation operator of one electron in the state τ"*

$a_\tau^\dagger$: *"creation operator of one electron in the state τ"*

Further, J represents the set of all electron energy eigenstates τ and J_0 is the subset of states, which are occupied in the collective electronic ground state. Its complement $J_* \equiv J \setminus J_0$ contains all the excited one-electron states. Based on these notations, we define the following auxiliary operators,

$c_\tau \equiv a_\tau^\dagger \quad \forall \tau \in J_0 \quad$ *"annihilation operator of a hole"*

$b_\tau \equiv a_\tau \quad \forall \tau \in J_* \quad$ *"annihilation operator of an electron"*

Their adjoints are consequently given by

$$c_\tau^\dagger = a_\tau \quad \forall \tau \in J_0 \quad \text{"creation operator of a hole"}$$

$$b_\tau^\dagger = a_\tau^\dagger \quad \forall \tau \in J_* \quad \text{"creation operator of an electron"}$$

In the second quantization the operator W is shown to become

$$W = -\sum_{..} w_{\tau\tau'}\, c_\tau^\dagger c_{\tau'} + \sum_{..} w_{\tau\tau'}\, b_\tau^\dagger c_{\tau'}^\dagger + \sum_{..} w_{\tau\tau'}\, c_\tau b_{\tau'} + \sum_{..} w_{\tau\tau'}\, b_\tau^\dagger b_{\tau'}$$

with
$$w_{\tau\tau'} \equiv \sum_{\mu=1}^{N} \frac{-Z_\mu e^2}{4\pi\varepsilon_0} \int_{\mathbb{R}^3} d^3x\, \frac{\varphi_\tau\left(\vec{x}\right)^* \varphi_{\tau'}\left(\vec{x}\right)}{\left|\vec{x} - \vec{R}_\mu^{(0)}\right|}$$

Thus the terms of $V^{res}_{e^- - modes}$ can be written in the second quantization. For the first order term we obtain explicitly

$$V^{res(1)}_{e^- - modes} = -\sum_{...} M^\alpha_{\tau\tau'}\, c_\tau^\dagger c_{\tau'} d_\alpha + \sum_{...} M^\alpha_{\tau\tau'}\, b_\tau^\dagger c_{\tau'}^\dagger d_\alpha + \sum_{...} M^\alpha_{\tau\tau'}\, c_\tau b_{\tau'} d_\alpha + \sum_{...} M^\alpha_{\tau\tau'}\, b_\tau^\dagger b_{\tau'} d_\alpha$$

$$-\sum_{...} M^\alpha_{\tau\tau'}\, c_\tau^\dagger c_{\tau'} d_\alpha^\dagger + \sum_{...} M^\alpha_{\tau\tau'}\, b_\tau^\dagger c_{\tau'}^\dagger d_\alpha^\dagger + \sum_{...} M^\alpha_{\tau\tau'}\, c_\tau b_{\tau'} d_\alpha^\dagger + \sum_{...} M^\alpha_{\tau\tau'}\, b_\tau^\dagger b_{\tau'} d_\alpha^\dagger$$

where
$$M^\alpha_{\tau\tau'} = \sqrt{\frac{\hbar}{2\omega_\alpha}}\, \mathcal{D}_\alpha\, w_{\tau\tau'} = \sqrt{\frac{\hbar}{2\omega_\alpha}}\, \frac{-e^2}{4\pi\varepsilon_0}\, \sum_{\mu=1}^{N} Z_\mu \vec{X}_{\alpha\mu} \cdot \frac{\partial}{\partial\vec{R}_\mu^{(0)}} \left[\int_{\mathbb{R}^3} d^3x\, \frac{\varphi_\tau\left(\vec{x}\right)^* \varphi_{\tau'}\left(\vec{x}\right)}{\left|\vec{x} - \vec{R}_\mu^{(0)}\right|} \right]$$

$\sum_{...}$ is the sum over all normal modes α and over the states τ and τ', on which the respective hole or electron operators are defined.

Note that equal electronic wave functions with different spins give two different states τ_1 and τ_2. If τ were only an index of the wave function, we had an additional sum over the two spin states in the expression of $M^\alpha_{\tau\tau'}$.

2.2.2 Discussion

The eight terms of $V^{res(1)}_{e^- - modes}$ correspond to different physical pictures shown in Fig. 1. All those terms describe interactions between one phonon and one electron. The interactions, which don't conserve the energy, have very small or vanishing matrix elements.

A similar derivation is used to obtain the further terms $V^{res(2)}_{e^- - modes}$, $V^{res(3)}_{e^- - modes}$, etc. $V^{res(2)}_{e^- - modes}$ contains 16 terms, $V^{res(3)}_{e^- - modes}$ 32 terms, $V^{res(4)}_{e^- - modes}$ 64 terms and so on. However, the corresponding matrix elements decrease rapidly as we go to higher order terms. It can thus be assumed that the first term contains the most important contribution in the sense that it yields the most probable interactions. The higher order

terms describe interactions, which involve several phonons: Generally, the term $V_{e^--modes}^{res(k)}$ gives the interaction between k phonons and one electron.

We emphasize that $V_{e^--modes}^{res}$ never gives interactions between phonons and *several* electrons. All electron-electron interactions are contained in the residual term $V_{electrons}^{equil,res}$, which has been introduced in chapter 0. Electron-phonon interactions, which involve several electrons are thus obtained by the simultaneous application of $V_{e^--modes}^{res}$ and $V_{electrons}^{equil,res}$.
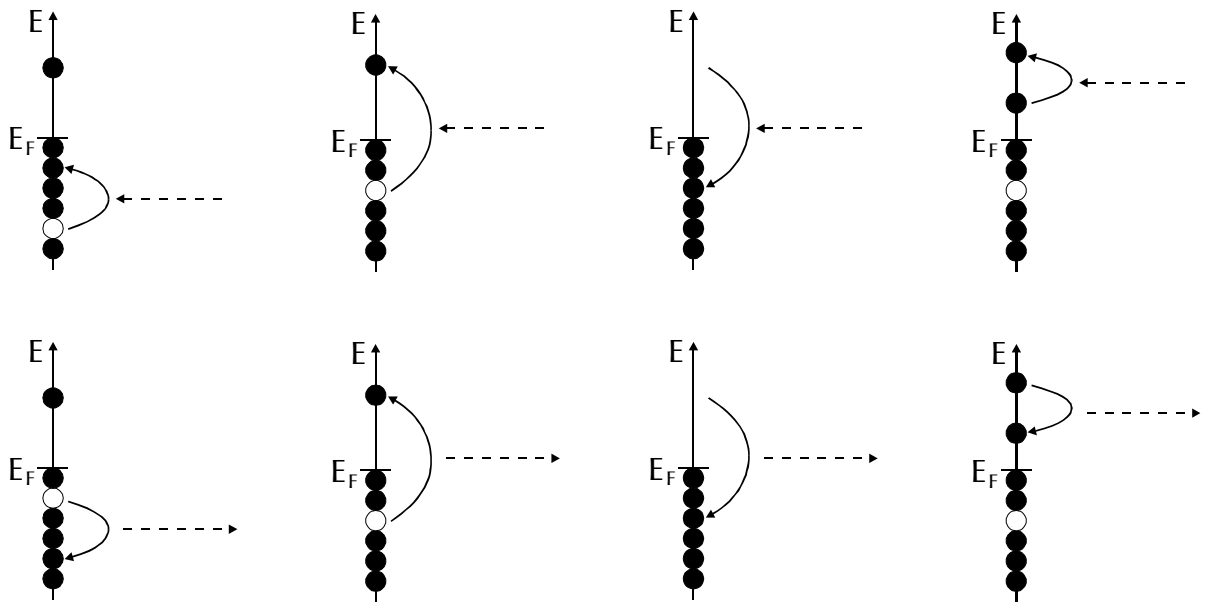
Fig. 1: **Visualization of the different first order interactions between phonon and electrons. The images are in the same order as the eight terms of the explicit expression. Filled circles represent electrons, empty circles holes and the dashed lines phonons. E_F is the Fermi energy of the molecule. The interactions, which don't conserve the energy, have very small or vanishing matrix elements.**

2.3 Electron-phonon interaction in perfect crystals

The goal of the present chapter is to apply the electron-phonon interaction of the general molecule to the particular case of a crystal. Therefore we make use of the particular structure of the electrons and normal modes, which result from the high symmetry of the crystal. On one hand this application serves as an important example of the general theory. On the other hand it gives a physical understanding of the perfect crystal, which is necessary to understand interactions in crystals with impurities or heterostructures.

Again the extended development is shown in appendix (8.1.3). Here, the general ideas are briefly mentioned and the result is discussed from a physical viewpoint.

2.3.1   From the molecule to the crystal

Passing from to the general molecule to the crystal we are subject to one conceptual change: The crystal electrons can be considered as either bound to specific ions or as valence electrons dispersed all over the structure. Every nucleus together with its bound electrons will be considered as one physical entity called "ion". Those ions are treated as point charges. In the general theory of the molecule, the nuclei become ions and the electrons become the valence electrons. To keep a record of this conceptual change, we write $V^{res}_{e^- - nuclei} \rightarrow V^{res}_{e^- - ions}$.

The mean positions of the ions of a crystal form a periodic structure, which is usually decomposed in a Bravais lattice BL and a basis B. Each ion μ is described by two vectors $\vec{l} \in BL$ and $\vec{b} \in B$, where $\vec{l}$ indicates the position of the primitive cell and $\vec{b}$ the location of the ion within the cell. The equilibrium position of the ion is thus given by $\vec{R}^{(0)}_{(\vec{l},\vec{b})} = \vec{l} + \vec{b}$.

2.3.2   Electrons and phonons in crystals

The mean electrical potential of a crystal has the periodicity of the underlying Bravais lattice. In this case the Bloch Theorem states, that the electronic energy eigenstates are of the form

$$\varphi_{\vec{k}}(\vec{r}) = u_{\vec{k}}(\vec{r}) e^{i\vec{k}\cdot\vec{r}}$$

where $u_{\vec{k}}(\vec{r})$ has the periodicity of the lattice. Further the functions $u_{\vec{k}}(\vec{r})$ can be chosen to be orthonormal.

Every wave function $\varphi_{\vec{k}}(\vec{r})$ gives two simultaneously accessible states, with opposite spins σ. A one-electron state τ is thus entirely described by a couple $(\vec{k},\sigma)$:

$$\tau \rightarrow (\vec{k},\sigma).$$

For any derivation in the reduced Hilbert space without spins, it is important to remember that equal wave functions with opposite spins are orthogonal. We shall add to the index σ,

$$\varphi_{\vec{k},\sigma}(\vec{r}) = u_{\vec{k}}(\vec{r}) e^{i\vec{k}\cdot\vec{r}},$$

and use the Kronecker Delta-function to mark the orthogonality,

$$\left(\varphi_{\vec{k}',\sigma'},\varphi_{\vec{k},\sigma}\right) = \int d^3r\,\varphi_{\vec{k}',\sigma'}^*(\vec{r})\,\varphi_{\vec{k},\sigma}(\vec{r})\,\delta_{\sigma\sigma'} = \delta_{\vec{k}\vec{k}'}\,\delta_{\sigma\sigma'}$$

The ionic motion of the crystal is again described in independent normal modes. Those modes are shown to be plane waves of the vibration amplitude, indexed by a wave vector $\vec{q}$ (see appendix). Each plane wave is associated with *3r* normal modes, where *r* is the number of basis points of the underlying crystal. The phonon annihilation and creation operators are called $d_{(\vec{q},j)}$ and $d_{(\vec{q},j)}^\dagger$, where $j = 1,...,3r$ is an additional index to distinguish between different normal modes with the same wave vector.

2.3.3 Residual interaction term

In the general theory the interaction term between electron and phonons $V_{e^--modes}^{res}$ has been developed in series. In the case of a crystal, the first order term is shown to be

$$V_{e^--ions}^{res(1)} = \sum_{(\vec{q},j),\vec{b},\vec{k},\vec{k}',\sigma} M_{\vec{b},\vec{k},\vec{k}'}^{(\vec{q},j)}\,a_{\vec{k}',\sigma}^\dagger\,a_{\vec{k},\sigma}\left(d_{(-\vec{q},j)}^\dagger + d_{(\vec{q},j)}\right)$$

with $$M_{\vec{b},\vec{k},\vec{k}'}^{(\vec{q},j)} = -i\sqrt{\frac{N\hbar}{16\pi^3 M_{\vec{b}}\omega_{(\vec{q},j)}}}\;\vec{\epsilon}_{(\vec{q},j),\vec{b}}\cdot\vec{q}\;\tilde{U}(\vec{q})\,e^{-i\vec{q}\cdot\vec{b}}\left[\int_{\mathbb{R}^3}d^3x\,e^{i\left(\vec{q}+\vec{k}+\vec{k}'\right)\cdot\vec{x}}\;u_{\vec{k}'}^*(\vec{x})u_{\vec{k}}(\vec{x})\right]$$

The factor $\vec{\epsilon}_{\vec{q},j}\in\mathbb{C}^{3r}$, called "polarization vector", is explained in appendix 8.1.3.

In the electron-hole-notation,

$$\begin{aligned}
V_{e^--modes}^{res(1)} = \;& -\sum_{...}M\,c_{\vec{k},\sigma}^\dagger c_{\vec{k}',\sigma}d_{\vec{q},j} + \sum_{...}M\,b_{\vec{k},\sigma}^\dagger c_{\vec{k}',\sigma}^\dagger d_{\vec{q},j} + \sum_{...}M\,c_{\vec{k},\sigma}b_{\vec{k}',\sigma}d_{\vec{q},j} + \sum_{...}M\,b_{\vec{k},\sigma}^\dagger b_{\vec{k}',\sigma}d_{\vec{q},j} \\
& -\sum_{...}M\,c_{\vec{k},\sigma}^\dagger c_{\vec{k}',\sigma}d_{\vec{q},j}^\dagger + \sum_{...}M\,b_{\vec{k},\sigma}^\dagger c_{\vec{k}',\sigma}^\dagger d_{\vec{q},j}^\dagger + \sum_{...}M\,c_{\vec{k},\sigma}b_{\vec{k}',\sigma}d_{\vec{q},j}^\dagger + \sum_{...}M\,b_{\vec{k},\sigma}^\dagger b_{\vec{k}',\sigma}d_{\vec{q},j}^\dagger
\end{aligned}$$

where the sum $\sum_{...}$ goes over all normal modes $\left(\vec{q},j\right)$, over all the basis vectors $\vec{b}\in B$, and over all the states $\left(\vec{k},\sigma\right)$ and $\left(\vec{k}',\sigma\right)$ on which the respective hole or excitation operators are defined.

2.3.4 Discussion

We first realize that the first order term of $V_{e^--modes}^{res}$ has the structure obtained in the case of the generic molecule. There are eight terms that describe different interactions between one electron and one phonon. However, in case of a crystal the matrix elements are easier to calculate. In praxis the difficult part is to know the ionic potential $U(\vec{r})$. It is needed to obtain the Fourier components $\tilde{U}(\vec{q})$ and to solve the

tential $U(\vec{r})$. It is needed to obtain the Fourier components $\tilde{U}(\vec{q})$ and to solve the eigensystem of the dynamical matrix (see appendix).

An important particularity of the crystal is the relation between the electron momentums $\vec{k}$ and $\vec{k}'$ and the phonon momentum $\vec{q}$. As shown in appendix 8.4.3 the sum $\vec{q} + \vec{k} - \vec{k}'$ has to be an element of the reciprocal lattice. We can also write

$$\vec{k}' = \vec{k} + \vec{q} - \vec{G}$$

where $\vec{G}$ is a reciprocal lattice vector. Since we only consider wave vectors $\vec{k}$, $\vec{k}'$, $\vec{q}$ inside the first Brillouin zone, there is only one possible solution for $\vec{G}$. The interaction is called "normal process" If $\vec{G} = 0$ and "umklapp process" if $\vec{G} \neq 0$. In the latter case $\vec{k} + \vec{q}$ lies outside the first Brillouin zone. $\vec{G}$ guaranties that $\vec{k}'$ is again in the first Brillouin zone (see Fig. 2).

Normal process
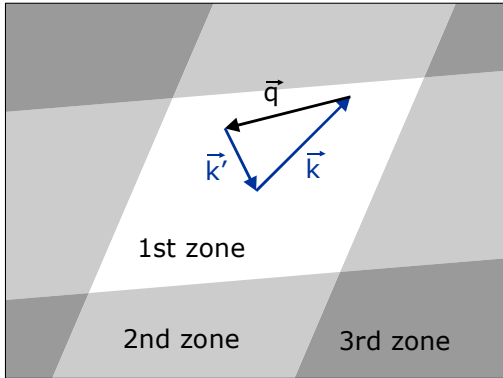
Umklapp process
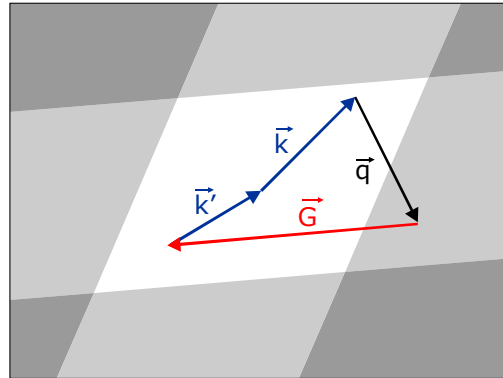
Fig. 2: Difference between normal and umklapp process in the reciprocal space.

We also mention an important application of the presented theory: Based on the explicit form of $V_{e^- - modes}^{res(1)}$ one can derive an effective interaction between electrons through intermediate interactions with phonons. By virtue of this effective interaction electrons tend to attract themselves at very low temperatures and to generate bosonic pairs, which form a Bose-Einstein condensate. The latter state is the superconducting state of a crystal.

Finally, we shine light on the fact that the crystal theory is somewhat too restrictive for the aimed application of quantum dots. In fact, $V_{e^- - modes}^{res(1)}$ only accounts for electrons in the Bloch state. Thus no other states, such as quantum dot electrons inside the crystal can be treated. Nevertheless the theory of the perfect crystal is essential to understand the physics of the imperfect crystals and heterostructures.

2.4 Electron-phonon interaction in polar crystals: "Fröhlich Hamiltonian"

This section presents a very different approach to electron-phonon interactions. It considers a diatomic crystal with two-point basis, in which optical modes cause polarization waves. We establish the interaction of a single electron in the crystal with this polarization waves. Since this approach is restricted to a particular set of crystals it is less general than the one described in chapter 2.3. However, it considers the interaction with a general electron state with no restriction to Bloch states.

The underlying physical model is first explained in detail. Then, the classical equations of motion are established using the classical theories of mechanics and electrodynamics. From the equations of motion we go over to the quantum mechanical interaction term while skipping a large part of mathematical development and the quantization. The mathematical development doesn't present a physical interest and the quantization is very similar to the quantization of the normal modes presented in appendix respective to the previous chapters.

2.4.1 Physical model

A perfect crystal with two ions per unit cell is considered as the dielectric medium of an electrodynamic description. It is subjected to a displacement field $\vec{D}$, which induces a polarization field $\vec{P}$. The resulting electric field is

$$\vec{E} = \frac{1}{\varepsilon_0}\left(\vec{D} - \vec{P}\right)$$

This is the field, which acts on charges that lie inside the crystal but don't belong to it. The "effective electric field", which acts on an ion of the crystal differs from $\vec{E}$ by the fact that the ion doesn't feel its own contribution to the polarization $\vec{P}$. An adequate approximation of this field is

$$\vec{E}_{eff} = \vec{E} + \frac{1}{3\varepsilon_0}\vec{P}$$

While the whole crystal acts like a dielectric medium, we consider a single electron inside the crystal as not belonging to the medium. This electron constitutes the charge distribution and fixes the displacement field $\vec{D}$ by the virtue of the Gauss law

$$\vec{\nabla} \cdot \vec{D}\left(\vec{x}\right) = -e\,\delta\left(\vec{x} - \vec{r}\right)$$

where $\vec{r}$ is the position of the electron.

2.4.2   Equations of motion

Polarization field

We first derive the dipole induced by a single ion with valence Z, which is displaced by a vector $\vec{u}$ from its equilibrium position.

1)   Due to its charge Ze the displaced ion yields a local dipole equal to $Ze\vec{u}$.

2)   When ions are displaced from their equilibrium positions, they suffer some deformation as a consequence of the overlap of the electronic shells with neighboring ions. This contribution is to a first approximation linear in the ionic displacement and gives rise to a small correction term equal to $-\lambda\vec{u}$, $\lambda > 0$.

3)   The electrons of the ion are further displaced by the local electric field $\vec{E}_{eff}$. This leads to a third polarization term, which is mainly linear in $\vec{E}_{eff}$. It is written as $\alpha\vec{E}_{eff}$, where α is called the "electronic polarizability".

The total microscopic dipole becomes

$$\vec{\xi} = Ze\vec{u} - \lambda\vec{u} + \alpha\vec{E}_{eff}$$

The constant λ can be considered as correction of the valence charge Ze. We can merely introduce a renormalized charge Z^*, such that $Z^*e \equiv Ze - \lambda$. Thus

$$\vec{\xi} = Z^*e\vec{u} + \alpha\vec{E}_{eff}$$

Next, we consider a single primitive cell with two ions. For a given displacement $\vec{u}_+$ and $\vec{u}_-$ of the positive and negative ion the local dipoles become

$$\vec{\xi}_+ = Z^*e\vec{u}_+ + \alpha_+\vec{E}_{eff}$$

$$\vec{\xi}_- = -Z^*e\vec{u}_- + \alpha_-\vec{E}_{eff}$$

where α_+ and α_- are the electronic polarizability of the positive and negative ion respectively. The mean polarization density inside the primitive cell is

$$\vec{P} = \frac{1}{V^{cell}}\left(\vec{\xi}_+ + \vec{\xi}_-\right) = \frac{1}{V^{cell}}\left[Z^*e\left(\vec{u}_+ - \vec{u}_-\right) + \left(\alpha_+ + \alpha_-\right)\vec{E}_{eff}\right]$$

where V^{cell} is the volume of the primitive cell. To simplify this expression, we introduce the relative displacement $\vec{w} \equiv \vec{u}_+ - \vec{u}_-$ and the total electronic polarizability $\alpha \equiv \alpha_+ + \alpha_-$. Then,

$$\vec{P} = \frac{1}{V^{cell}}\left(Z^*e\,\vec{w} + \alpha\,\vec{E}_{eff}\right)$$

The effective electric field $\vec{E}_{eff}$ is not directly accessible. Therefore we express it as a function of $\vec{E}$ and $\vec{P}$ and solve again for $\vec{P}$. We obtain

$$\vec{P} = \left[\frac{Z^*e}{V^{cell}}\,\frac{3\varepsilon_0 V^{cell}}{3\varepsilon_0 V^{cell} - \alpha}\right]\vec{w} + \left[\frac{\alpha}{V^{cell}}\,\frac{3\varepsilon_0 V^{cell}}{3\varepsilon_0 V^{cell} - \alpha}\right]\vec{E}$$

which is a first "equation of motion".

Ionic motion

The ions are subjected to electrical forces, which are supposed to be decomposed in a short-range and a long-range component. The short-range force comes from the electrostatic interaction between two ions of the same unit cell. The long-range force is due to the interaction with all the other ions through the global polarization field. We can thus write

$$\vec{F} = \vec{F}^{short} + \vec{F}^{long}$$

$$\vec{F}^{short} = \begin{cases} -K\left(\vec{u}_+ - \vec{u}_-\right) = -K\,\vec{w} & \text{positive ions} \\ +K\left(\vec{u}_+ - \vec{u}_-\right) = +K\,\vec{w} & \text{negative ions} \end{cases}$$

$$\vec{F}^{long} = \begin{cases} +Z^*e\,\vec{E}_{eff} & \text{positive ions} \\ -Z^*e\,\vec{E}_{eff} & \text{negative ions} \end{cases}$$

where we have introduced the short-range force constant $K > 0$.

Newton's equation of motion yields

$$m_+\ddot{\vec{u}}_+ = -K\left(\vec{u}_+ - \vec{u}_-\right) + Z^*e\,\vec{E}_{eff} \qquad \text{and} \qquad m_-\ddot{\vec{u}}_- = +K\left(\vec{u}_+ - \vec{u}_-\right) - Z^*e\,\vec{E}_{eff}$$

Combining those equations we obtain

$$\mu\ddot{\vec{w}} = -K\,\vec{w} + Z^*e\left(\vec{E} + \frac{\vec{P}}{3\varepsilon_0}\right)$$

where $\qquad \mu \equiv \dfrac{m_+ m_-}{m_+ + m_-} \qquad$ "reduced mass" $\qquad$ and $\qquad \vec{w} \equiv \vec{u}_+ - \vec{u}_- \qquad$ "relative position"

Using the expression of $\vec{P}$, we obtain a second equation of motion,

$$\ddot{\vec{w}} = \left[-\frac{K}{\mu} + \frac{Z^{*2}e^2}{\mu\left(3\varepsilon_0 V^{cell} - \alpha\right)}\right]\vec{w} + \left[\frac{Z^*e}{\mu}\,\frac{3\varepsilon_0 V^{cell}}{3\varepsilon_0 V^{cell} - \alpha}\right]\vec{E}$$

Solving the equations of motion

The results of two previous sections are summarized in the following system of equations

(1) $\quad \ddot{\vec{w}} = b_{11}\vec{w} + b_{12}\vec{E}$

(2) $\quad \vec{P} = b_{21}\vec{w} + b_{22}\vec{E}$

As shown in [38] the b-coefficients can be related to measurable quantities: b_{12}, b_{21} and b_{22} are functions of the relative dielectric constants in a static (ε_r) and high frequency (ε_∞) field. b_{11} can be expressed as a function of the longitudinal optical phonon frequency ω_{LO}. This is a very important conclusion since it means that all the employed microscopic quantities don't have to be measured.

In order to solve for the three unknown variables $\vec{E}$, $\vec{P}$ and $\vec{w}$, a third equation is needed. We suppose that the motion of the ions is too slow for induction phenomena to occur, which means that $\vec{B} = 0$. Thus, another equation is given by

(3a) $\quad \vec{\nabla} \times \vec{E} = 0$

This relation leads to longitudinal plane wave solutions and excludes transverse ones. We note that a vector field is only partially determined by its curl. To complete the equation, an expression for its divergence is needed. We can use the Gauss law $\vec{\nabla} \cdot \vec{D}(\vec{x}) = -e\,\delta(\vec{x} - \vec{r})$ combined with the relation $\vec{D} = \varepsilon_0\vec{E} + \vec{P}$. This gives the last equation

(3b) $\quad \vec{\nabla} \cdot \vec{E}(\vec{r}') = -e\,\delta(\vec{r}' - \vec{r}) - \dfrac{1}{\varepsilon_0}\vec{\nabla} \cdot \vec{P}$

The equations (1), (2), (3a), (3b) constitute a complete set of equations to solve for $\vec{E}$, $\vec{P}$ and $\vec{w}$.

2.4.3 Fröhlich Hamiltonian

The solution of the equation of motion is obtained by introducing a cubic volume V in which all the physical functions have to satisfy the periodic boundary conditions. The mathematical derivation of the solution is long but doesn't present a lot of physical aspects. Therefore we don't present it here and refer the reader to [39]. The solution of the crystal motion can be decomposed in normal modes, which physically represent longitudinal waves of the polarization field. When quantifying those polarization modes we obtain a Hamiltonian governing the interaction between the polarization modes and the single electron. This Hamiltonian has first been derived by H. Fröhlich [40] in 1949 (see original text in appendix 8.7.4). Its explicit form is

$$H^{Fröhlich}_{e^- - phonons} = \sum_{\vec{q}} \left(g_{\vec{q}} \, e^{i\vec{q}\cdot\vec{r}} \, d_{\vec{q}} + g_{\vec{q}}^* \, e^{-i\vec{q}\cdot\vec{r}} \, d_{\vec{q}}^\dagger \right), \text{ where } g_{\vec{q}} = -i\sqrt{\frac{\hbar\omega_{LO}\, e^2}{2\varepsilon_0\, V\, q^2}\left(\frac{1}{\varepsilon_\infty} - \frac{1}{\varepsilon_r}\right)}$$

The wavevectors $\vec{q}$ associated with the polarization modes satisfy the periodic boundary conditions of the quantization volume V. The polarization modes are expressed in second quantization by the annihilation and creation operators of longitudinal optical phonons $d_{\vec{q}}$ and $d_{\vec{q}}^\dagger$. Since there is only one longitudinal optical mode per wave vector $\vec{q}$ we don't need the degeneracy index j introduced in chapter 2.3. The electron position operator $\vec{r}$ has not yet been transformed to second quantization. We like to write the interaction Hamiltonian in the same form as in chapter 2.2 and 2.3. Thus, it is extended to the $n-electron$ formalism although we don't account for interaction terms which involve more than one electron. The second quantization of the electronic coordinates is achieved by (see [41])

$$H^{Fröhlich}_{e^- - phonons} = \sum_{\vec{q}} \; \sum_{\tau,\tau'\in J} \left(M^{\vec{q}}_{\tau\tau'} \, a_\tau^\dagger a_{\tau'} d_{\vec{q}} + M^{\vec{q}*}_{\tau\tau'} \, a_\tau^\dagger a_{\tau'} d_{\vec{q}}^\dagger \right)$$

$$\text{where} \qquad M^{\vec{q}}_{\tau\tau'} = -i\sqrt{\frac{\hbar\omega_{LO}\, e^2}{2\varepsilon_0\, V\, q^2}\left(\frac{1}{\varepsilon_\infty} - \frac{1}{\varepsilon_r}\right)} \int_{\mathbb{R}^3} d^3x \; e^{i\vec{q}\cdot\vec{x}} \psi_\tau^*\left(\vec{x}\right)\psi_{\tau'}\left(\vec{x}\right)$$

This interaction is again written in the electron-hole-notation

$$
\begin{aligned}
H^{Fröhlich}_{e^- - phonons} = \; & -\sum_{\dots} M^{\vec{q}}_{\tau\tau'} \, c_\tau^\dagger c_{\tau'} d_{\vec{q}} \; + \sum_{\dots} M^{\vec{q}}_{\tau\tau'} \, b_\tau^\dagger c_{\tau'}^\dagger d_{\vec{q}} + \sum_{\dots} M^{\vec{q}}_{\tau\tau'} \, c_\tau b_{\tau'} d_{\vec{q}} + \sum_{\dots} M^{\vec{q}}_{\tau\tau'} \, b_\tau^\dagger b_{\tau'} d_{\vec{q}} \\
& -\sum_{\dots} M^{\vec{q}}_{\tau\tau'} \, c_\tau^\dagger c_{\tau'} d_{\vec{q}}^\dagger \; + \sum_{\dots} M^{\vec{q}}_{\tau\tau'} \, b_\tau^\dagger c_{\tau'}^\dagger d_{\vec{q}}^\dagger + \sum_{\dots} M^{\vec{q}}_{\tau\tau'} \, c_\tau b_{\tau'} d_{\vec{q}}^\dagger + \sum_{\dots} M^{\vec{q}}_{\tau\tau'} \, b_\tau^\dagger b_{\tau'} d_{\vec{q}}^\dagger
\end{aligned}
$$

where the sum $\sum_{\dots}$ goes over all reciprocal lattice vectors $\vec{q}$ and over the states τ and τ', on which the respective hole or excitation operators are defined.

2.4.4 Discussion

We discuss the framework and the limitations of the Fröhlich interaction.

A comparison of the Fröhlich Hamiltonian to the general electron-phonon interaction of chapter 2.2 immediately shows that Fröhlich only constitutes a first order term. Explicitly, the Fröhlich interaction is linear in the normal mode coordinates and thus only describes interactions with one phonon. This limitation arises from the linearity of the underlying physical model: The polarization field $\vec{P}$, the electric field $\vec{E}$ and the ionic displacement $\vec{w}$ were assumed to depend linearly on each other.

It is further necessary to emphasize the difference between "polar" and "optical" modes. Any crystal consisting of a Bravais lattices and basis with more than one ion possesses both acoustic and optical modes. In acoustic modes the ions at different

basis points oscillate with equal phase, in optical modes the phases are shifted. If the ions at different basis sites are all equal, such as in diamond, the ionic motion does not induce a polarization field. Thus the modes of a monatomic crystal are called "non-polar acoustic" and "non-polar optical". However, if the ions of the crystal basis are different, their valence charges are generally different and the ionic motion causes a polarization field. The modes of a diatomic or multi-atomic crystals are thus referred to as "polar acoustic" and "polar optical". Fig. 3 shows the modes in case of a crystal with a two-point basis. From the images it is obvious that polar acoustic modes cause very weak polarization fields compared to the polar optical ones. In practice the term "polar mode" is thus often used as a synonym of "optical mode" in the case of a polar crystal, although rigorously one should say "polar optical mode".
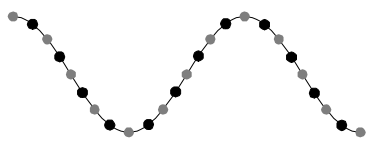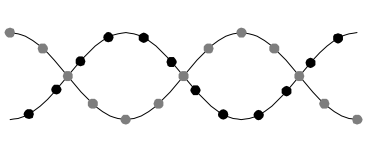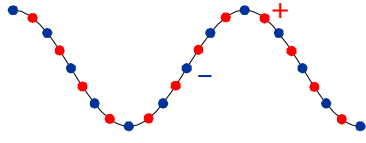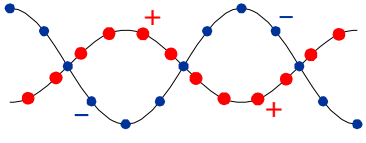
	"acoustic mode"	"optical mode"
"non-polar mode" (two-point basis with equal valence charges) Examples: Si, Diamond		
"polar mode" (two-point basis with different valence charges) Examples: GaAs, AlAs, InAs, InSb		(Fröhlich Hamiltonian)

Fig. 3: **Distinction between acoustic, optical, polar and non-polar modes of a crystal with two-point basis. The Fröhlich Hamiltonian only applies to the polar optical modes (right, bottom).**

In the derivation of the Fröhlich Hamiltonian we consider a polar crystal with two different ions per basis. They are supposed to move in opposite directions, which leads to oscillations with opposite phases, thus to optical modes. Therefore, we conclude that the Fröhlich interaction only accounts for "polar optical modes".

Further, the derivation is based on the assumption that magnetic induction phenomena can be neglected. Thus transverse optical modes have been excluded. This assumption is justified by two considerations. First, at low temperatures the ionic motion can be shown to be slow enough, that the influence of induction is negligible compared to the electrostatic interaction. Second, the energy spectrum of the interacting electron is often discrete with large energy spacings (e.g. in quantum dots). If the electronic energy quanta are large compared to the energy quanta of the acoustic phonons, then the interaction can be expected to be small.

Finally, we emphasize that the Fröhlich interaction only accounts for one-electron interactions. When transcribing the Fröhlich Hamiltonian to the multiple electron formalism all the electrons are considered to interact separately with the polar optical phonon. This is in agreement with the general derivation of chapter 2.2. In 2.2.2 it was explained that interactions with several electrons are obtained by the simultaneous application of the electron-electron interaction $V_{electrons}^{equil,res}$. Thus the fact that Fröhlich works with a single electron doesn't represent a conceptual limitation.

To conclude the discussion, the application field of the Fröhlich Hamiltonian is summarized in the following compact form:

> The Fröhlich Hamiltonian describes to first order (in the normal mode coordinates) the electrostatic interaction between a single but general electron state and the longitudinal optical phonons in a diatomic crystal with two-point basis.

3 General quantum dot systems and analytical results

We shall introduce a quite general quantum dot system with an appropriate mathematical representation. Then, we develop analytical tools to solve the polaron dynamics and to reveal important physical interpretations.

3.1 Physical model

We consider an arbitrary quantum dot formed by a heterostructure in a semiconductor consisting of a diatomic crystal with two-point basis. Those specifications are necessary for the Fröhlich interaction to be valid, as we could show in section 2.4.4.

Within the Born-Oppenheimer approximation (see 2.1.2), we shall consider the electronic and ionic components of the crystal as decoupled up to remaining interactions between electronic and ionic excitations. By virtue of the harmonic approximation, the ionic state of motion is decomposed in independent normal modes (see 2.1.2). Applying the scheme of second quantization, this leads to consider the crystal as a gas quantized excitations called "phonons". Those phonons are restricted to bulk phonons. As for the electrons, we do not need to specify the method to evaluate their dynamics (e.g. mean field or k·p-method). We shall, however, suppose that the electronic ground states and the excited states confined to the quantum dot are known. Further, we adopt the "electron-hole"-semantics. Thus, the term "electron" always refers to an excitation above the collective ground state, such as an electron confined to the quantum dot.

We assume that the phonon gas and the electrons interact exclusively through the Fröhlich interaction. In section 2.4 this interaction is shown to exhibit a first order contribution (in the normal mode coordinates) of the electrostatic interaction between a single but general electron state and the longitudinal optical phonons in a diatomic crystal with a two-point basis. Thus, only the longitudinal optical phonons are involved in our considerations. We shall therefore restrict the crystal description to a gas of LO-phonons.

The whole system is considered at sufficiently low temperatures for the electron and phonon numbers to be restricted to zero and one.

3.2   Mathematical representation

3.2.1   System representation (Hilbert space)

The electron confined in the quantum dot is represented in the Hilbert space $\mathcal{H}_e$ of dimension n. The n energy eigenstates are noted $|1\rangle, ..., |n\rangle$, ordered with increasing energies. We call g the degeneracy of the most excited energy level. Thus the set of "not fully excited" energy eigenstates is $|1\rangle, ..., |n-g\rangle$.

The LO-phonon gas introduced in section 3.1 is completely described by the number of excitations in every normal mode (see 2.1.2). We shall call N the number of normal modes and $\vec{q}_i$, $i = 1, ..., N$, the respective wavevector. Those vectors are confined to a primitive cell of the reciprocal lattice, usually taken as the first Brillouin zone. Further, they are chosen to satisfy the periodic boundary conditions of an arbitrary quantization volume V (see 2.4.3). We emphasize that this volume is a purely mathematical tool, since it is topologically impossible to realize a three-dimensional object with periodic boundary conditions in all dimensions. In the framework of the low temperature approximation, the total number of phonons is at most one, which translates in saying that each normal mode is at most once excited. A suitable basis of this model contains the zero-phonon state $|0\rangle$ and the N one-phonon states $|1\vec{q}_i\rangle$.

Together with the vector product defined by the orthonormality of those states, they span a Hilbert space $\mathcal{H}_{ph}$ of dimension $N + 1$.

The strength of the Fröhlich interaction is inversely proportional to the norm of the wavevector $\vec{q}_i$. Thus, the predominant contribution comes from small wavevectors close to the zone center, where the phonon dispersion is very narrow. We shall therefore take the phonons as monochromatic, their energy being equal to

$$\varepsilon_{LO}(\vec{q}_i) = \varepsilon_{LO} \equiv \hbar\omega_{LO}.$$

The combined system of electron and crystal is represented in a tensor product space $\mathcal{H}_e \otimes \mathcal{H}_{ph}$. We decide on writing the non-entangled product states as

$$|electron\,state \quad phonon\,state\rangle \equiv |electron\,state\rangle \otimes |phonon\,state\rangle$$

Product states of an electron states on the most excited level and an arbitrary one-phonon state are only reached through anti-resonant interaction. This interaction doesn't conserve the energy and the corresponding coupling term is very small. Therefore, such states can be safely neglected. Finally, the relevant Hilbert space $\mathcal{H}$ is spanned by the "tensor product basis"

$$\left\{ \left| 1\ 0 \right\rangle, \left| 2\ 0 \right\rangle, ..., \left| n\ 0 \right\rangle, \left| 1\ 1\vec{q}_i \right\rangle, \left| 2\ 1\vec{q}_i \right\rangle ..., \left| n-g\ 1\vec{q}_i \right\rangle : i = 1...N \right\},$$

where g is the degeneracy of the most excited electron level. This space exhibits $n + (n-g)N$ dimensions. Fig. 4 shows a visualization of the tensor product basis states in the particular case of three electron levels.
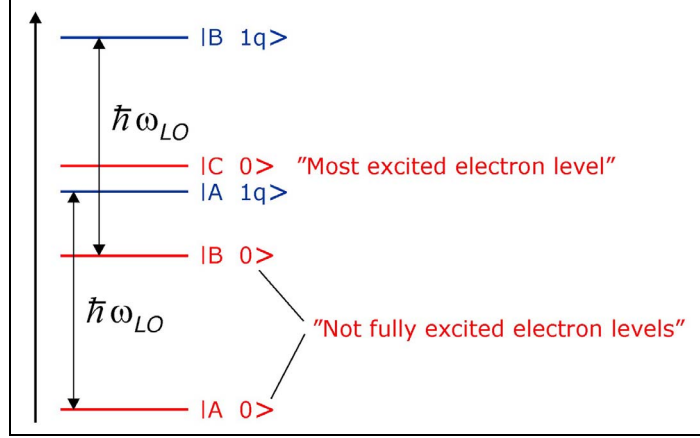
Fig. 4: Representation of the zero-phonon states (red) and the one-phonon states (blue) included in our quantum dot model with three electron levels A, B, C.

3.2.2 System evolution (Hamiltonian)

The system evolution is governed by a Hamiltonian operator

$$H = H^{free} + H^{Fröhlich}$$

The one-body term

$$H^{free} = \left(\sum_{\tau} \varepsilon_{\tau} a_{\tau}^{\dagger} a_{\tau} \right) \otimes 1_{ph} + 1_e \otimes \left(\varepsilon_{L0} \sum_{i=1}^{N} d_{\vec{q}_i}^{\dagger} d_{\vec{q}_i} \right)$$

describes the free evolution of the electrons confined in the quantum dot and the free evolution of the LO-bulk-phonons. This free evolution inherently comprehends the Born-Oppenheimer approximation (nuclei-electron decoupling), the harmonic approximation (nuclei-nuclei decoupling) and a suitable approximation for the mean interaction between electrons, such as given by Hartree-Fock. Extended explanations to these approximations were developed in section 2.1.

The interaction term, taken as the Fröhlich Hamiltonian, has the form

$$H^{Fröhlich} = \sum_{i=1}^{N} \sum_{\tau, \tau'} \left(M_{\tau\tau'}^{\vec{q}_i} a_{\tau}^{\dagger} a_{\tau'} d_{\vec{q}_i} + M_{\tau\tau'}^{\vec{q}_i *} a_{\tau'}^{\dagger} a_{\tau} d_{\vec{q}_i}^{\dagger} \right)$$

with

$$M_{\tau\tau'}^{\vec{q}_i} = -i \sqrt{\frac{\hbar \omega_{LO} e^2}{2\varepsilon_0 V q_i^2} \left(\frac{1}{\varepsilon_\infty} - \frac{1}{\varepsilon_r} \right)} \int_{\mathbb{R}^3} d^3x\ e^{i\vec{q}_i \cdot \vec{x}} \psi_\tau^* (\vec{x}) \psi_{\tau'} (\vec{x}) = \frac{\lambda}{q_i \sqrt{V}} \int_{\mathbb{R}^3} d^3x\ e^{i\vec{q}_i \cdot \vec{x}} \psi_\tau^* (\vec{x}) \psi_{\tau'} (\vec{x})$$

The sum over $\vec{q}_i$ goes over all the reciprocal space vectors inside the first Brillouin zone, which yield plane waves with the periodicity of the quantization volume V (see 2.4.3).

In the product state basis introduced above, the Hamiltonian has the following matrix representation:

$$H = \begin{pmatrix} \varepsilon_1 & & & X & \cdots\cdots\cdots\cdots\cdots & X \\ & \ddots & & \vdots & & \vdots \\ & & \varepsilon_n & X & \cdots\cdots\cdots\cdots\cdots & X \\ X & \cdots & X & \varepsilon_1 + \varepsilon_{LO} & & \\ & & & & \ddots & \\ & & & & & \varepsilon_1 + \varepsilon_{LO} \\ & & & & & & \varepsilon_2 + \varepsilon_{LO} \\ & & & & & & & \ddots \\ & & & & & & & & \ddots \\ X & \cdots & X & & & & & & & \varepsilon_{n-g} + \varepsilon_{LO} \end{pmatrix}$$

The diagonal elements come from the free evolution term, whereas the two off diagonal blocks contain the Fröhlich coupling elements. The dimension number of this Hamiltonian is equal to $n + (n - g)N$ and thus depends on the number of normal modes N, which is proportional to the quantization volume V. N is generally large and becomes infinite if V becomes infinite.

Previous theoretical investigations emphasized that the evolution problem of such a quantum dot system is hardly approached by perturbation theory [30, 31, 32, 33]. However, finding the non-approximate evolution given by a very large Hamiltonian, which means diagonalizing a high dimensional matrix, represents a complex numerical task. We will nevertheless introduce analytical simplifications, which drastically reduce the dimension of the relevant Hilbert space. Those analytical simplifications and a set of tools for physical interpretation will be developed of the following section.

3.3   Analytical results and interpretation tools

This section summarizes some analytical key results. In particular, we introduce a non-orthonormal basis, which we call the "natural basis", to represent all the quantum dot polarons. This basis allows us to investigate the substructure of the polaron space and to associate a physical image to each polaron.

We will emphasize the physical aspects, while keeping the mathematical derivations brief. The mathematical developments are expended in the appendix (8.1).

3.3.1   Hilbert space reduction, "Natural Basis"

We intend to determine the evolution described by the Hamiltonian $H = H^{free} + H^{Fröhlich}$. This task is equivalent to finding all the eigenstates and eigenenergies of this Hamiltonian – a high dimensional diagonalization problem.

Recent research activities have revealed that the solution of this problem yields a small number of polaron states, which are coupled to the quantum dot electronic states, and a large number of dispersed bulk phonons [30, 31, 32, 34].

In this work, we show the existence of an orthogonal decomposition of $\mathcal{H}$ in spaces that are stable under the action of H. In particular, we introduce a stable subspace $\mathcal{H}_{red}$, "called reduced space", which contains all the quantum dot polarons, i.e. polarons that couple to certain quantum dot electronic states. We reveal that this space exhibits a small dimension allowing numerical methods to work efficiently. Finally, we show that $\mathcal{H}_{red}$ contains all the zero-phonon states – states that are often taken as initial states of a relaxation process. By virtue of those particular features, we shall restrict our considerations to $\mathcal{H}_{red}$.

First, we note that $\mathcal{H}$ can be decomposed in zero-phonon and one-phonon sub-spaces:

$$\mathcal{H} = \mathcal{H}_{0ph} \oplus \mathcal{H}_{1ph} = \mathcal{H}_{0ph} \oplus \left(\overset{n-g}{\underset{\tau=1}{\oplus}} \mathcal{H}_{1ph+\tau} \right)$$

where $\mathcal{H}_{0ph} \equiv vect \left(\left\{ \left| \tau \ \ 0 \right\rangle : \tau = 1, ..., n \right\} \right)$ "zero-phonon subspace"

$\mathcal{H}_{1ph+\tau} \equiv vect \left(\left\{ \left| \tau \ \ 1\vec{q}_i \right\rangle : i = 1, ..., N \right\} \right)$ "one-phonon subspace of electron τ"

For each electron energy eigenstate $\tau = 1...n$ we define the orthogonal projector

$$P_{1ph+\tau} : \mathcal{H} \rightarrow \mathcal{H}_{1ph+\tau}$$

Further, we define the subspaces

$\mathcal{H}_{A,\tau} \equiv P_{1ph+\tau} \left(H \mathcal{H}_{0ph} \right) \subseteq \mathcal{H}_{1ph+\tau}$ and their orthogonal complements

$\mathcal{H}_{B,\tau} \perp \mathcal{H}_{A,\tau}$ such that $\mathcal{H}_{A,\tau} \oplus \mathcal{H}_{B,\tau} = \mathcal{H}_{1ph+\tau}$

In this way, we are led to the following orthogonal decomposition of $\mathcal{H}$,

$$\mathcal{H} = \mathcal{H}_{0ph} \oplus \left(\mathcal{H}_{A,1} \oplus \mathcal{H}_{B,1} \right) \oplus ... \oplus \left(\mathcal{H}_{A,n-g} \oplus \mathcal{H}_{B,n-g} \right) = \mathcal{H}_{0ph} \oplus \left(\overset{n-g}{\underset{\tau=1}{\oplus}} \mathcal{H}_{A,\tau} \right) \oplus \left(\overset{n-g}{\underset{\tau=1}{\oplus}} \mathcal{H}_{B,\tau} \right)$$

In appendix 8.2.1 we prove that the particular structure of the Fröhlich Hamiltonian and the monochromaticity of the LO-phonon spectrum imply that all the subspaces $\mathcal{H}_{B,\tau}$ are stable, i.e. $H \mathcal{H}_{B,\tau} \subseteq \mathcal{H}_{B,\tau} \quad \forall \tau$. This is an essential feature that we shall ex-

ploit in the following. As all the states of a given space $\mathcal{H}_{B,\tau}$ have the same energy equal to $\varepsilon_{LO} + \varepsilon_\tau$, it follows that the spaces $\mathcal{H}_{B,\tau}$ are highly degenerate eigenspaces of the evolution operator. In physical terms, those spaces represent the large bath of superpositions of degenerate one-phonon states, which do not couple to confined electron states.

We address particular attention to the remaining orthogonal part, which we call "reduced space $\mathcal{H}_{red}$". From the decomposition shown above it follows that

$$\mathcal{H}_{red} \equiv \mathcal{H}_{0\,ph} \oplus \left(\bigoplus_{\tau=1}^{n} \mathcal{H}_{A,\tau} \right) = \mathcal{H}_{0\,ph} \oplus \left(\bigoplus_{\tau=1}^{n} P_{1ph+\tau} \left(H\mathcal{H}_{0ph} \right) \right) \qquad \text{"reduced space"}$$

This space exhibits a list of four physical key properties:

- $\mathcal{H}_{red}$ is stable under the action of H, i.e. $H\mathcal{H}_{red} \subseteq \mathcal{H}_{red}$. Consequently a state vector initially contained in $\mathcal{H}_{red}$ stays inside $\mathcal{H}_{red}$ over time. This follows directly from the stability of its orthogonal complements $\mathcal{H}_{B,\tau}$.

- $\mathcal{H}_{red}$ is the only subspace of $\mathcal{H}$ that couples different electron states. In other words, $\mathcal{H}_{red}$ contains all the eigenstates of the full Hamiltonian H, which involve several electron states. This immediately derives from the feature that all the spaces $\mathcal{H}_{B,\tau}$ only contain uncoupled states.

- As shown in appendix 8.2.1, $\mathcal{H}_{red}$ exhibits a small number of dimensions that is independent of the number of normal modes, $dim\left(\mathcal{H}_{red}\right) = n\left(n - g + 1\right)$. n is the number of electron eigenstates and g the degeneracy of the most excited level.

- $\mathcal{H}_{red}$ contains all the zero-phonon states, which are often considered as initial states.

In consequence of those fundamental features, the reduced subspace $\mathcal{H}_{red}$ of the orthogonal decomposition

$$\mathcal{H} = \mathcal{H}_{red} \oplus \mathcal{H}_{B,1} \oplus \ldots \oplus \mathcal{H}_{B,n-g}$$

constitutes the physically interesting space.

Natural basis

A basis of the reduced Hilbert space $\mathcal{H}_{red}$ is naturally obtained by summing the basis vectors of its subparts (see definition above). We shall call this basis the "natural basis":

$$\left\{ \left| v\ 0 \right\rangle,\ \sum_{i=1}^{N} \left| \tau\ 1\vec{q}_i \right\rangle \left\langle \tau\ 1\vec{q}_i \middle| H \middle| v\ 0 \right\rangle,\ v = 1 \ldots n,\ \tau = 1 \ldots n - g \right\} \qquad \text{"natural basis"}$$

Ferreira, Verzelen and Bastard have emphasized [42] that only one-phonon superpositions of the type $\sum_{i=1}^{N} \left| \tau\ 1\vec{q}_i \right\rangle \left\langle \tau\ 1\vec{q}_i \middle| H \middle| v\ 0 \right\rangle$ are involved in electron-phonon coupling regimes. Our affirmation, that the subspace $\mathcal{H}_{red}$ contains all the quantum dot polarons agrees well with this statement.

It might surprise that we decide to use this non-orthonormal basis. We will, however, show, that the natural basis allows to develop analytical tools to classify the polarons, to give them a simple mathematical expression and to associate a physical image to each polaron. Furthermore, the vectors of the natural basis have themselves interesting physical interpretations. As for the zero-phonon states $\left| v\ 0 \right\rangle$, they can be interpreted as isolated electron states. The one-phonon states $\sum_{i=1}^{N} \left| \tau\ 1\vec{q}_i \right\rangle \left\langle \tau\ 1\vec{q}_i \middle| H \middle| v\ 0 \right\rangle$ yield the following physical interpretation:

- They are sums of one-phonon tensor product states associated with one fixed electron state τ. The weight of each such states is given by $f(\vec{q}_i) = \left\langle \tau\ 1\vec{q}_i \middle| H \middle| v\ 0 \right\rangle$. The inverse Fourier transform of this function gives the physically meaningful "vibrational density function". Since $\left\langle \tau\ 1\vec{q}_i \middle| H \middle| v\ 0 \right\rangle$ is itself mainly proportional to the Fourier transform of the wave function product $\psi_\tau \psi_v$ (see Fröhlich Hamiltonian in 3.2), its inverse Fourier transform is again proportional to $\psi_\tau \psi_v$. This function is localized in the quantum dot, since its two factors are localized. We conclude that the one-phonon basis states of the natural basis are normal mode superpositions that are localized in the quantum dot!

- The one-phonon states of the natural basis can also be viewed as the states $H \left| v\ 0 \right\rangle$ projected on the one-phonon subspace associated with the electron state τ. This image immediately reveals that the one-phonon states of the natural basis couple to the zero-phonon states.

A critical discussion on the use of the natural basis is held in chapter 6.

Some other insight

Up to here, the orthogonal decomposition of the Hilbert space $\mathcal{H}$ was presented from an abstract viewpoint. Two additional viewpoints may help to sharpen our understanding:

- Matrix representation:

    There is a partially orthogonal basis of the Hilbert space $\mathcal{H}$, in which the matrix representation of the Hamiltonian operator H is bloc-diagonal:

$$
H' = \begin{pmatrix}
\boxed{H_{red}} & & & \\
& \boxed{H_{B,\tau=1}} & & \\
& & \ddots & \\
& & & \boxed{H_{B,\tau=n-g}}
\end{pmatrix}
$$

    This matrix is obtained from the initial matrix H by a similarity transformation, which implies the existence of a non-singular matrix S such that $H' = S^{-1}HS$.

- Conserved physical quantity:

    The system evolution conserves a quantity x that is different from the energy. This quantity is associated with a hermitian operator X, which commutes with the Hamiltonian operator H, $[H, X] = 0$. Such an operator is easily obtained by combining all the orthogonal projectors on the different stable subspaces. For example,

$$
X \equiv \sum_{\tau=1}^{n-g} \tau \cdot \left(projector \, on \, H_{B,\tau} \right)
$$

    In this way,

$$
[H, X] = 0 \qquad \text{and} \qquad X|\psi\rangle = x|\psi\rangle \quad \text{with} \quad x = \begin{cases} 0 \;\; if \;\; |\psi\rangle \in \mathcal{H}_{red} \\ \tau \;\; if \;\; |\psi\rangle \in \mathcal{H}_{B,\tau} \end{cases}
$$

3.3.2 Physical symmetries and substructure of the reduced Hilbert space

After having developed a suitable representation of quantum dot polarons in a general quantum dot model in the previous section, we shall now investigate the consequences of a spatial symmetry. In particular, we show that a symmetry plane allows

to decompose the reduced polaron space $\mathcal{H}_{red}$, introduced in the previous section, in two decoupled subsets.

We introduce this subject with a general remark about a single spatial symmetry. Let us suppose that the quantum dot system obeys a symmetry represented by the symmetry operator $\mathcal{P}$, which commutes with the Hamiltonian $[H,\mathcal{P}] = 0$. It follows that the eigenstates of H can be chosen to be simultaneous eigenstates of $\mathcal{P}$. The respective eigenvalues are noted p. From the commutation property it follows that p represents a conserved physical quantity and that the system evolves independently inside different eigenspaces of $\mathcal{P}$. Therefore, the total Hamiltonian can be solved independently for each eigenvalue of the symmetry operator. Thus, the Hilbert space $\mathcal{H}_{red}$ yields an orthogonal decomposition in decoupled subspaces, each of which is associated with a different eigenvalue of $\mathcal{P}$.

In this work, we investigate pyramidal quantum dots that exhibit three vertical symmetry planes, which constitute the symmetry group C$_{3V}$ (see Fig. 5).
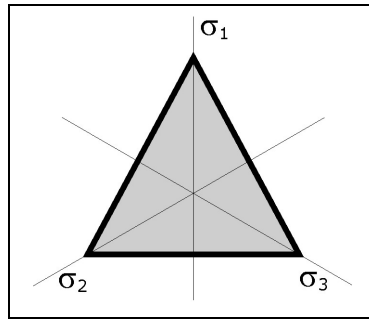
Fig. 5: **Vertical symmetry planes (σ_1, σ_2, σ_3) of the pyramidal quantum dot investigated in this work. Those symmetries define the group C$_{3V}$. The considerations of this paragraph only use one the symmetry plane σ_1, which constitutes the group C$_S$.**

In this case, the quantum dot yields three symmetry operators, which do not commute mutually. Thus, our previous considerations about the general symmetry operator $\mathcal{P}$ are not easily extendable. An efficient investigation of the symmetry group C$_{3V}$ requires group theory. In the frame of this work, we decide on restricting the symmetry considerations to the group C$_S$ that consists in one symmetry plane taken as σ_1. This allows us to bypass group theory and to develop conclusions for the polaron states of a more general quantum dot system. We could nevertheless lose certain additional features related to the higher symmetry.

We define $\mathcal{P}$ as the symmetry operator associated with the symmetry plane σ_1, which is associated with x-z-plane. Thus, the symmetry operator $\mathcal{P}$ inverses the y-coordinate and exhibits two different eigenvalues $p = \pm 1$, called "y-parity". From the preliminary remark of this section it follows, that the Hilbert space $\mathcal{H}_{red}$ can be decomposed in two decoupled orthogonal parts associated with a different y-parity,

$$\mathcal{H}_{red} = \mathcal{H}_{red}^{+} \oplus \mathcal{H}_{red}^{-}$$

In the appendix (8.2.2), this general result is developed in a pedestrian way in order to obtain another insight as well as to find the suitable natural basis associated with the two restrictions of $\mathcal{H}_{red}$. If the electron eigenstates of the Hamiltonian are chosen to be simultaneous eigenstates of the symmetry operator, we prove that the bases of $\mathcal{H}_{red}^{+}$ and $\mathcal{H}_{red}^{-}$ are simple subsets of the "natural basis". Explicitly we find (see 8.2.2):

$$\mathcal{H}_{red}^{+} : \left\{ \left| v\ 0 \right\rangle, \sum_{i=1}^{N} \left| \tau\ 1\vec{q}_{i} \right\rangle \left\langle \tau\ 1\vec{q}_{i} \right| H \left| v\ 0 \right\rangle, v = 1...n, \tau = 1...n-g, p_{v} = +1 \right\}$$

$$\mathcal{H}_{red}^{-} : \left\{ \left| v\ 0 \right\rangle, \sum_{i=1}^{N} \left| \tau\ 1\vec{q}_{i} \right\rangle \left\langle \tau\ 1\vec{q}_{i} \right| H \left| v\ 0 \right\rangle, v = 1...n, \tau = 1...n-g, p_{v} = -1 \right\}$$

$\mathcal{H}_{red}^{+}$ is of dimension $n_{+}(n-g+1)$ and $\mathcal{H}_{red}^{-}$ is of dimension $n_{-}(n-g+1)$, where n_{+} and n_{-} are the number of electron eigenstates with positive and negative parity, respectively.

The decomposition of $\mathcal{H}_{red}$ in two decoupled orthogonal subspaces implies that the matrix representation of the Hamiltonian H_{red} becomes further bloc-diagonal:

$$H_{red} = \begin{pmatrix} \boxed{\begin{array}{c} H_{red}^{+} \\[1em] {\scriptstyle n_{+}(n-g+1) \times n_{+}(n-g+1)} \end{array}} & \\ & \boxed{\begin{array}{c} H_{red}^{-} \\[1em] {\scriptstyle n_{-}(n-g+1) \times n_{-}(n-g+1)} \end{array}} \end{pmatrix}$$

3.3.3 Degeneracies and "zero-shift polaron states"

We show the existence of coupled eigenstates of H_{red} with no energy shift relative to the free evolution spectrum. Such eigenstates appear in consequence of the degeneracy of certain electron eigenstates.

In section 3.3.1 we could demonstrate that the set of eigenstates of the reduced Hamiltonian H_{red} contains all the eigenstates of the full Hamiltonian H, which superpose different electron eigenstates. In return, it can be shown that every eigenstate of H_{red} is a superposition of different electron states. We emphasize, however, that certain eigenstates of H_{red} might be pure superpositions of different degenerate elec-

tron eigenstates. Such eigenstates of H_{red} are also eigenstates of the free Hamiltonian H^{free}, although they couple different electron states. In the following, we agree on calling those states "zero-shift eigenstates".

In the present quantum dot system, the electron energy eigenstates are either non-degenerate or twice degenerate due to the spatial symmetry with respect to the x-z-plane (spin degeneracy is neglected). Let us consider two degenerate electron states $|\tau_+\rangle$ and $|\tau_-\rangle$, where the sign refers to the wave function's parity along the y-coordinate.

In appendix 8.2.3 we show that H_{red} yields eigenstates of the form

$$|\psi_0\rangle = \sum_v \left[a_v \sum_{i=1}^{N} |\tau_+ \; 1\vec{q}_i\rangle \langle \tau_+ \; 1\vec{q}_i | H | v \; 0\rangle + b_v \sum_{i=1}^{N} |\tau_- \; 1\vec{q}_i\rangle \langle \tau_- \; 1\vec{q}_i | H | v \; 0\rangle \right],$$

where v ranges over the n_p electron states with parity p.

Those eigenstates have a strictly non-shifted energy equal to

$$\varepsilon_{\tau_+} + \varepsilon_{LO} \equiv \varepsilon_{\tau_-} + \varepsilon_{LO} \equiv \varepsilon_{\tau} + \varepsilon_{LO}.$$

More precisely, if an electron level ε_τ, below the most excited level, is degenerate (2x), then it gives rise to n_p linearly independent eigenvectors of H_{red}^p with zero energy shifts with respect to the spectrum of the free Hamiltonian. For the total reduced Hamiltonian H_{red} it follows the existence of $n \left(= n_+ + n_- \right)$ linearly independent zero-shift eigenvectors with energies equal to $\varepsilon_\tau + \varepsilon_{LO}$. Let us call d is the number of degenerate electron levels below the most excited level or, as we shall say, the number of "not fully excited electron levels" (see Fig. 4, section 3.2.1). Then, the total number of strictly non-shifted states adds up to $n \cdot d$.

We emphasize that the choice of zero-shift eigenvectors is not unique. Since the zero-shift eigenvectors associated with one degenerate level τ have an identical energy $\varepsilon_\tau + \varepsilon_{LO}$, they span an eigenspace $\mathcal{H}_{red}^{zero,\tau}$. As there are n linear independent zero-shift eigenstates, the energy $\varepsilon_\tau + \varepsilon_{LO}$ is n-times degenerated and $\mathcal{H}_{red}^{zero,\tau}$ has dimension n. Every superposition of zero-shift eigenstates inside $\mathcal{H}_{red}^{zero,\tau}$ is again a zero-shift eigenstate of H_{red}. Furthermore, we mention that the large bath of uncoupled polarons contains many more eigenstates with an energy equal to $\varepsilon_\tau + \varepsilon_{LO}$. In fact, all the states contained in the subspaces $\mathcal{H}_{B,\tau+}$ and $\mathcal{H}_{B,\tau-}$ introduced in section 3.3.1 have the energy $\varepsilon_\tau + \varepsilon_{LO}$. Any superposition of zero-shift eigenstates of $\mathcal{H}_{red}^{zero,\tau}$ and states from $\mathcal{H}_{B,\tau+}$ and $\mathcal{H}_{B,\tau-}$ is again an eigenstate of H.

At this point, one might wonder about the difference between "zero-shift states" and the large bath of uncoupled polarons. The crucial point about the zero-shift states is that they couple different electron states, even though those electron states are degenerate. A zero-shift state can never be expressed as a superposition of vectors from the uncoupled subspaces $\mathcal{H}_{B,\tau+}$ and $\mathcal{H}_{B,\tau-}$ since those spaces are both orthogonal to $\mathcal{H}_{red}$, in which the zero-shift states are contained. Furthermore, they are superpositions of natural basis states. Therefore they represent physically localized crystal deformations (see "Natural basis", 3.3.1), unlike the delocalized functions of $\mathcal{H}_{B,\tau+}$ and $\mathcal{H}_{B,\tau-}$. We conclude that the "zero-shift eigenstates" are indeed a particular category of coupled eigenstates.

3.3.4   Strong coupling subspaces

We shall investigate now the strength of all the matrix elements of the reduced Hamiltonian associated with the quantum dot polarons. These considerations will allow us to identify strong coupling subspaces inside $\mathcal{H}_{red}$ with weak mutual interaction.

The following notations are recalled: n is the number of electron state, g is the degeneracy of the most excited level and d is the number of not fully excited degenerate electron levels.

In the appendix (8.2.4) we prove that for each electron index $v = 1,...,n$ the subspace

$$\mathcal{H}_{red}^{v} \equiv vect\left\{\left|v\ 0\right\rangle,\ \sum_{i=1}^{N}\left|\tau\ 1\vec{q}_i\right\rangle\left\langle\tau\ 1\vec{q}_i\left|H\right|v\ 0\right\rangle,\ \tau = 1...n-g\right\}$$

contains $n-g-d+1$ orthogonal vectors with strong mutual coupling. In return, those vectors are very weakly coupled to all the other subspaces $\mathcal{H}_{red}^{\mu}$, $\mu \neq v$. This has crucial consequences for the diagonalization of H_{red}: There are $n-g-d+1$ eigenvectors of H_{red} with dominant contribution of $\mathcal{H}_{red}^{v}$ and quasi vanishing contribution of all the other subspaces $\mathcal{H}_{red}^{\mu}$, $\mu \neq v$. A good approximation of these eigenvectors is thus obtained by diagonalizing H_{red}^{v}, defined as the restriction of H_{red} to $\mathcal{H}_{red}^{v}$.

Altogether, there are n subspaces $\mathcal{H}_{red}^{v}$. Thus, H_{red} has $n(n-g-d+1)$ eigenvectors, which are nearly contained in only one of the subspaces $\mathcal{H}_{red}^{v}$.

Finally, we show in appendix 8.2.4 that an eigenstate of H_{red}, which is nearly contained in a space $\mathcal{H}_{red}^{v}$, can never be one of the "zero-shift states" introduced in the previous section. Since there are $n \cdot d$ such "zero-shift states" and $n(n-g-d+1)$

eigenstates associated with strong coupling subspaces, any of the $n(n-g+1)$ quantum dot polarons is either a zero-shift state or an eigenstate associated with a strong coupling subspace.

3.3.5   Similar subspaces

We argue in this section that the strong coupling subspaces $\mathcal{H}_{red}^{v+}$ and $\mathcal{H}_{red}^{v-}$ associated with the two degenerate electron states $|v_+\rangle$ and $|v_-\rangle$ are similar restrictions of the Hamiltonian H_{red}. Therefore, those subspaces have similar eigenvectors and eigenvalues. In particular, we prove in appendix 8.2.5 that the diagonal matrix elements of the Hamiltonian, restricted do the subspaces $\mathcal{H}_{red}^{v+}$ and $\mathcal{H}_{red}^{v-}$, are analytically equal. To demonstrate this statement we need to introduce the normalized natural basis of $\mathcal{H}_{red}^{v+}$ and $\mathcal{H}_{red}^{v-}$ introduced in section 3.3.1.

3.3.6   Overview: Three types of polaron states

Let us now summarize the important steps of section 3.3 and give a conclusive classification of the polarons in quantum dots.

We have represented the quantum dot system in a Hilbert space $\mathcal{H}$ and described its evolution by the Hamiltonian operator $H = H^{free} + H^{Fröhlich}$. The particular structure of this operator allowed us to restrict the physical considerations to a "reduced subspace" $\mathcal{H}_{red}$, which excludes the large and highly degenerate set of bulk polarons.

A mathematical representation of $\mathcal{H}_{red}$ is given by the non-orthonormal basis

$$\left\{ |v\ 0\rangle,\ \sum_{i=1}^{N} |\tau\ 1\vec{q}_i\rangle \langle \tau\ 1\vec{q}_i | H | v\ 0\rangle,\ v = 1...n,\ \tau = 1...n-g \right\},$$

Using this basis and taking into account one symmetry plane, we could show that the reduced subspace $\mathcal{H}_{red}$ exhibits the following substructure:

- $\mathcal{H}_{red}$ can be decomposed in two decoupled, orthogonal subspaces associated with symmetric and antisymmetric electronic wave functions. Bases of those spaces are simple subsets of the natural basis. (see 3.3.1)

- If the system posses degenerate electron levels below the most excited level, there are "zero-shift eigenstates" inside $\mathcal{H}_{red}$. They couple different degenerate electron states. (see 3.3.2)

- $\mathcal{H}_{red}$ contains n nearly independent strong coupling subspaces, one for each electron level $v = 1,...,n$. Those strong coupling subspaces have bases, which are simple subsets of the natural basis. (see 3.3.4)

- Due to degenerate electron states, certain strong coupling subspaces reveal similar polaron states. (see 3.3.5)

Further, we emphasize the completeness of the above classification by saying that all the quantum dot polaron states are either "zero-shift states" or states, which are nearly contained in one of the strong coupling subspaces. Consequently, we are led to the following final classification of the polarons in our quantum dot:

- **"bulk polarons"**

  Energy eigenstates of H, which do not couple different electron states. Those states are orthogonal to $\mathcal{H}_{red}$ and represent the large majority of the polarons. Their energies are non-shifted with respect to the free evolution spectrum. Physically, they correspond to superpositions, which are not localized in the quantum dot. Such polarons are characterized by the electron index τ of their subspace $\mathcal{H}_{B,\tau}$.

- **"normal quantum dot polarons"**

  Energy eigenstates of H, which couple different electron states and yield an energy that is shifted relative to the free evolution spectrum. Those states are contained in $\mathcal{H}_{red}$ and associated with one of its strong coupling subspaces $\mathcal{H}_{red}^{v}$. Such polarons are characterized by the electron index v of the corresponding strong coupling subspace $\mathcal{H}_{red}^{v}$. Further, they yields the property of quasi-degeneracy if v is a degenerate electron level.

- **"zero-shift quantum dot polarons"**

  Energy eigenstates of H, which couple degenerate electron states and yield a strictly non shifted energy. Those states are contained in a zero-shift subspace $\mathcal{H}_{red}^{zero,\tau} \subset \mathcal{H}_{red}$. Their energy is equal to $\varepsilon_{\tau} + \varepsilon_{LO}$. Those polarons are characterized by the electron index τ of the zero-shift subspace.

This classification concludes the analytical discussion of this section.

4 Present physical system

We shall now introduce a model of an actual quantum dot together with an appropriate analytical representation and numerical implementation.

4.1 Model overview and previous computations

The quantum system of interest consists in GaAs/GaAlAs quantum dots grown by organometallic chemical vapor deposition in inverted tetrahedral pyramids on patterned (111)B GaAs substrates. The created dot is embedded in complex one- and two-dimensional barriers, i.e. quantum wires and quantum wells, presented in Fig. 6 as modeled by F. Michelini [2]. The system belongs to the symmetry group C_{3V}, i.e. it exhibits three vertical symmetry planes with a mutual angle of 120°.
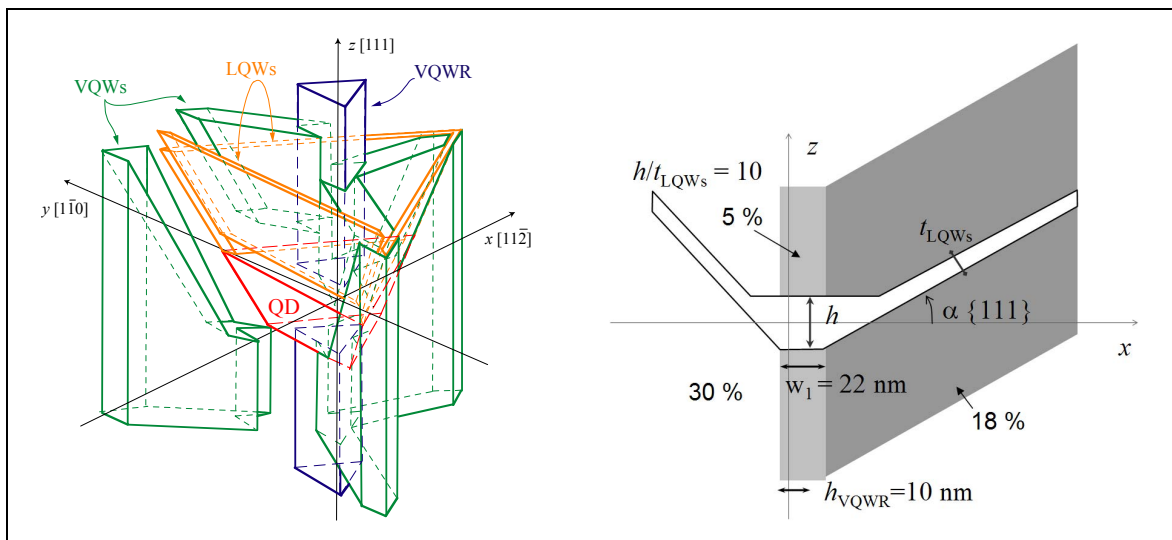
Fig. 6: **Model of the pyramidal quantum dot (10nm); source: [2].**

        LEFT: **3D visualization. QD = "quantum dot", VQWR = "vertical quantum wire", VQW = "vertical quantum well", LQW = "lateral quantum well".**

        RIGHT: **Projection on the x-z-plane (symmetry plane). The different zones of the heterostructure contain different fractions of Al, that are indicated by their percentage values.**

In the next chapter, the studies are carried out for three different dot heights *h=10 nm, 7.5 nm, 5 nm*.

4.2   Previously computed electron states

The envelope functions of the confined electron states in the quantum dots have been evaluated numerically using the k·p-method [1, 2] with a finite element scheme. In the case of $h = 10nm$, the quantum dot yields three confined energy levels: the first and the third are non-degenerated and the second is twice degenerated (spinless case). Fig. 7 shows isosurface plots of the respective envelope functions for the 10nm-dot. The states labeled $|A\rangle$, $|B_+\rangle$ and $|C\rangle$ yield even envelope functions along the y-axis, whereas $|B_-\rangle$ has an odd envelope function.
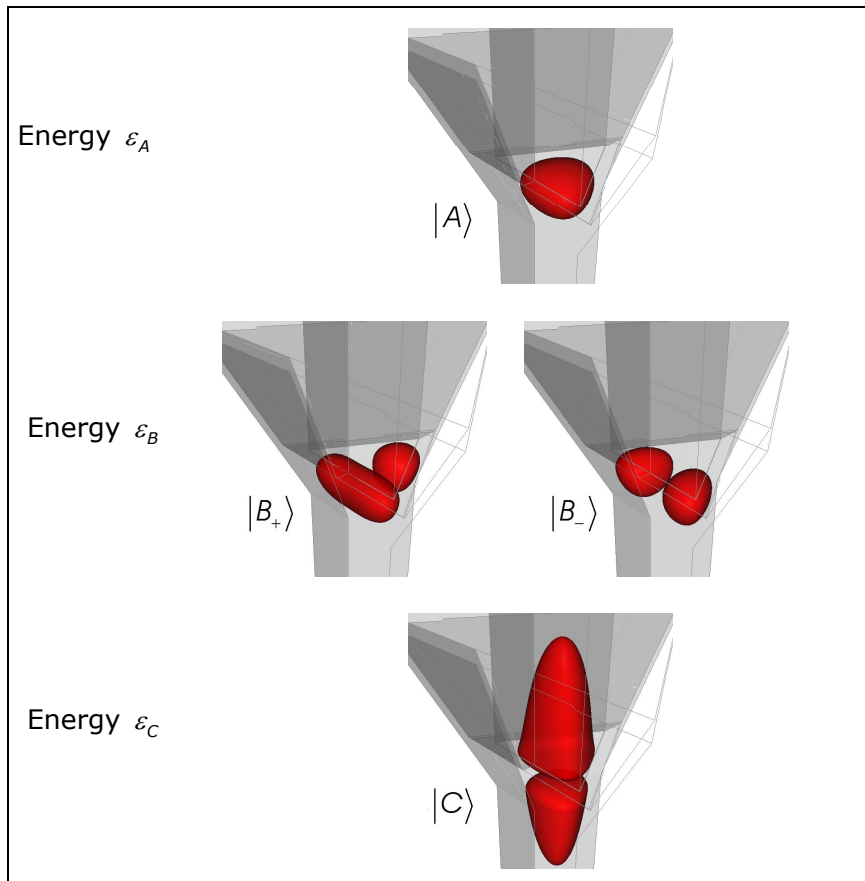
Fig. 7:   **Envelope functions of the electron eigenstates in the pyramidal quantum dot (10nm) as computed by F. Michelini [2]. The notation of the states used in this report is indicated.**

The energies of these electron states are shown in Tab. 1. For the 5nm dot only two levels (three states) are bound.

	ε_A [meV]	ε_B [meV]	ε_C [meV]
10nm dot	43.08	72.22	84.91
7.5nm dot	51.67	83.22	86.89
5nm dot	63.36	97.14	unbound

Tab. 1:   **Energies of the electron eigenstates in the pyramidal quantum dot, computed by F. Michelini [2].**

4.3   Numerical implementation

In this work, we have developed and embedded suitable numerical tools to compute the polaron states in the pyramidal quantum dots. In particular, we use an adaptive irregular discretization of the reciprocal space to efficiently represent the phonon continuum. In this frame, we transcribe the Fröhlich Hamiltonian, usually valid for regular discretization, in a scheme of irregular discretization. The direct space discretization is accomplished with the finite element method already used to compute the electronic envelope functions [1, 2].

Numerical methods and mathematical developments are expended in the appendix (8.3). Here we shall only present some leading ideas relative to the reciprocal space discretization, which are new in this work.

The Fröhlich matrix elements are subject to strong variation with the wavevector $\vec{q}$. A good discretization accounts for this dependence by a varying point density. The latter is achieved by an irregular discretization, which is adaptively refined in the regions of strong variation of the Fröhlich elements.

We prove in the appendix (8.3.3) that, in an irregular discretization, the volume Ω_i surrounding a given wave vector $\vec{q}_i$ enters in the calculation of the Fröhlich elements. Therefore, each vector $\vec{q}_i$ is assigned a volume Ω_i, taken as the volume of its Wigner-Seitz-cell.

To generate the well adapted irregular mesh, we start with a regular mesh with a small number of nodes. Then, the Wigner-Seitz-volume of each mesh node is computed and the Fröhlich matrix elements are evaluated. The mesh neighbors with the highest fluctuation of their Fröhlich elements are added a new node in between. The same procedure is repeated until the convergence of the polaron spectrum is reached. The convergence criterion is fulfilled if the maximal variation of all the polaron energies between two successive steps is smaller than a preset threshold.

A three-dimensional visualization of the adaptively generated irregular mesh of the first Brillouin zone is shown in Fig. 24. The three images are different zooming stages of the same mesh.
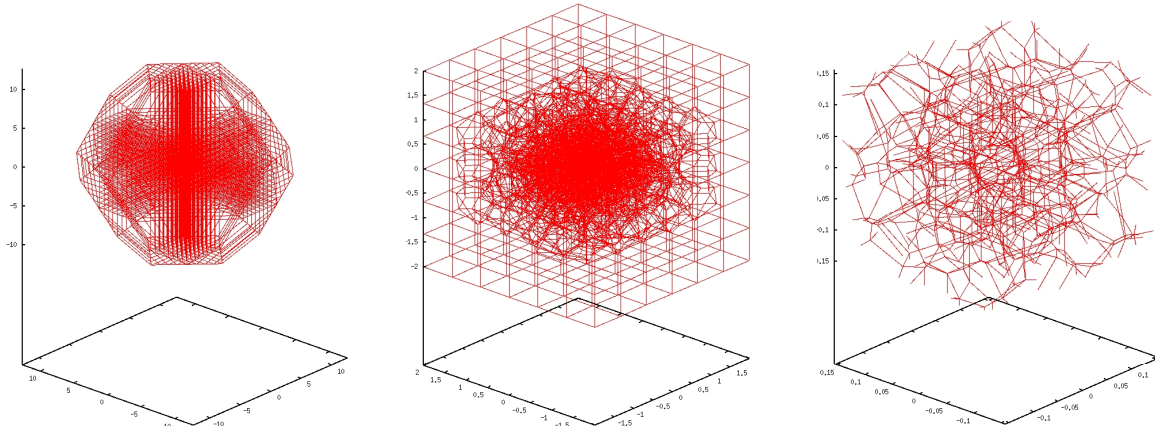
Fig. 8: **Adaptive discretization of the first Brillouin zone. Only the Wigner-Seitz-cells are drawn. Left: total zone, middle: zoomed to center by a factor 10, right: zoomed to center by a factor 100.**

This adaptive construction of an irregular discretization with simultaneous evaluation of the Wigner-Seitz volume defines a complex computational problem that demands sophisticated program structures. Yet, this effort is justified by the following advantages:

- The polaron spectrum computed based on an adaptive irregular mesh is shown to converge with about *500* wavevectors $\vec{q}_i$, whereas an optimized regular mesh requires more than *100'000* wavevectors. (convergence threshold = *1µeV*).

- Our mesh adapts itself to an arbitrary set of envelope functions. Thus, the method can be used without modifications to investigate other dot structures.

- The structure of the adaptively created mesh, carefully visualized, gives itself an insight in the physics.

Further explanations can be found in the appendix (8.3).

5 Computational results and interpretation

In this chapter we discuss and interpret the computational results. The quantum dot system has been explained in chapter 4. The results obtained for quantum dots with two and three electron levels are grouped in different sections 5.1 and 5.2, respectively.

5.1 Quantum dot with two electron levels

We present the results for a pyramidal quantum dot, where the second electron level is twice degenerate. Three different dot heights have been investigated: 10nm, 7.5nm and 5nm. In the latter case, the dot size is in deed small enough to contain only two electron energies, whereas for the 10nm and 7.5nm quantum dot a third level appears, which we neglect.

5.1.1 Electronic structure and polaron basis

The tensor product basis (electron state $\otimes$ phonon state) of the full Hilbert space $\mathcal{H}$ writes (section 3.2)

$$\left\{ \left| A\ 0 \right\rangle, \left| B_+\ 0 \right\rangle, \left| B_-\ 0 \right\rangle, \left| A\ 1\vec{q}_i \right\rangle, i = 1,...,N \right\}$$

where N is the number of normal modes. Those product states are the eigenstates of the free evolution without Fröhlich interaction. The corresponding free energies for the different dot sizes are given in Tab. 2.

	ε_A [meV] (non-degenerate)	ε_B [meV] (2× degenerate)	$\varepsilon_A + \varepsilon_{LO}$ [meV] (N× degenerate)
10nm dot	43.08	72.22	78.98
7.5nm dot	51.67	83.22	87.57
5nm dot	63.36	97.14	99.26

Tab. 2: Energies of the tensor product states of the two-level system

In section 3.3.1 we have introduced the reduced subspace $\mathcal{H}_{red}$ containing all the quantum dot polaron states. This space has six dimensions according to the general considerations of section 3.3.1. Its "natural basis" is composed of the three zero-phonon states

$$\left\{ \left| A\ 0 \right\rangle, \left| B_+\ 0 \right\rangle, \left| B_-\ 0 \right\rangle \right\}$$

and the three one-phonon states

$$\left\{\sum_{i=1}^{N}\left|A\ 1\vec{q}_i\right\rangle\left\langle A\ 1\vec{q}_i\left|H\right|A\ 0\right\rangle, \sum_{i=1}^{N}\left|A\ 1\vec{q}_i\right\rangle\left\langle A\ 1\vec{q}_i\left|H\right|B_+\ 0\right\rangle, \sum_{i=1}^{N}\left|A\ 1\vec{q}_i\right\rangle\left\langle A\ 1\vec{q}_i\left|H\right|B_-\ 0\right\rangle\right\}$$

The quantum dot polarons have been computed numerically using the numerical methods described in section 4.3. The convergence threshold has been set to $0.001meV$.

5.1.2   Computational results

Polaron energies

Fig. 9 depicts an overview of the polaron energies obtained for the three different dot heights (10nm, 7.5nm, 5nm). Blue lines indicate the free evolution spectrum without Fröhlich interaction, which we have numerically shown in Tab. 2. Red lines show the polaron energies with inclusion of the Fröhlich interaction. Short notations attached to each level allude to the classification of the respective polaron states. This classification is developed in the interpretation part (5.1.3). We mention, however, that certain computed energy levels, are equal up to the convergence precision. They have been added the suffix "quasi-degenerate", which accounts for the impossibility of deciding numerically whether the degeneracies are analytical. This important question will be addressed in section 5.1.3.
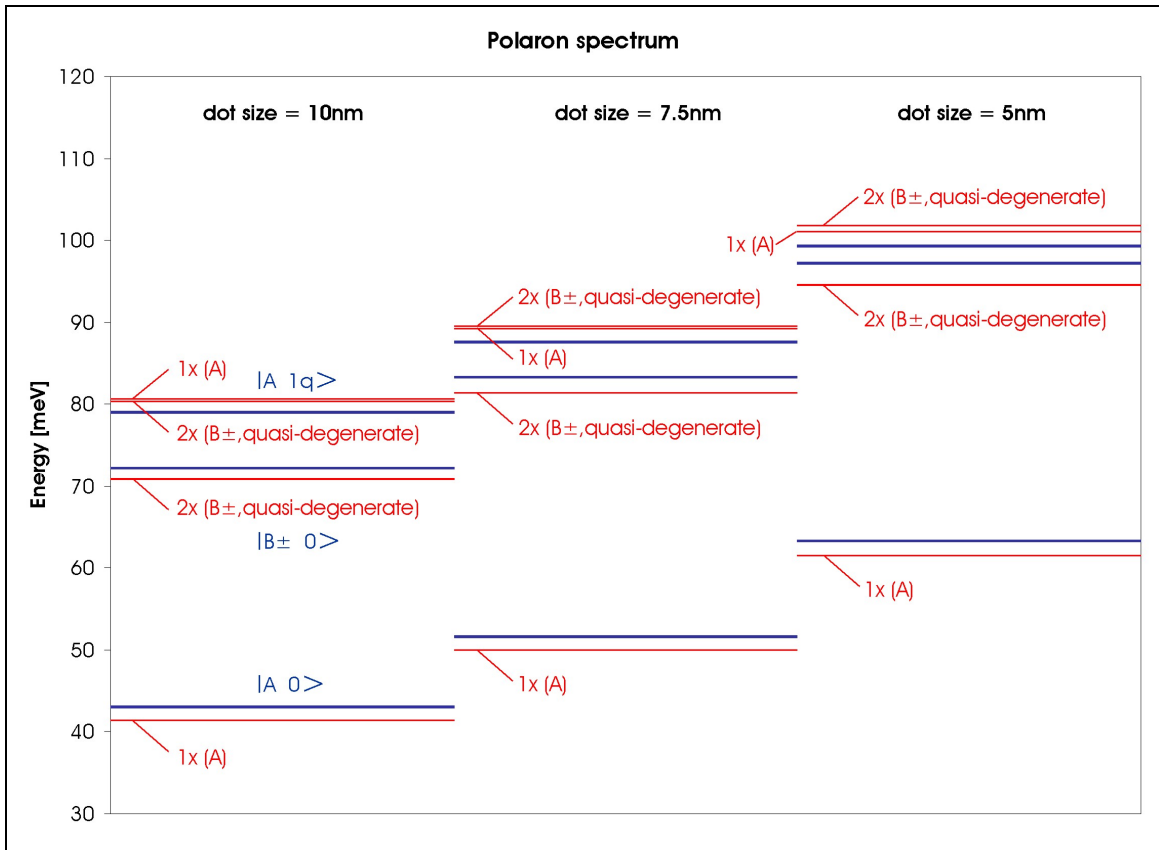

Fig. 9:   **Polaron spectrum of the two-level system for the three dot sizes. Blue lines indicate the free evolution spectrum, red lines include Fröhlich interaction.**

Polaron eigenvectors in the natural basis

We shall normalize the natural basis to represent the polaron states, in order to render the vector components comparable. We emphasize, however, that the normalized natural basis is still non-orthogonal. Tab. 3 shows the computed polaron vectors of the 10nm quantum dot, represented in this basis and suitably ordered for interpretation purposes. Smaller dot sizes (7.5nm and 5nm) reveal quite similar polaron states. The respective numerical tables are found in appendix **Fehler! Verweisquelle konnte nicht gefunden werden.**.

2 level system size = 10nm	Energy [meV]	State Vector					
		Subspace A		Subspace B+		Subspace B-	
		|A 0>	|A 1q> (|A 0>)	|B+ 0>	|A 1q> (|B+ 0>)	|B- 0>	|A 1q> (|B- 0>)
polaron state 1	41.470	0.9792	0.2029	0.0001	0.0003	0.0000	0.0000
polaron state 6	80.590	0.2029	0.9791	0.0064	0.0138	0.0000	0.0000
polaron state 3	70.827	0.0002	0.0002	0.9246	0.3810	0.0000	0.0000
polaron state 4	80.377	0.0030	0.0170	0.3809	0.9245	0.0000	0.0000
polaron state 2	70.825	0.0000	0.0000	0.0000	0.0000	0.9237	0.3832
polaron state 5	80.378	0.0000	0.0000	0.0000	0.0000	0.3832	0.9237

Tab. 3: **Polaron eigenvectors of the two-level system expressed in the normalized natural basis, 10nm dot**

The state numbers are ordered with increasing energy. Red fields indicate the most important components and yellow fields all the other components larger than 0.1. Blue fields stand for analytically vanishing components, as derived from the symmetry considerations of section 3.3.2. For the one-phonon natural basis vectors, the following abbreviations have been used in the table:

$$
\left| A\ 1q \right\rangle \left(\left| A\ 0 \right\rangle \right) \equiv \frac{\sum_{i=1}^{N} \left| A\ 1\vec{q}_i \right\rangle \left\langle A\ 1\vec{q}_i \left| H \right| A\ 0 \right\rangle}{\left\| \sum_{i=1}^{N} \left| A\ 1\vec{q}_i \right\rangle \left\langle A\ 1\vec{q}_i \left| H \right| A\ 0 \right\rangle \right\|}
$$

$$
\left| A\ 1q \right\rangle \left(\left| B_+\ 0 \right\rangle \right) \equiv \frac{\sum_{i=1}^{N} \left| A\ 1\vec{q}_i \right\rangle \left\langle A\ 1\vec{q}_i \left| H \right| B_+\ 0 \right\rangle}{\left\| \sum_{i=1}^{N} \left| A\ 1\vec{q}_i \right\rangle \left\langle A\ 1\vec{q}_i \left| H \right| B_+\ 0 \right\rangle \right\|}
$$

$$
\left| A\ 1q \right\rangle \left(\left| B_-\ 0 \right\rangle \right) \equiv \frac{\sum_{i=1}^{N} \left| A\ 1\vec{q}_i \right\rangle \left\langle A\ 1\vec{q}_i \left| H \right| B_-\ 0 \right\rangle}{\left\| \sum_{i=1}^{N} \left| A\ 1\vec{q}_i \right\rangle \left\langle A\ 1\vec{q}_i \left| H \right| B_-\ 0 \right\rangle \right\|}
$$

The six vectors of the natural basis are ascribed to three subspaces indexed by the letters A, B+ and B− . Those are the "strong coupling subspaces" introduced in the analytic developments of section 3.3.4. In the respective notation they write

"Subspace A" $\equiv \mathcal{H}_{red}^{A}$,   "Subspace B+" $\equiv \mathcal{H}_{red}^{B+}$,   "Subspace B−" $\equiv \mathcal{H}_{red}^{B-}$.

Polaron eigenvectors in the tensor product basis

Tab. 4 gives the polaron vectors represented in the tensor product basis (electron state $\otimes$ phonon state). The coloring scheme matches with the previous table.

2 level system size = 10nm	Energy [meV]	State Vector			
		|A 0>	|B+ 0>	|B- 0>	all |A 1q>
polaron state 1	41.470	0.9792	0.0001	0.0000	0.2029
polaron state 6	80.590	0.2029	0.0064	0.0000	0.9792
polaron state 3	70.827	0.0002	0.9246	0.0000	0.3810
polaron state 4	80.377	0.0030	0.3809	0.0000	0.9246
polaron state 2	70.825	0.0000	0.0000	0.9237	0.3832
polaron state 5	80.378	0.0000	0.0000	0.3832	0.9237

Tab. 4: **Polaron eigenvectors of the two-level system expressed in the tensor product basis, 10nm dot**

In order to reveal the meaning of this representation and to motivate the results presented below, we are led to some analytical explanations. Every polaron vector yields a tensor product basis representation of the type

$$c_A \left| A\ 0 \right\rangle + c_{B_+} \left| B_+\ 0 \right\rangle + c_{B_-} \left| B_-\ 0 \right\rangle + \sum_{i=1}^{N} \xi\left(\vec{q}_i\right) \left| A\ 1\vec{q}_i \right\rangle ,$$

where c_A , c_{B_+} , c_{B_-} .and $\xi\left(\vec{q}_i\right)$ are complex coefficients.

In Tab. 4, the first three columns under "state vector" show the complex magnitudes of the coefficients c_A , c_{B_+} and c_{B_-} . The forth column is the module of the vectors' projection on the one-phonon subspace, calculated as $\sqrt{\sum_{i=1}^{N} \left| \xi\left(\vec{q}_i\right) \right|^2}$. The discrete functions $\xi\left(\vec{q}_i\right)$, might be physically interpreted as "normal mode distribution functions". They will be depicted graphically. Before doing so, we should nevertheless acquire some insight about those functions.

Discussion of the polaron eigenvectors

From the natural basis representation (section Tab. 3) we conclude that the polaron states appear in pairs, which lie exactly or almost exactly in one of the three subspaces A, B+ or B− . Each such subspace contains only one one-phonon state of the natural basis and thus only one type of normal mode distribution function. For the subspace A, for example, the one-phonon basis vector (without normalization) writes

$$\sum_{i=1}^{N} \left| A \ 1\vec{q}_i \right\rangle \left\langle A \ 1\vec{q}_i \left| H \right| A \ 0 \right\rangle$$

Thus, the polaron states contained in this subspace have normal mode distribution functions $\xi(\vec{q}_i)$ proportional to $\left\langle A \ 1\vec{q}_i \left| H \right| A \ 0 \right\rangle$. In the same way, we find that the strong coupling subspaces B+ and B− exhibit a particular type of normal mode distribution functions. Explicitly we find,

Subspace A: $\qquad \xi(\vec{q}_i) \sim \left\langle A \ 1\vec{q}_i \left| H \right| A \ 0 \right\rangle$

Subspace B+: $\qquad \xi(\vec{q}_i) \sim \left\langle A \ 1\vec{q}_i \left| H \right| B_+ \ 0 \right\rangle$

Subspace B−: $\qquad \xi(\vec{q}_i) \sim \left\langle A \ 1\vec{q}_i \left| H \right| B_- \ 0 \right\rangle$

This argument reveals that two polarons associated with the same subspace have almost proportional functions $\xi(\vec{q}_i)$, which essentially depend on the phonon distribution function of a one-phonon state in the natural basis. Therefore, we can restrict ourselves to the visualization of only one function $\xi(\vec{q}_i)$ per strong coupling subspace. In the present case, the polaron states 1 and 6 are contained in the subspace A, the states 3 and 4 in the subspace B+ and the states 2 and 5 in the space B−. For these three pairs, some one-dimensional representations of the functions $\xi(\vec{q}_i)$ are shown in the first row of Fig. 10. Properly speaking, the figures show the modules of the functions $\xi(\vec{q}_i)$ along the qx-, qy-, and qz-directions. The images in the second row depict the isosurfaces of the functions' module, implicitly defined by

$\left| \xi(\vec{q}) \right| = const$, where the $\xi(\vec{q})$ is a continuous linear interpolation of $\xi(\vec{q}_i)$.

Since phase information is lost in these representations, we mention that the functions of the left and the middle column are symmetrical, whereas those of the right column are antisymmetric with respect to the x-z-plane. This reflects the y-parity of the underlying subspaces (section 3.3.2). Further, we emphasize that the small irregularities on the isosurfaces are not related to physical aspects. They are caused by the inexact discretization of the reciprocal space for q-values far from the zone center. In fact, we recall our implementation of an adaptive discretization method that only refines the reciprocal space meshing of numerically relevant zones (section 4.3).

Of partial interest is the inversed Fourier transforms of the normal mode distribution functions $\xi(\vec{q}_i)$. Those transforms are physically interpreted as "vibrational density functions" of the crystal. We emphasize that only longitudinal optical vibrations are considered in the present model (section 3.1). These density functions are repre-

sented in the third row of Fig. 10. Again, the images show isosurfaces, implicitly defined by

$$\left| \hat{\xi}\left(\vec{r}\right) \right| = const \text{ , where } \hat{\xi}\left(\vec{r}\right) = \int d^3q \ e^{i\vec{q}\cdot\vec{r}} \ \xi\left(\vec{q}\right)$$

Finally, the forth row shows isosurfaces of the electronic envelope functions ψ_A, ψ_{B_+} and ψ_{B_-} used for comparison. The orientation and the scale of these images is the same as in the third row. We already mention the remarkable similarity of the electronic envelope function and the vibrational density functions. This similarity will be discussed in section 5.1.3.

All the images of Fig. 10 refer to the 10nm quantum dot. The respective results for the dot sizes of 7.5nm and 5nm are presented in appendix **Fehler! Verweisquelle konnte nicht gefunden werden.**. Here we only show one example of the small dependence of the vibrational density function on the dot size (see Fig. 11).

Polaron states 1 and 6

$$\xi\left(\vec{q}_i\right) \sim \left\langle A \ 1\vec{q}_i \left| H \right| A \ 0 \right\rangle$$

Polaron states 3 and 4

$$\xi\left(\vec{q}_i\right) \sim \left\langle A \ 1\vec{q}_i \left| H \right| B_+ \ 0 \right\rangle$$

Polaron states 2 and 5

$$\xi\left(\vec{q}_i\right) \sim \left\langle A \ 1\vec{q}_i \left| H \right| B_- \ 0 \right\rangle$$
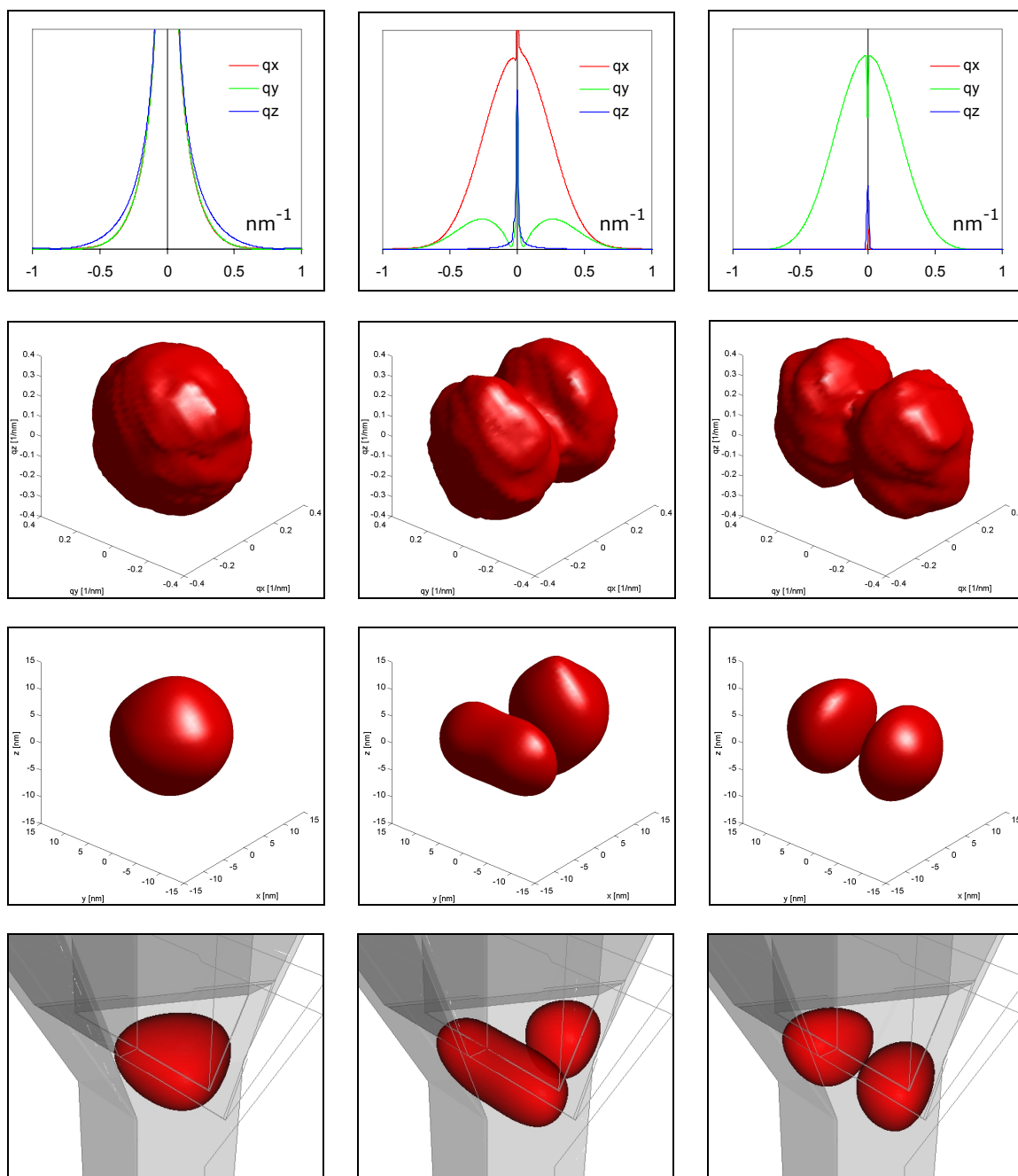
Fig. 10: **Row 1: Normal mode density functions, 1D plot of modules along qx,qy,qz.**
Row 2: Normal mode density functions, 3D isosurfaces of the module in q-space
Row 3: Vibrational density functions, 3D isosurfaces of the mod. in direct space
Row 4: Electronic envelope functions, 3D isosurfaces of the modules in direct space, same orientation and scale as row 3 [2]
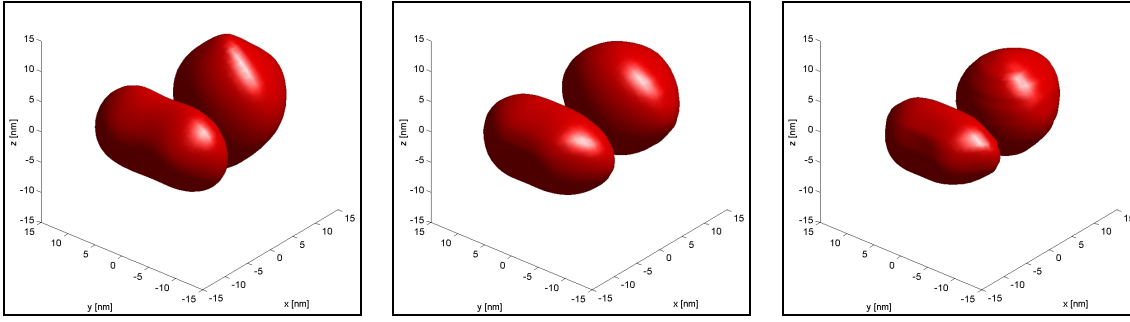
Fig. 11: Vibrational density functions in direct space (3D isosurfaces of the modules),
Left: 10nm dot, Middle: 7.5nm dot, Right: 5nm dot

5.1.3 Interpretation of the quantum dot polaron states

Let us discuss our numerical results more in detail using the analytical tools developed in section 3.3.

General structure of the energy spectrum

The energy spectrum shown in Fig. 9 reveals that one polaron energy lies close to the energy of the state $|A\ 0\rangle$, two polaron energies lie close to $|B_{\pm}\ 0\rangle$ and three lie close to $|A\ 1\vec{q}\rangle$. This feature could have been predicted from our natural basis, used to represent the quantum dot polaron states (section 3.3.1). In fact, the those basis states write:

$$\left\{ |A\ 0\rangle, |B_{+}\ 0\rangle, |B_{-}\ 0\rangle, \sum_{i=1}^{N} |A\ 1\vec{q}_{i}\rangle\langle A\ 1\vec{q}_{i}|H|A\ 0\rangle, \sum_{i=1}^{N} |A\ 1\vec{q}_{i}\rangle\langle A\ 1\vec{q}_{i}|H|B_{+}\ 0\rangle, \sum_{i=1}^{N} |A\ 1\vec{q}_{i}\rangle\langle A\ 1\vec{q}_{i}|H|B_{-}\ 0\rangle \right\}$$

We can numerically show, that the off-diagonal matrix elements of the Hamiltonian in this basis are small compared to the diagonal ones. Thus, one can expect that the polarons have energies close to the free energies of those basis states. This leads indeed to one polaron energy in the vicinity of $|A\ 0\rangle$, two close to $|B_{\pm}\ 0\rangle$ and three close to $|A\ 1\vec{q}\rangle$.

Global classification of polarons states

For completeness we mention that the large majority of polarons are "bulk polarons" (section 3.3.6), which are is spread over the dispersed bulk. Mathematically, those states are orthogonal to $\mathcal{H}_{red}$, defined as the small space of quantum dot polarons. The six remaining polarons are "normal quantum dot polarons" (section 3.3.6), defined as quantum dot polaron states with non-vanishing energy shift. There are no "zero-shift polarons". This affirmation is revealed numerically by the fact that none of the six polaron energies overlaps a free evolution energy (see Fig. 9), but it also derives from analytic considerations. In fact, we have shown in section 3.3.3 that only

electronic degeneracies on a level below the most excited level can cause "zero-shift polarons". In the present case, however, the only degenerate level ε_B is itself the most excited level. In consequence there are no "zero-shift polarons" in the two-level system.

Symmetry plane and independent subspaces

From now on, we restrict ourselves to the reduced space $\mathcal{H}_{red}$, which only contains the six quantum dot polarons. In the section 3.3.2 we have shown that the plane-symmetry of the pyramidal quantum dot implies that $\mathcal{H}_{red}$ contains two decoupled orthogonal parts, called $\mathcal{H}_{red}^+$ and $\mathcal{H}_{red}^-$, associated with different parities of the electronic wave functions. Applying our general developments of this section to the present case, those spaces become

$$\mathcal{H}_{red}^+ : \quad \left\{ \left| A\ 0 \right\rangle, \left| B_+\ 0 \right\rangle, \sum_{i=1}^{N} \left| A\ 1\vec{q}_i \right\rangle \left\langle A\ 1\vec{q}_i \left| H \right| A\ 0 \right\rangle, \sum_{i=1}^{N} \left| A\ 1\vec{q}_i \right\rangle \left\langle A\ 1\vec{q}_i \left| H \right| B_+\ 0 \right\rangle \right\}$$

$$\mathcal{H}_{red}^- : \quad \left\{ \left| B_-\ 0 \right\rangle, \sum_{i=1}^{N} \left| A\ 1\vec{q}_i \right\rangle \left\langle A\ 1\vec{q}_i \left| H \right| B_-\ 0 \right\rangle \right\}$$

We conclude that $\mathcal{H}_{red}^+$ contains the subspaces A and B+ used to present the results (5.1.2), and $\mathcal{H}_{red}^-$ is identified with the subspace B− . The numerical computation has indeed revealed the analytically exact decoupling of $\mathcal{H}_{red}^+$ and $\mathcal{H}_{red}^-$ by the fact that four states came out with numerically vanishing contribution of $\mathcal{H}_{red}^-$ and two states with vanishing contribution of $\mathcal{H}_{red}^+$ (see Tab. 3 of the previous section).

Weakly coupled and independent "strong coupling subspaces"

We further identify the subspaces A, B+ and B− with the "strong coupling subspaces" that we have introduced in section 3.3.4. There we have justified the small mutual coupling of those spaces. Of course, there is no coupling at all between the space B− and the other two spaces because of the plane-symmetry discussed above. The affirmation of section 3.3.4 is, however, that even the spaces A and B+ are only weakly coupled. The numerical computation is in good agreement with this prediction as can be seen in Tab. 3.

Types of superpositions

We wonder about the types of superpositions found in each quantum dot polaron. Therefore, we will consider each strong coupling subspace (A, B+, B−) separately. The subspace A is spanned by the basis (section 3.3.4)

$$\left\{ \left| A\ 0 \right\rangle, \sum_{i=1}^{N} \left| A\ 1\vec{q}_i \right\rangle \left\langle A\ 1\vec{q}_i \left| H \right| A\ 0 \right\rangle \right\}$$

This basis only involves one electron state $\left| A \right\rangle$. Thus, the two polarons 1 and 6 contained in this subspace do not involve different electron states, but still superpose the zero-phonon states with one-phonon states.

As for the subspace B+, a suitable basis is given by (section 3.3.4)

$$\left\{ \left| B_+\ 0 \right\rangle, \sum_{i=1}^{N} \left| A\ 1\vec{q}_i \right\rangle \left\langle A\ 1\vec{q}_i \left| H \right| B_+\ 0 \right\rangle \right\}$$

It follows that the two polarons 3 and 4 contained in this space do involve the two electron states $\left| B_+ \right\rangle$ and $\left| A \right\rangle$. At the same time, they involve the superpositions of zero-phonon states with one-phonon states. However, it should be stressed that these polarons are entangled superpositions of electronic and phononic parts and thus those parts cannot be treated separately.

The consequences for the states 2 and 5 in the strong coupling subspace B− are the same up to the sign difference.

Degeneracies

The numerical results show evidence for two degeneracies between the polarons associated with the subspaces B+ and B− (see Fig. 9). We ascribe those degeneracies to an additional symmetry, which we did not include in the analytical considerations. In fact, the pyramidal quantum dot exhibits three vertical symmetry planes that constitute the symmetry group C_{3V}. In the analytical investigations of the system symmetry, we have exploited only one symmetry plane, which constitutes the group C_S. The real symmetry, which is higher, causes the degeneracy of the electron states $\left| B_+ \right\rangle$ and $\left| B_- \right\rangle$ and implies a relation between their respective envelope functions.

Since phonons exhibit a spherical symmetry and the pyramidal quantum dots the symmetry C_{3V}, the composed polaron system belongs again to the symmetry group C_{3V}. Therefore, the polarons yield the same symmetry ass the electrons, which justifies the degeneracy between the states associated with the subspaces B+ and B−. Thus, we interpret the polaron energies, numerically classified as quasi-degenerate, as indeed analytically degenerate.

Vibrational density function

A physical picture of each polaron is given by the respective "vibrational density function" (see row 3 of Fig. 10). This function reveals some crucial features. First, it shows that the crystal vibrations associated with one of the six polarons are highly confined to the quantum dot. Second, the comparison between the images of row 3

and 4 of Fig. 10 yields that the electronic envelope functions are very similar to the vibrational density functions $\xi\left(\vec{q}_i\right)$ of the respective strong coupling subspace. We explain this feature by a closer look at the functions $\xi\left(\vec{q}_i\right)$. In fact, they are all proportional to Fröhlich matrix elements, which depend on $\vec{q}_i$ by the Fröhlich integral

$$\int d^3x \; e^{i\vec{q}\cdot\vec{x}} \, \psi_A(\vec{x})\psi_\nu(\vec{x}) \, ,$$

where ν is the electron index of the strong coupling subspace.

Since $\psi_A(\vec{x})$ is an s-like envelope function it is nearly isotropic. In consequence, the inverse Fourier transform of the integral above is again similar to $\psi_\nu(\vec{x})$. This explains the similarity between the electronic envelope functions and the vibrational density functions in the two-level quantum dot.

Dot size dependence

The dot size dependence of the polaron energies is revealed in Fig. 9. First, we note that the polaron coupling increases with decreasing dot size, meaning that the energy shifts become larger. We associate this feature with the increasing confinement of the electron states and the close-up of the free energies of the states $\left| A \; 1q \right\rangle$ and $\left| B \; 0 \right\rangle$ with decreasing dot size.

An interesting particularity is observed with the two highest energy levels, one of which is twice degenerate (see Fig. 9). Those levels are exchanged when passing from the 10nm quantum dot to the 7.5nm dot. Continuity considerations imply that in between the two levels there is an accidental degeneracy, giving rise to a three fold degeneracy. This crossing is compatible with our previous conjecture about the influence of symmetry on degeneracies.

5.2　　Quantum dot with three electron levels

In this section, we present computational results relative to the 10nm quantum dot with three electron levels, where the second level is twice degenerate. These results are in many aspects similar to the two-level system. Therefore, we shall explain them more briefly and focus on the differences with the previous case.

5.2.1　　Electronic structure and polaron basis

The tensor product basis (electron state $\otimes$ phonon state) of the Hilbert space $\mathcal{H}$ writes

$$\left\{ \left| A\ 0 \right\rangle, \left| B_+\ 0 \right\rangle, \left| B_-\ 0 \right\rangle, \left| C\ 0 \right\rangle, \left| A\ 1\vec{q}_i \right\rangle, \left| B_+\ 1\vec{q}_i \right\rangle, \left| B_-\ 1\vec{q}_i \right\rangle, i = 1, \ldots, N \right\}$$

where N is the number of normal modes. Those product states are the eigenstates of the free evolution without Fröhlich interaction. The respective energies are shown in Tab. 5.

zero-phonon product states	one-phonon product states
$\varepsilon_A = 43.08\,meV$	$\varepsilon_A + \varepsilon_{LO} = 78.98\,meV$
$\varepsilon_B = 72.22\,meV$	$\varepsilon_B + \varepsilon_{LO} = 108.12\,meV$
$\varepsilon_C = 84.01\,meV$	

Tab. 5:   Energies of the tensor product states of the three-level system

The reduced subspace $\mathcal{H}_{red}$ containing all the polaron states of physical interest has 16 dimensions according to our general analytic derivations (3.3.1). The natural basis is given by the four zero-phonon states

$$\left\{ \left| A\ 0 \right\rangle, \left| B_+\ 0 \right\rangle, \left| B_-\ 0 \right\rangle, \left| C\ 0 \right\rangle \right\}$$

and the twelve one-phonon states

$$\left\{ \sum_{i=1}^{N} \left| A\ 1\vec{q}_i \right\rangle \left\langle A\ 1\vec{q}_i \right| H \left| v\ 0 \right\rangle, \sum_{i=1}^{N} \left| B_+\ 1\vec{q}_i \right\rangle \left\langle B_+\ 1\vec{q}_i \right| H \left| v\ 0 \right\rangle, \sum_{i=1}^{N} \left| B_-\ 1\vec{q}_i \right\rangle \left\langle B_-\ 1\vec{q}_i \right| H \left| v\ 0 \right\rangle, v = A, B_+, B_-, C \right\}$$

The quantum dot polarons of such a system have been computed numerically using the numerical methods described in section 4.3. The convergence threshold has again been set to *0.001meV* .

5.2.2   Computational results

Polaron energies

To investigate the energy shift with increasing Fröhlich coupling, we have introduced a constant called "tuning factor". This factor multiplies the Fröhlich constant, such that its value *1* corresponds to the true physical situation. In a series of independent computations, this tuning factor was varied from *0* to *2* . The polaron energies as a function of the tuning factor are given in Fig. 12. The short notations attached to each level indicate the classification of the respective polaron states. This classification is developed in the interpretation part (5.2.3). Similarly to the case of two electron levels, quasi-degenerate levels appear (section 5.1.2). Those levels are labeled "quasi-degenerate".
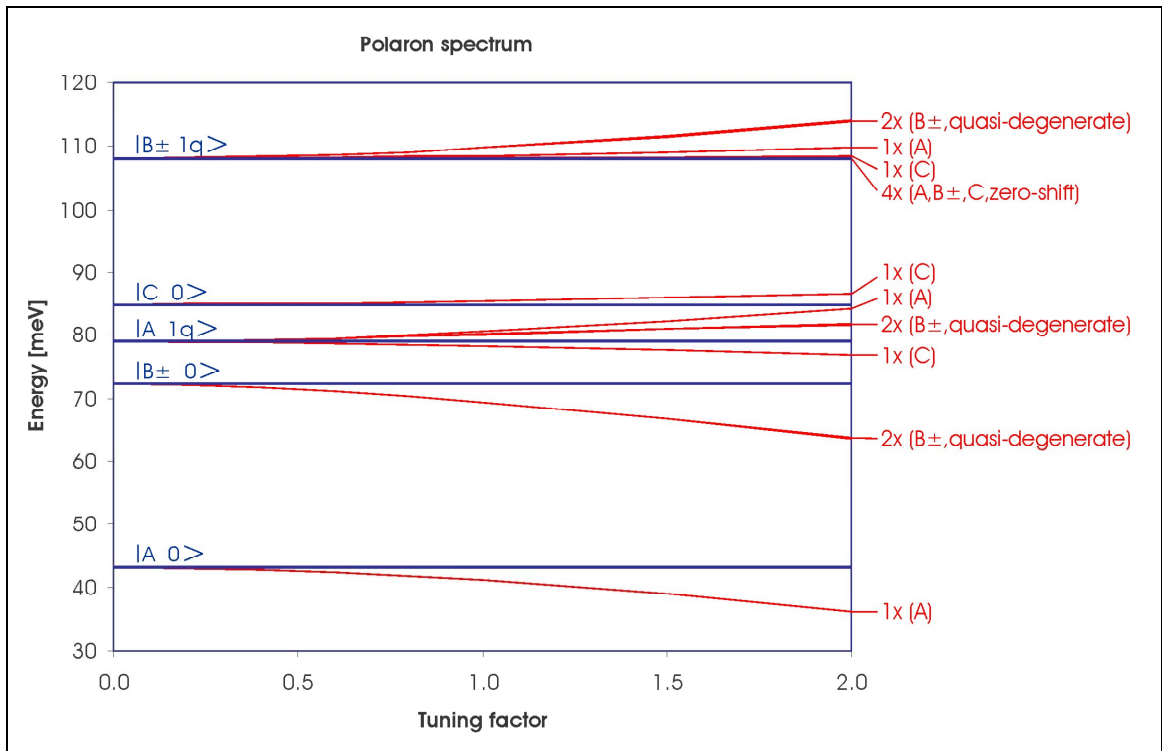
Fig. 12: Polaron spectrum of the three-level system. Blue lines indicate the free evolution spectrum without Fröhlich interaction (F. Michelini [2]), red lines include Fröhlich interaction. The tuning factor multiplies the Fröhlich coupling constant. The value 1.0 corresponds to the true physical situation.

Polaron eigenvectors in the natural basis

The polaron vectors represented in the normalized natural basis are shown in Tab. 6. They are suitably ordered to facilitate the interpretation.

3 level system size = 10nm	Energy [meV]	State Vector															
		Subspace A				Subspace B+				Subspace C				Subspace B-			
		|A 0>	|A 1q> (|A 0>)	|B+ 1q> (|A 0>)	|B- 1q> (|A 0>)	|B+ 0>	|A 1q> (|B+ 0>)	|B+ 1q> (|B+ 0>)	|B- 1q> (|B+ 0>)	|C 0>	|A 1q> (|C 0>)	|B+ 1q> (|C 0>)	|B- 1q> (|C 0>)	|B- 0>	|A 1q> (|B- 0>)	|B+ 1q> (|B- 0>)	|B- 1q> (|B- 0>)
polaron state 1	41.21	0.978	0.198	0.048	0.049	0.000	0.000	0.000	0.001	0.000	0.001	0.001	0.000	0.000	0.000	0.000	0.000
polaron state 7	80.51	0.196	0.980	0.024	0.024	0.000	0.001	0.000	0.000	0.012	0.015	0.001	0.000	0.000	0.000	0.000	0.000
polaron state 14	108.47	0.074	0.019	0.693	0.695	0.000	0.000	0.001	0.010	0.016	0.001	0.054	0.052	0.000	0.000	0.000	0.000
polaron state 3	69.53	0.000	0.000	0.000	0.000	0.927	0.326	0.175	0.058	0.000	0.001	0.001	0.000	0.000	0.000	0.000	0.000
polaron state 5	80.09	0.000	0.001	0.000	0.000	0.315	0.945	0.082	0.027	0.000	0.002	0.000	0.000	0.000	0.000	0.000	0.000
polaron state 15	109.70	0.000	0.000	0.000	0.000	0.202	0.022	0.929	0.308	0.000	0.000	0.004	0.000	0.000	0.000	0.000	0.000
polaron state 8	85.38	0.004	0.005	0.001	0.001	0.000	0.000	0.000	0.000	0.955	0.288	0.046	0.047	0.000	0.000	0.000	0.000
polaron state 4	78.40	0.002	0.025	0.000	0.000	0.000	0.001	0.000	0.000	0.287	0.958	0.011	0.011	0.000	0.000	0.000	0.000
polaron state 13	108.22	0.005	0.001	0.176	0.176	0.000	0.000	0.003	0.003	0.065	0.004	0.709	0.721	0.000	0.000	0.000	0.000
polaron state 11	108.12	0.000	0.000	0.179	1.093	0.000	0.000	0.125	1.188	0.000	0.000	0.437	0.345	0.000	0.000	0.000	0.000
polaron state 9	108.12	0.000	0.000	0.740	0.388	0.000	0.000	0.390	0.358	0.000	0.000	0.058	0.087	0.000	0.000	0.000	0.000
polaron state 10	108.12	0.000	0.000	0.065	0.711	0.000	0.000	0.021	0.868	0.000	0.000	0.575	0.625	0.000	0.000	0.000	0.000
polaron state 2	69.53	0.000	0.000	0.000	0.000	0.000	0.000	0.000	0.000	0.000	0.000	0.000	0.000	0.927	0.326	0.058	0.175
polaron state 6	80.09	0.000	0.000	0.000	0.000	0.000	0.000	0.000	0.000	0.000	0.000	0.000	0.000	0.315	0.945	0.027	0.082
polaron state 16	109.70	0.000	0.000	0.000	0.000	0.000	0.000	0.000	0.000	0.000	0.000	0.000	0.000	0.202	0.022	0.308	0.929
polaron state 12	108.12	0.000	0.000	0.000	0.000	0.000	0.000	0.000	0.000	0.000	0.000	0.000	0.000	0.000	0.000	0.949	0.315

Tab. 6: Polaron eigenvectors of the three-level system represented in the normalized natural basis

The state numbers are ordered with increasing energy. For the 4 "zero-shift states" (see analytical derivations 3.3.3), the non-zero coefficients are colored green. For the other 12 states with shifted energies, red fields mark the main contribution, dark yellow fields other important coefficients (>0.2) and bright yellow fields slightly important coefficients (>0.02). All the white fields contain very small, but non-vanishing values, whereas blue stands for analytically vanishing coefficients.

For the one-phonon basis vectors, the following abbreviations have been used:

$$\left| \tau \ 1q \right\rangle \left(\left| \nu \ 0 \right\rangle \right) \equiv \frac{\sum_{i=1}^{N} \left| \tau \ 1\vec{q}_i \right\rangle \left\langle \tau \ 1\vec{q}_i \left| H \right| \nu \ 0 \right\rangle}{\left\| \sum_{i=1}^{N} \left| \tau \ 1\vec{q}_i \right\rangle \left\langle \tau \ 1\vec{q}_i \left| H \right| \nu \ 0 \right\rangle \right\|}$$

The sixteen basis vectors are grouped in four "strong coupling subspaces" indexed by the letters A, B+, B− and C. In the notation used in section 3.3, they are noted $\mathcal{H}_{red}^{A}$, $\mathcal{H}_{red}^{B+}$, $\mathcal{H}_{red}^{B-}$ and $\mathcal{H}_{red}^{C}$, respectively.

We emphasize that the four zero-shift polarons (with green coefficients) are degenerate. Every superposition of those states is again an eigenstate. Thus, the shown coefficients only represent one linearly independent choice.

Polaron eigenvectors in the tensor product basis

The following tables show the polaron eigenvectors in the tensor product basis (electron state ⊗ phonon state). The coloring corresponds to the one of the previous table.

3 level system size = 10nm	Energy [meV]	State Vector						
		zero-phonon subspace				one-phonon subspace		
		|A 0>	|B+ 0>	|B- 0>	|C 0>	all |A 1q>	all |B+ 1q>	all |B- 1q>
polaron state 1	41.21	0.978	0.000	0.000	0.000	0.198	0.048	0.049
polaron state 7	80.51	0.196	0.000	0.000	0.012	0.980	0.024	0.024
polaron state 14	108.47	0.074	0.000	0.000	0.016	0.019	0.704	0.706
polaron state 3	69.53	0.000	0.927	0.000	0.000	0.326	0.175	0.058
polaron state 5	80.09	0.000	0.315	0.000	0.000	0.945	0.082	0.027
polaron state 15	109.70	0.000	0.202	0.000	0.000	0.022	0.929	0.308
polaron state 8	85.38	0.004	0.000	0.000	0.955	0.288	0.046	0.047
polaron state 4	78.40	0.002	0.000	0.000	0.287	0.958	0.011	0.011
polaron state 13	108.22	0.005	0.000	0.000	0.065	0.005	0.700	0.712
polaron state 11	108.12	0.000	0.000	0.000	0.000	0.000	0.464	0.886
polaron state 9	108.12	0.000	0.000	0.000	0.000	0.000	0.738	0.675
polaron state 10	108.12	0.000	0.000	0.000	0.000	0.000	0.590	0.807
polaron state 2	69.53	0.000	0.000	0.927	0.000	0.326	0.058	0.175
polaron state 6	80.09	0.000	0.000	0.315	0.000	0.945	0.027	0.082
polaron state 16	109.70	0.000	0.000	0.202	0.000	0.022	0.308	0.929
polaron state 12	108.12	0.000	0.000	0.000	0.000	0.000	0.949	0.315

Tab. 7: **Polaron eigenvectors of the three-level system represented in the tensor product basis.**

In the tensor product basis, every state vector has the decomposition

$$c_A\left|A\ 0\right\rangle + c_{B+}\left|B_+\ 0\right\rangle + c_{B-}\left|B_-\ 0\right\rangle + c_C\left|C\ 0\right\rangle + \sum_{i=1}^{N}\xi\left(\vec{q}_i\right)\left|A\ 1\vec{q}_i\right\rangle + \sum_{i=1}^{N}\eta\left(\vec{q}_i\right)\left|B_+\ 1\vec{q}_i\right\rangle + \sum_{i=1}^{N}\zeta\left(\vec{q}_i\right)\left|B_+\ 1\vec{q}_i\right\rangle,$$

where c_A, c_{B+}, c_{B-}, c_C as well as $\xi\left(\vec{q}_i\right)$, $\eta\left(\vec{q}_i\right)$, $\zeta\left(\vec{q}_i\right)$ are complex coefficients.

The three functions $\xi\left(\vec{q}_i\right)$, $\eta\left(\vec{q}_i\right)$, $\zeta\left(\vec{q}_i\right)$ are again interpreted as "normal mode density functions" associated with the electron indices A, B_+ and B_-, respectively.

In Tab. 7 the four columns under "zero-phonon subspace" show the modules of the coefficients c_A, c_{B+}, c_{B-} and c_C. The three columns under "one-phonon subspace" give the magnitude of the vectors' projection on the one-phonon subspaces associated with the three electron indices A, B_+ and B_-. Explicitly, they are obtained from the functions $\xi\left(\vec{q}_i\right)$, $\eta\left(\vec{q}_i\right)$, $\zeta\left(\vec{q}_i\right)$ by

$$\text{"All }|A\ 1q>\text{"}=\sqrt{\sum_{i=1}^{N}\left|\xi\left(\vec{q}_i\right)\right|^2}\qquad\text{"All }|B_+\ 1q>\text{"}=\sqrt{\sum_{i=1}^{N}\left|\eta\left(\vec{q}_i\right)\right|^2}\qquad\text{"All }|B_-\ 1q>\text{"}=\sqrt{\sum_{i=1}^{N}\left|\zeta\left(\vec{q}_i\right)\right|^2}$$

We point out an important conclusion from the natural basis representation: The 12 shifted polaron states (all except the four with green coefficients) are nearly contained in one of the four strong coupling subspaces. Yet, polarons contained in the same strong coupling subspace have proportional normal mode density functions $\xi\left(\vec{q}_i\right)$, $\eta\left(\vec{q}_i\right)$, $\zeta\left(\vec{q}_i\right)$ (see extended explication of 5.1.2). They are indeed proportional to certain Fröhlich matrix elements as shown in Tab. 8.

	proportional function of $\xi\left(\vec{q}_i\right)$	proportional function of $\eta\left(\vec{q}_i\right)$	proportional function of $\zeta\left(\vec{q}_i\right)$
Subspace A $\left(\equiv\mathcal{H}_{red}^{A}\right)$	$\left\langle A\ 1\vec{q}_i\middle|H\middle|A\ 0\right\rangle$	$\left\langle B_+\ 1\vec{q}_i\middle|H\middle|A\ 0\right\rangle$	$\left\langle B_-\ 1\vec{q}_i\middle|H\middle|A\ 0\right\rangle$
Subspace B+ $\left(\equiv\mathcal{H}_{red}^{B_+}\right)$	$\left\langle A\ 1\vec{q}_i\middle|H\middle|B_+\ 0\right\rangle$	$\left\langle B_+\ 1\vec{q}_i\middle|H\middle|B_+\ 0\right\rangle$	$\left\langle B_-\ 1\vec{q}_i\middle|H\middle|B_+\ 0\right\rangle$
Subspace B− $\left(\equiv\mathcal{H}_{red}^{B_-}\right)$	$\left\langle A\ 1\vec{q}_i\middle|H\middle|B_-\ 0\right\rangle$	$\left\langle B_+\ 1\vec{q}_i\middle|H\middle|B_-\ 0\right\rangle$	$\left\langle B_-\ 1\vec{q}_i\middle|H\middle|B_-\ 0\right\rangle$
Subspace C $\left(\equiv\mathcal{H}_{red}^{C}\right)$	$\left\langle A\ 1\vec{q}_i\middle|H\middle|C\ 0\right\rangle$	$\left\langle B_+\ 1\vec{q}_i\middle|H\middle|C\ 0\right\rangle$	$\left\langle B_-\ 1\vec{q}_i\middle|H\middle|C\ 0\right\rangle$

Tab. 8: **Types of "normal mode distribution functions" in each strong coupling subspace**

Graphical representations in the reciprocal space of these 12 functions can be found in appendix **Fehler! Verweisquelle konnte nicht gefunden werden.**. Here, we focus on their inverse Fourier transforms that are interpreted as "vibrational density functions" of the longitudinal optical crystal vibrations. In contrast to the two-level system, we deal now with three such functions and not just one. They are associated

with different electron states and appear in entangled superpositions. Those three functions are shown for the four strong coupling subspaces in Fig. 13 to Fig. 16.
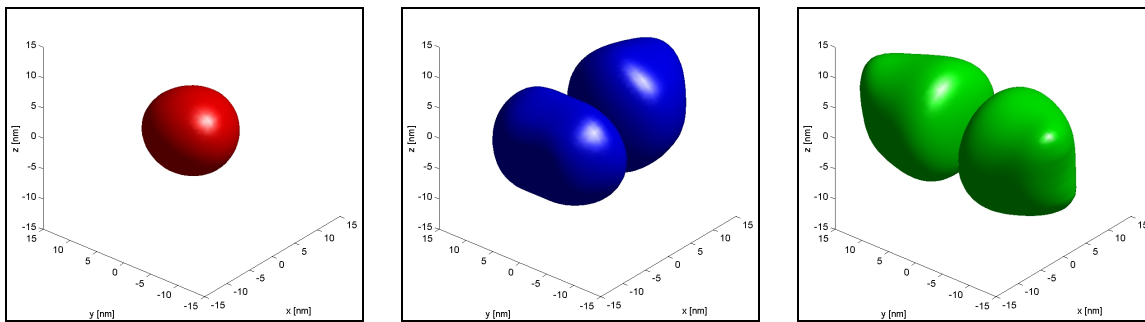

Fig. 13: Vibrational density functions of the polaron states nearly contained in the subspace A.
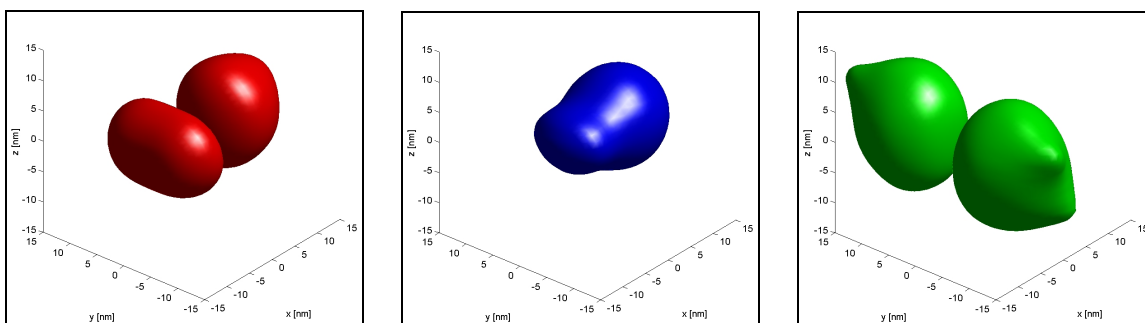

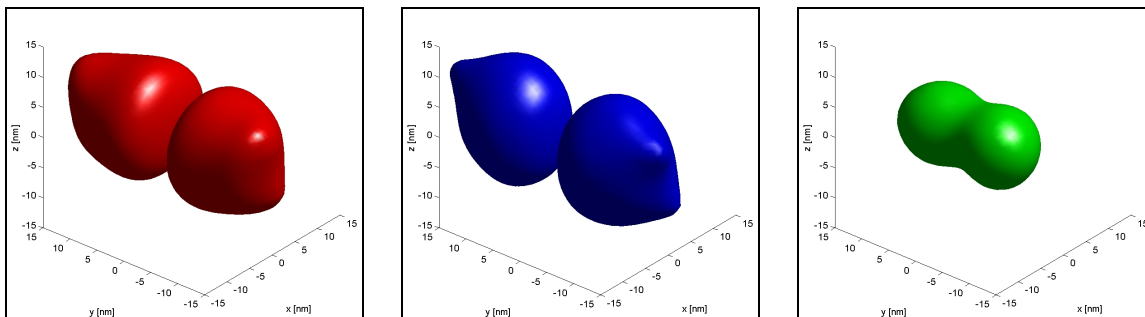**Fig. 14:** Vibrational density functions of the polaron states nearly contained in the subspace B_+ .
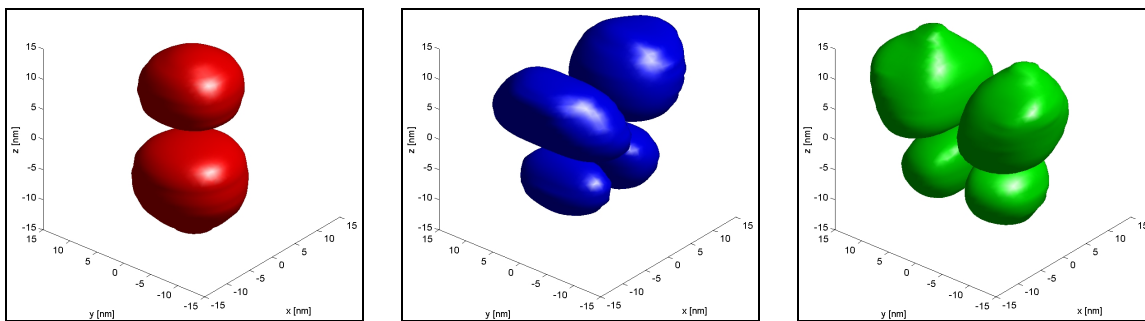

Fig. 15: Vibrational density functions of the polaron states nearly contained in the subspace B_- .

Fig. 16: Vibrational density functions of the polaron states nearly contained in the subspace C.

So far, we have focused on the 12 shifted polaron states. Let us now consider the four "zero-shift polarons" (section 3.3.3). By their nature, those states involve only pairs one-phonon states with degenerate electron index. Explicitly, they contain contributions from $\left| B_+ \ 1\vec{q}_i \right\rangle$ and $\left| B_- \ 1\vec{q}_i \right\rangle$, but there is strictly no contribution from $\left| A \ 1\vec{q}_i \right\rangle$. Thus, the function $\xi\left(\vec{q}_i\right)$ vanishes for all $\vec{q}_i$. Furthermore, the choice of the coefficients $\eta\left(\vec{q}_i\right)$ and $\zeta\left(\vec{q}_i\right)$ is not unique, since all the four zero-shift polarons are degenerate. A linearly independent choice has already been fixed in the natural basis representation (see green fields, Tab. 6). The polaron state 12 does not mix strong coupling subspaces, since it is ascribed to the only antisymmetric subspace B− . The vibrational density functions of this state are proportional to the ones shown in Fig. 15 (blue and green). For the other three zero-shift states the vibrational density functions are depicted in Fig. 17.
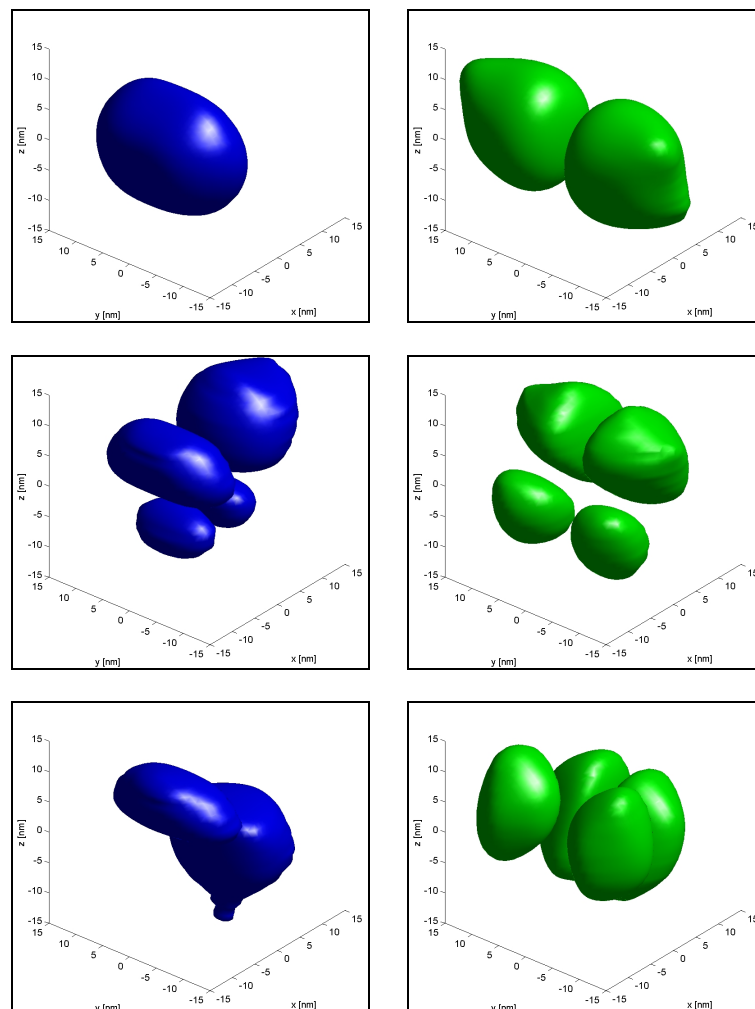
Fig. 17: **Vibrational density functions of the three symmetrical zero-shift polarons "9", "10" and "11".**

Again, the respective normal mode density functions in q-space are shown in appendix **Fehler! Verweisquelle konnte nicht gefunden werden.**.

5.2.3 Interpretation of the quantum dot polarons

General structure of the energy spectrum

Similarly to the case of two electron levels (section 5.1.3), the structure of the natural basis predicts how many polaron energies are associated with each energy of the free spectrum.

The natural basis (section 3.3.1) is given by the four zero-phonon states

$$\left\{ \left| A\ 0 \right\rangle, \left| B_+\ 0 \right\rangle, \left| B_-\ 0 \right\rangle, \left| C\ 0 \right\rangle \right\}$$

and the twelve one-phonon states

$$\left\{ \sum_{i=1}^{N} \left| A\ 1\vec{q}_i \right\rangle \left\langle A\ 1\vec{q}_i \left| H \right| v\ 0 \right\rangle, \sum_{i=1}^{N} \left| B_+\ 1\vec{q}_i \right\rangle \left\langle B_+\ 1\vec{q}_i \left| H \right| v\ 0 \right\rangle, \sum_{i=1}^{N} \left| B_-\ 1\vec{q}_i \right\rangle \left\langle B_-\ 1\vec{q}_i \left| H \right| v\ 0 \right\rangle, v = A, B_+, B_-, C \right\}$$

If follows from this representation that every free energy gives rise to a certain number of polarons according to Tab. 9. This affirmation is in well agreement with the numerical results shown in Fig. 12.

$\left\| A\ 0 \right\rangle$	$\left\| B_\pm\ 0 \right\rangle$	$\left\| C\ 0 \right\rangle$	$\left\| A\ 1q \right\rangle$	$\left\| B_\pm\ 1q \right\rangle$
1	2	1	4	8

Tab. 9: Number of quantum dot polarons associated with each free energy of the three-level system.

Effect of the additional electron levels

The polaron ground state energy offers an ideal tool to illustrate the effects of the additional electron level with respect to the two-level system, since the ground state energy can never be lifted by an interaction term. Its down-shift is somehow a measure of the interaction strength. For the two-level system the polaron ground state energy lies at 41.5meV, corresponding to a shift of –1.6meV. As for the three-level system the same level lies at 41.2meV, corresponding to a shift of –1.9meV. This reveals a small, but non negligible contribution of third electron level to the polaron ground state energy. The influence of this electron level on the first excited polaron energy is even higher. Whereas the two-level system exhibits a shift of –1.4meV, the three-level system yields –2.7meV. This strong variation relies on the proximity of the third electron state to the first excited polaron level. For more excited polaron energies, the discussions becomes more complicated because the additional zero- and one-phonon states of the three-level system give contradictory contributions to the polaron energy-shifts.

Global classification of polaron states

First, there is a large majority of "bulk polarons" without coupling to the quantum dot electronic states as explained in the case of two levels (section 5.1.3). All the remaining states are contained in the reduced space $\mathcal{H}_{red}$, defined as the small space of quantum dot polarons. Our analytical derivation of the "zero-shift states" presented in section 3.3, implies the existence of four "zero-shift states" in the present three-level system. In fact, we recall that each degenerate electron level, which lies strictly below the most excited level, gives a number of "zero-shift states" equal to the total number of electron states. The present quantum dot yields one degenerated electron level (ε_B) and the total number of electron states, including degenerate states, equals four. Thus, we obtain indeed four "zero-shift polaron states" on the level of the state $\left| B_\pm\ 1q \right\rangle$. This prediction is in agreement with the computational result: The energies of the polarons 9, 10, 11 and 12 all are numerically equal to the free energy of $\left| B_\pm\ 1q \right\rangle$ (see Tab. 6).

All the other quantum dot polarons are "normal quantum dot polarons" in the classification scheme, which we have introduced in this work (section 3.3.6). Finally, we conclude that the quantum dot has a large set of bulk "polarons", twelve "normal quantum dot polarons" and four "zero-shift polarons".

Symmetry plane and independent subspaces

We have shown the detailed consequences of this symmetry in the frame for two electron levels (section 5.1.3). In the case of three levels, the symmetric subspace $\mathcal{H}_{red}^+$ contains the subspaces A, B+ and C (section 5.2.2), whereas the antisymmetric complement $\mathcal{H}_{red}^-$ is identified with the subspace B−. The analytical decoupling of those two parts agrees with the numerical evidence found in Tab. 6.

Strong coupling subspaces

The analytical derivations of section 3.3.4 predict that there are four "strong coupling subspaces", one associated with each electron index A, B+, B− and C. Those spaces have only weak mutual coupling. In order to visualize the polaron states we have already widely used this particular feature (section 5.2.2).

Superposition types

By contrast with the case of two levels, all the 16 polarons superpose several electron states. This is for example shown in the natural basis representation of Tab. 6. However, it appears that the three polarons associated with the strong coupling subspace C involve superpositions of the electron state $\left| C \right\rangle$. Further, it is numerically

obvious (Tab. 6) that the four "zero-shift states" only superpose the two electron states $\left|B_+\right\rangle$ and $\left|B_-\right\rangle$ as predicted by the analytical considerations (section 3.3.3). The remaining nine polarons involve superpositions of the electron states $\left|A\right\rangle$, $\left|B_+\right\rangle$ and $\left|B_-\right\rangle$. Concerning the phonon component of the polarons, we emphasize that the four "zero-shift superpositions" involve only one-phonon states (see ??? for analytical, Tab. 6 for numerical), whilst the remaining twelve polarons involve also zero-phonon states.

Degeneracies

The numerical results show evidence for three degeneracies between the polarons associated with the subspaces B+ and B− (see Fig. 12). Like in the two-level system, we ascribe those degeneracies to an additional symmetry (C_{3V}), which we did not include in the analytical considerations. Thus, the high numerical similarities of the pairs of so-called "quasi-degenerate" states are most likely analytical degeneracies.

6 Discussion

A number of different aspects of this work needs to be discussed. First, we shall address the strong coupling regime in quantum dots. Second, our results for the quantum dot with two electron levels are compared with the results of other groups. Third, we discuss the relevance of our analytical results.

Evidence of strong coupling

A typical signature of a strong coupling regime is the failure of the perturbation theory. In Fig. 18 the red lines represent some of the pyramidal quantum dot polaron energies as a function of the Fröhlich coupling constant, whilst the black lines were derived from first order perturbation theory and the green line gives one example of second order perturbation. The large difference between the non-perturbative method and both (!) perturbative approaches for a tuning factor of 1 points out the limitations of perturbation theory. This evidence of strong coupling is in good agreement with recently published results [30, 31, 32, 33].
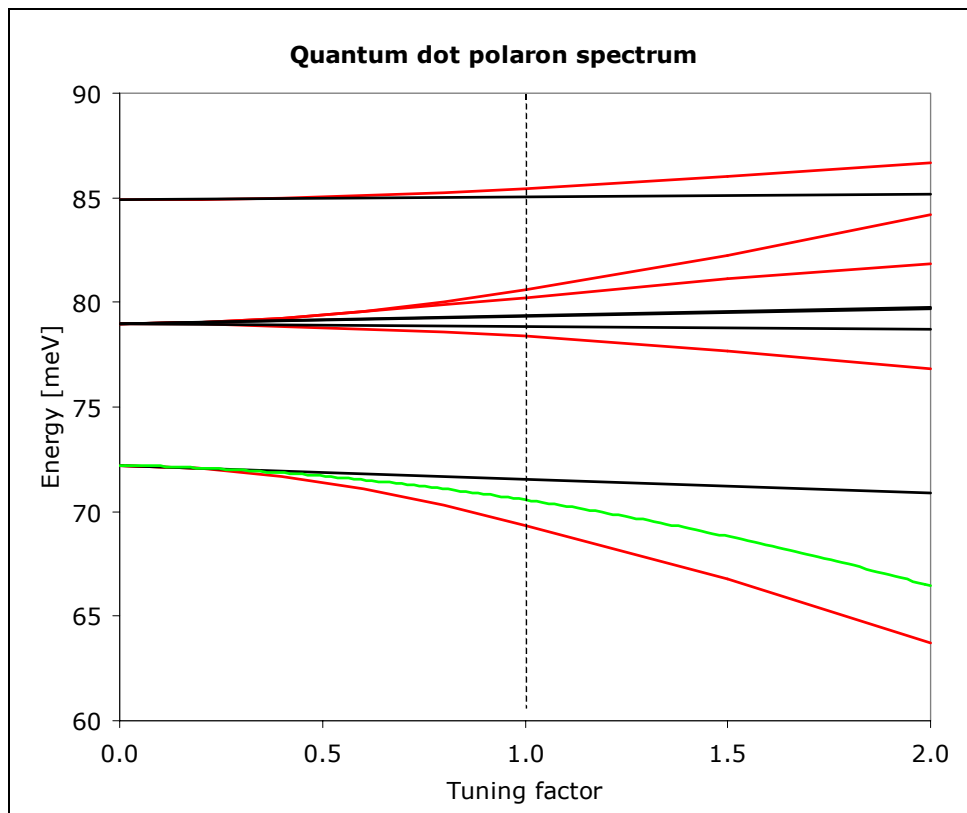
Fig. 18: Polaron energies calculated in the non-perturbative scheme used in this work (red) and in a first order perturbative approach (black). The artificial tuning factor multiplies the Fröhlich constant allowing to control the interaction strength.

Discussion of the quantum dot with two electron levels

The polaron states in diverse quantum dots with two electron levels have been investigated recently (see for example Verzelen et al. 2000, [33]). In opposition to many of those cases, our quantum dot presents the particular feature, that its first excited electron level lies below the ground state level combined with one LO-phonon. To compare the differences of the respective polaron spectra, we shall consider the example of a quantum dot with cylindrical symmetry [33]. Its second electron level is twice degenerate (like in our case) and the free evolution sates are referred to as $|S0\rangle$, $|S1\rangle$ and $|P\pm 0\rangle$. For the pyramidal quantum dot the respective notations were $|A0\rangle$, $|A1q\rangle$ and $|B\pm 0\rangle$. Fig. 19 shows the electron and polaron spectra of the two quantum dots. We note that the free evolution states $|S1\rangle$ and $|P\pm 0\rangle$ are inverted with respect to $|A1q\rangle$ and $|B\pm 0\rangle$.
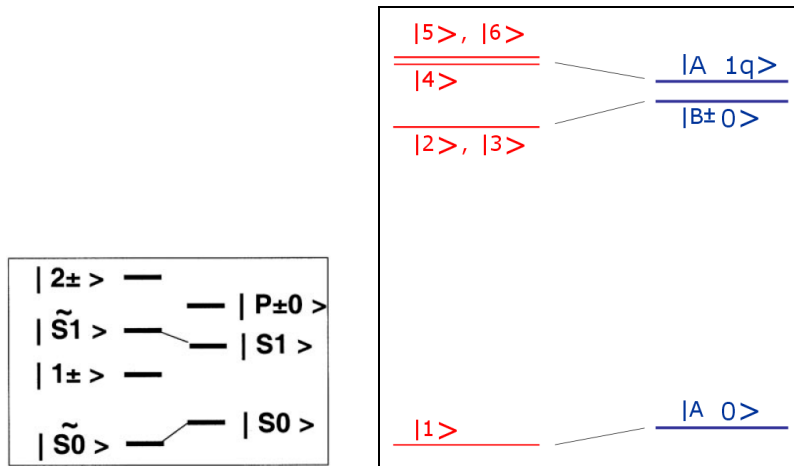
Fig. 19: **LEFT: Energy spectra of the polarons (left) and electrons (right) corresponding to the cylindrical quantum dot studied by Bastard et al. [33].**

RIGHT: Energy spectra of our quantum dot (dot size = 5nm)

The two polaron spectra qualitatively differ by the fact that the polaron $|\tilde{S1}\rangle$ has an energy in between the two free evolution states $|S1\rangle$ and $|P\pm 0\rangle$, whereas the corresponding state $|4\rangle$ lies above the two levels $|A1q\rangle$ and $|B\pm 0\rangle$. We argue that the polaron state $|\tilde{S1}\rangle$ (or $|4\rangle$) always yields a higher energy than $|S1\rangle$ (or $|A1q\rangle$). This comes from the strong Fröhlich interaction between $|S1\rangle$ and $|S0\rangle$ (or $|A1q\rangle$ and $|A0\rangle$), which is indeed much stronger than the interaction between $|S1\rangle$ and $|P\pm 0\rangle$ (or $|A1q\rangle$ and $|B\pm 0\rangle$). In fact, the Fröhlich integral between two s-functions overweighs the one between an s- and a p-function. In the analytic scheme developed in this work, $|S1\rangle$ and $|S0\rangle$ are part of the same "strong coupling subspace", which only interacts weakly with the subspace of $|P\pm 0\rangle$.

Natural basis and subsequent concepts

In this work, we introduced a non-orthonormal basis of quantum dot polarons, which we decided to call the "natural basis". It contains the all the free electron states plus the one-phonon states of the type $\sum_{i=1}^{N} \left| \tau\ 1\vec{q}_i \right\rangle \left\langle \tau\ 1\vec{q}_i \left| H \right| \nu\ 0 \right\rangle$ (section 3.3.1). This form of one-phonon basis states is coherent with the recent conclusion that pure electron states can only couple to precisely those states (Ferreira, Verzelen and Bastard [43]).

Through analytical investigations of the Fröhlich interaction between this non-orthonormal natural basis states, we have proved the following key properties of quantum dot polarons:

- Independent of analytical symmetries, we could prove that the total reduced Hilbet space, defined as the space containing all the quantum dot polarons, contains subspaces with weak mutual interaction, which we called "strong coupling subspaces". Many quantum dot polarons are nearly contained in one of those subspaces. Further, we could identify the number of strong coupling subspaces with the number of electron states confined to the quantum dot and derive the number of polarons associated with each strong coupling subspace.

- If the quantum dot presents certain degeneracies (see 3.3.4), the system exhibits quantum dot polarons with strictly non-vanishing energy-shift. Unlike the bulk polarons those "zero-shift quantum dot polarons" superpose different degenerate electron states and represent localized crystal excitations in the quantum dot.

To the best of our knowledge neither the concept of "zero-shift quantum dot polarons" nor the concept of "strong coupling subspaces" seem to have been pointed out before. We are convinced that both concepts reveal new physical insight in the dynamics of quantum dots, such as shown in chapter 5.

7   Conclusion

Our objective was to compute and to study the polaron states in a pyramidal GaAs/AlGaAs quantum dot. Mathematical analysis, computational developments and physical interpretations have allowed us to answer many questions and to discover at least as new many questions (!), which will inspire our future research.

For example, we have raised the problem of the three-fold rotational symmetry of the quantum dot, which leads to observable consequences, namely degeneracies, in the polaron spectrum. A suitable tool to handle this symmetry relies on group theory and thus we propose to investigate the substructure of the quantum dot polaron space using group theory.

Further, the inclusion of the quantum wire electronic states is a promising perspective in the view of additional polaron energy shift. Those quantum wire electron states constitute a continuum decomposed in one-dimensional normal modes. This representation is similar to the normal mode representation of the crystal vibrations. We shall thus conjecture that a new basis could simplify the description of coupled quantum wire states, analogically to the "natural basis" for polarons.

Finally, we are ready to face the problem of capture and relaxation. The capture of charge carriers from the quantum wire might be influenced by strong coupling and be treated with a non-perturbative approach such as outlined in the previous paragraph. The relaxation inside the quantum dot is partially driven by phonon-phonon interactions as emphasized by Verzelen et al. [33]. We shall study this relaxation path in the future.

Epilogue

This research project has been a real pleasure to me and I gratefully acknowledge the society, the school and the people who allow me to focus on abstract interests. Particularly, I'd like to thank Dr. Fabienne Michelini and Dr. Marc-André Dupertuis for their active help along the project. Further, my gratitude is directed to Dr. François Reuse who has sharpened my physical understanding by his excellent essays [e.g. 34] and several clarifying discussions.

8   Appendix

8.1   Extended discussion of electron-crystal interaction

This section is an extension of chapter 2 giving detailed mathematical developments.

8.1.1   Extension of section 2.1.2

Nuclei-electron decoupling: "Born-Oppenheimer approximation"

Inside the reduced space $\mathcal{H}_{electrons}$, the Hamiltonian $H_{electrons}$ describes an unstable dynamic of negative particles that all repel each other. In the same way H_{nuclei} describes an unstable system of positive particles in the space $\mathcal{H}_{nuclei}$. In this section, we shall include the mean effect of the nuclei in the electron Hamiltonian $H_{electrons}$ and the mean effect of the of the electrons in the nuclei Hamiltonian $\boxed{H_{nuclei}}$. Finally, the electron and the nuclei dynamics yield stable solutions, which are close to the solution of the full Hamiltonian. This approximate decoupling of the electronic and nuclear motion is globally referred to as the "Born-Oppenheimer approximation".

In a first step, we give an approximate Hamiltonian describing the nuclei dynamics in the subspace $\mathcal{H}_{nuclei}$, which accounts for the mean influence of the electrons. The commonly used approximation is an "adiabatic approximation". It considers the electrons as slaves without inertia. They follow instantaneously the relatively slow nuclear motion. Mathematically, the electrons are considered to be always in the ground state around the instantaneous nuclear configuration. To do so, we regard the nuclei as classical particles located in the positions $\vec{R}.^{class}$ at a given moment in time. The electrons contribute to the nuclear dynamics by the mean of a potential $E_0\left(\vec{R}.^{class}\right)$, which is the electronic ground state energy of the instantaneous nuclear configuration. Explicitly, it is the ground state energy of the time independent Schrödinger equation

$$\left\{\sum_{\nu=1}^{n} \frac{\vec{p}_{\nu}^{2}}{2m_e} + \frac{e^2}{8\pi\varepsilon_0} \sum_{\nu\neq\nu'} \frac{1}{\left|\vec{r}_{\nu} - \vec{r}_{\nu'}\right|} - \frac{e^2}{4\pi\varepsilon_0} \sum_{\mu=1}^{N} \sum_{\nu=1}^{n} \frac{Z_{\mu}}{\left|\vec{r}_{\nu} - \vec{R}_{\mu}^{class} \cdot 1_{electrons}\right|}\right\} |\psi\rangle = E\left(\vec{R}.^{class}\right)|\psi\rangle$$

Including this contribution, the nuclei potential becomes

$$\frac{e^2}{8\pi\varepsilon_0} \sum_{\mu\neq\mu'} \frac{Z_{\mu}}{\left|\vec{R}_{\mu}^{class} - \vec{R}_{\mu'}^{class}\right|} + E_0\left(\vec{R}.^{class}\right)$$

This potential has stable solutions. It namely allows obtaining the classical equilibrium configuration $\vec{R}.^{(0)}$ of the nuclei. This configuration minimizes the potential energy, i.e.

$$\frac{\partial}{\partial \vec{R}_\mu^{(0)}} \left[\frac{e^2}{8\pi\varepsilon_0} \sum_{\mu\neq\mu'} \frac{Z_\mu}{\left|\vec{R}_\mu^{(0)} - \vec{R}_{\mu'}^{(0)}\right|} + E_0\left(\vec{R}.^{(0)}\right) \right] = 0 \qquad \forall \mu = 1...N$$

If this equation yields several solutions, the absolute minimum is chosen. To keep the electronic contribution to the nuclei Hamiltonian small, it is convenient to subtract $E_0\left(\vec{R}.^{(0)}\right)$ from the potential above, such that the final potential yields

$$\frac{e^2}{8\pi\varepsilon_0} \sum_{\mu\neq\mu'} \frac{Z_\mu}{\left|\vec{R}_\mu^{class} - \vec{R}_{\mu'}^{class}\right|} + E_0\left(\vec{R}.^{class}\right) - E_0\left(\vec{R}.^{(0)}\right)$$

It is a function of classical position variables. By virtue of the spectral theorem or a Taylor development it is extended to an operator function of quantum mechanical operators. In such a way we obtain an approximate Hamiltonian describing the nuclear dynamics in the adiabatic approximation,

$$H_{nuclei}^{adia} = \sum_{\mu=1}^{N} \frac{\vec{P}_\mu^2}{2M_\mu} + \frac{e^2}{8\pi\varepsilon_0} \sum_{\mu\neq\mu'} \frac{Z_\mu}{\left|\vec{R}_\mu - \vec{R}_{\mu'}\right|} + \left[E_0\left(\vec{R}.\right) - E_0\left(\vec{R}.^{(0)}\right) \right]$$

In a second step, we look for an approximate electronic Hamiltonian in the subspace $\mathcal{H}_{electrons}$, which accounts for the mean influence of the nuclei. This is generally done by assuming that the nuclei are classical charges retained in the equilibrium positions $\vec{R}.^{(0)}$. They act on the electrons by Coulomb interaction, such that

$$H_{electrons}^{equil} = \sum_{v=1}^{n} \frac{\vec{p}_v^2}{2m_e} + \frac{e^2}{8\pi\varepsilon_0} \sum_{v\neq v'} \frac{1}{\left|\vec{r}_v - \vec{r}_{v'}\right|} - \frac{e^2}{4\pi\varepsilon_0} \sum_{\mu=1}^{N} \sum_{v=1}^{n} \frac{Z_\mu}{\left|\vec{r}_v - \vec{R}_\mu^{(0)} \cdot 1_{electrons}\right|}$$

We have thus found an approximate Hamiltonian that separates the electronic and nuclear dynamics from one another:

$$H^{Born-Oppenheimer} = H_{electrons}^{equil} \otimes 1_{nuclei} + 1_{electrons} \otimes H_{nuclei}^{adia}$$

This approximation is referred to as "Born-Oppenheimer approximation". It differs from the original Hamiltonian $H_{molecule}$ by a residual correction term

$$V_{e^- - nuclei}^{res} = -\frac{e^2}{4\pi\varepsilon_0} \sum_{\mu=1}^{N} \sum_{v=1}^{n} \left[\frac{Z_\mu}{\left|\vec{r}_v \otimes 1_{nuclei} - 1_{electrons} \otimes \vec{R}_\mu\right|} - \frac{Z_\mu}{\left|\vec{r}_v - \vec{R}_\mu^{(0)} \cdot 1_{electrons}\right|} \otimes 1_{nuclei} \right]$$

$$- 1_{electrons} \otimes \left[E_0\left(\vec{R}.\right) - E_0\left(\vec{R}.^{(0)}\right) \cdot 1_{nuclei} \right]$$

Finally,

$$H_{molecule} = H_{electrons}^{equil} \otimes 1_{nuclei} + 1_{electrons} \otimes H_{nuclei}^{adia} + V_{e^--nuclei}^{res}$$

where $H_{electrons}^{equil} = \sum_{v=1}^{n} \frac{\vec{p}_v^2}{2m_e} + \frac{e^2}{8\pi\varepsilon_0} \sum_{v\neq v'} \frac{1}{|\vec{r}_v - \vec{r}_{v'}|} - \frac{e^2}{4\pi\varepsilon_0} \sum_{\mu=1}^{N} \sum_{v=1}^{n} \frac{Z_\mu}{|\vec{r}_v - \vec{R}_\mu^{(0)} \cdot 1_{electrons}|}$

$$H_{nuclei}^{adia} = \sum_{\mu=1}^{N} \frac{\vec{P}_\mu^2}{2M_\mu} + \frac{e^2}{8\pi\varepsilon_0} \sum_{\mu\neq\mu'} \frac{Z_\mu}{|\vec{R}_\mu - \vec{R}_{\mu'}|} + \left[E_0\left(\vec{R}.\right) - E_0\left(\vec{R}.^{(0)}\right) \right]$$

$$V_{e^--nuclei}^{res} = -\frac{e^2}{4\pi\varepsilon_0} \sum_{\mu=1}^{N} \sum_{v=1}^{n} \left[\frac{Z_\mu}{|\vec{r}_v \otimes 1_{nuclei} - 1_{electrons} \otimes \vec{R}_\mu|} - \frac{Z_\mu}{|\vec{r}_v - \vec{R}_\mu^{(0)} \cdot 1_{electrons}|} \otimes 1_{nuclei} \right]$$

$$- 1_{electrons} \otimes \left[E_0\left(\vec{R}.\right) - E_0\left(\vec{R}.^{(0)}\right) \cdot 1_{nuclei} \right]$$

Nuclei-nuclei decoupling: "Harmonic normal modes"

The next step is to decouple the nuclear coordinates from one another inside the re-
duced space $\mathcal{H}_{nuclei}$. The standard method consists in neglecting the anharmonic part
of the potential energy around the equilibrium configuration and to perform a canoni-
cal transformation giving rise to independent normal modes. The energy quanta of
each such mode are referred to as "phonons".

Harmonic approximation

We consider the nuclei as classical point charges located in $\{\vec{R}_\mu\}$. The potential

$$V_{nuclei}^{adia} = \frac{e^2}{8\pi\varepsilon_0} \sum_{\mu\neq\mu'} \frac{Z_\mu}{|\vec{R}_\mu - \vec{R}_{\mu'}|} + \left[E_0\left(\vec{R}.\right) - E_0\left(\vec{R}.^{(0)}\right) \right]$$

is developed in series around the equilibrium configuration $\vec{R}.^{(0)}$. To simplify the no-
tation, we introduce the displacement vectors $\vec{Q}_\mu \equiv \vec{R}_\mu - \vec{R}_\mu^{(0)}$,

$$V_{nuclei}^{adia} = \underbrace{\frac{e^2}{8\pi\varepsilon_0} \sum_{\mu\neq\mu'} \frac{Z_\mu}{|\vec{R}_\mu^{(0)} - \vec{R}_{\mu'}^{(0)}|}}_{V_{nuclei}^{adia,(0)}} + \underbrace{\frac{1}{2!} \sum_{(\mu,i),(\mu',j)} \frac{\partial V_{nuclei}^{adia}\left(\vec{Q}.\right)}{\partial Q_\mu^i \partial Q_{\mu'}^j}\bigg|_{\vec{Q}.=0} Q_\mu^i Q_{\mu'}^j}_{V_{nuclei}^{adia,harm}} + \underbrace{O(3)}_{V_{nuclei}^{adia,res}}$$

There is no linear term, since the equilibrium configuration corresponds to a mini-
mum of the potential energy. The residual term $V_{nuclei}^{adia,res}$ contains the anharmonic con-
tribution to the interaction potential. Neglecting this residual term yields the "har-

monic approximation". Further we neglect the constant contribution $V_{harm}^{adia,(0)}$, which simply shifts the energy scale.

Finally,

$$H_{nuclei}^{adia,harm} = \sum_{\mu=1}^{N} \frac{\vec{P}_\mu^2}{2M_\mu} + V_{nuclei}^{adia,harm}\left(\vec{Q}.\right)$$

Classical normal mode solution

It always exists is a particular set of canonically conjugate coordinates, in which the Hamiltonian $H_{nuclei}^{adia,harm}$ becomes decoupled. To demonstrate it, we shall adapt the following tensor notations:

$$P \equiv \begin{pmatrix} P_1^x \\ P_1^y \\ P_1^z \\ \vdots \\ P_N^z \end{pmatrix} \in \mathbb{R}^{3N}, \quad Q \equiv \begin{pmatrix} Q_1^x \\ Q_1^y \\ Q_1^z \\ \vdots \\ Q_N^z \end{pmatrix} \in \mathbb{R}^{3N} \qquad \text{"momentum and displacement vec-}$$

tor"

$$\mathcal{M}_{(\mu,i),(\mu',j)} \equiv M_\mu \, \delta_{\mu\mu'} \, \delta_{ij} \in M_{3N \times 3N} \qquad i,j = 1,2,3 \qquad \text{"mass matrix", diagonal, positive}$$

$$\mathcal{D}_{(\mu,i),(\mu',j)} \equiv \left. \frac{\partial V_{nuclei}^{adia}\left(\vec{Q}.\right)}{\partial Q_\mu^i \partial Q_{\mu'}^j} \right|_{\vec{Q}.=0} \in M_{3N \times 3N} \qquad \text{"dynamical matrix", symmetrical,}$$

positive

Thereby, the Hamiltonian takes the simple form

$$H_{nuclei}^{adia,harm} = \frac{1}{2}\left(P^T \mathcal{M}^{-1} P + Q^T \mathcal{D} Q\right)$$

In appendix 8.4.1 it is proved that the non-symmetrical matrix $\left(\mathcal{M}^{-1}\mathcal{D}\right)$ has positive non-degenerate eigenvalues ω_α^2,

$$\left(\mathcal{M}^{-1}\mathcal{D}\right) X_\alpha = \omega_\alpha^2 \, X_\alpha$$

The with eigenvectors X_α can be orthonormalized in the sense

$$X_\alpha^T \mathcal{M} X_\beta = \delta_{\alpha\beta}$$

They constitute a basis of $\mathbb{R}^{3N}$, in which we shall decompose the nuclei coordinates:

$$Q = \sum_\alpha Q_\alpha X_\alpha \qquad \text{and} \qquad P = \sum_\alpha P_\alpha \mathcal{M} X_\alpha$$

Those relations define a set of new coordinates

$$Q_\alpha = X_\alpha^T \mathcal{M} Q \qquad \text{and} \qquad P_\alpha = X_\alpha^T P$$

which can be verified to be canonically conjugate. In those coordinates the Hamiltonian looks like

$$H_{nuclei}^{adia,harm} = \sum_\alpha \left(P_\alpha^2 + \omega_\alpha^2 Q_\alpha^2 \right)$$

Thereby we have proved the existence of a canonical transformation, which decouples the nuclei coordinates, and derived its explicit form. What do the new coordinates physically represent? Each couple (Q_α, P_α) describes an independent harmonic oscillator with angular frequency ω_α. Since the ionic displacements depend linearly on Q_α, each couple (Q_α, P_α) describes a collective harmonic oscillation of all the nuclei at one same frequency. Therefore the new coordinates are called "normal mode coordinates". There are $3N$ modes: 3 global translations, 3 global rotations and $3N-6$ vibrations. The set of all those modes is called $\mathcal{A}$.

Quantum mechanical normal mode solution, phonons

The $3N$ modes are independent properties of motion of the nuclei system. Therefore, each mode α can be assigned a restricted orthogonal subspace $\mathcal{H}_{mode\,\alpha}$ of the full space $\mathcal{H}_{nuclei}$. The full space is isomorphic to the product space $\mathcal{F}_{modes}$ defined by

$$\mathcal{H}_{nuclei} \quad \sim \quad \mathcal{F}_{modes} \equiv \bigotimes_{\alpha \in \mathcal{A}} \mathcal{H}_{mode\,\alpha}$$

This space is called "Fock space of normal modes".

Q_α and P_α are considered as quantum mechanical operators acting in this space. The commutation relations of the nuclei coordinates transform to

$$\left[Q_\alpha, P_\beta \right] = i\hbar \delta_{\alpha\beta} \cdot \mathbf{1}_{modes} \qquad \left[Q_\alpha, Q_\beta \right] = 0 \qquad \left[P_\alpha, P_\beta \right] = 0$$

We remind, that operators belonging to different normal modes naturally commute because they act on different parts of the product space. This is not related to exchange symmetries of identical particles.

The dynamics of the nuclei system is given by the Hamiltonian operator

$$H_{modes}^{adia,harm} = \sum_{\alpha \in \mathcal{A}} \left(P_\alpha^2 + \omega_\alpha^2 Q_\alpha^2 \right) = \sum_{\alpha \in \mathcal{A}} H_{mode\,\alpha}$$

The operator $H_{mode\,\alpha}$ describes a quantum mechanical harmonic oscillator in the space $\mathcal{H}_{mode\,\alpha}$ and acts trivially on all other modes. The standard way to solve the dynamics described by $H_{mode\,\alpha}$ is to introduce the "annihilation operator" and "creation operator" of one energy quanta,

$$d_\alpha = \frac{\omega_\alpha Q_\alpha + i\, P_\alpha}{\sqrt{2\hbar\omega_\alpha}} \qquad \text{and} \qquad d_\alpha^\dagger = \frac{\omega_\alpha Q_\alpha - i\, P_\alpha}{\sqrt{2\hbar\omega_\alpha}}$$

They can be shown to satisfy the following commutation relations

$$\left[d_\alpha, d_\beta^\dagger\right] = \delta_{\alpha\beta} \cdot 1_{modes} \qquad \left[d_\alpha, d_\beta\right] = 0 \qquad \left[d_\alpha^\dagger, d_\beta^\dagger\right] = 0$$

and the Hamiltonian becomes

$$H_{mode\,\alpha} = \hbar\omega_\alpha d_\alpha^\dagger d_\alpha$$

The operator $N_\alpha = d_\alpha^\dagger d_\alpha$ is hermitian and its spectrum can be shown to contain all non-negative integers. Therefore, the energy eigenstates of each mode α correspond to equally-spaced discrete energies, separated by $\hbar\omega_\alpha$. Further, the spectrum is non-degenerate. Thus a complete set of commuting observables is given by $\{N_\alpha\}$. The corresponding orthogonal basis is noted

$$\left\{\left|n_\alpha, n_\beta, n_\gamma, ...\right\rangle : n_\alpha, n_\beta, ... \in \{0, 1, 2, 3, ...\}\right\}$$

Physically, the vector $\left|n_\alpha, n_\beta, n_\gamma, ...\right\rangle$ represents a state, where the mode α is $n_\alpha - times$ excited, i.e. it has an energy $n_\alpha\hbar\omega_\alpha$, and so on. The annihilation and creation operators act on the basis vectors as follows

$$d_\alpha\left|.., n_\alpha, ..\right\rangle = \sqrt{n_\alpha}\left|.., n_{\alpha-1}, ..\right\rangle \qquad \text{and} \qquad d_\alpha^\dagger\left|.., n_\alpha, ..\right\rangle = \sqrt{n_\alpha + 1}\left|.., n_{\alpha+1}, ..\right\rangle$$

which justifies their names. In section "Bosonic second quantization" (8.1.2) we will see that this mathematical structure exactly corresponds to the one used to describe a system of identical bosons. This leads us to consider the nuclei vibrations as composed by bosonic particles, called "phonons", which can occupy any of the modes $\alpha \in \mathcal{A}$.

The full dynamic beyond the harmonic approximation is described by the Hamiltonian

$$H_{modes}^{adia} = \sum_{\alpha \in \mathcal{A}} \left(P_\alpha^2 + \omega_\alpha^2 Q_\alpha^2\right) + V_{modes}^{adia,res}$$

where $V_{modes}^{adia,res} = V_{nuclei}^{adia,res}(Q.)$ contains the anharmonic part of the potential. This term is not diagonal and therefore yields interactions between the normal modes or "phonon-phonon-interactions".

8.1.2   Extension of section 2.2

First, this term is developed in series. This allows distinguishing important contributions from less important ones. Second, the different terms of the series are expressed in the notation of second quantization. This allows considering the interaction

as a sum of elementary interactions between single quanta of vibration and electrons.

Development in series

Starting with the residual interaction term between electrons and modes

$$V^{res}_{e^--modes} = -\frac{e^2}{4\pi\varepsilon_0} \sum_{\mu=1}^{N} \sum_{v=1}^{n} \left[\frac{Z_\mu}{\left|\vec{r}_v \otimes 1_{modes} - 1_{electrons} \otimes \vec{R}_\mu(Q.)\right|} - \frac{Z_\mu}{\left|\vec{r}_v - \vec{R}_\mu^{(0)} \cdot 1_{electrons}\right|} \otimes 1_{modes} \right]$$

$$- 1_{electrons} \otimes \left[E_0\left(\vec{R}.(Q.)\right) - E_0\left(\vec{R}.^{(0)}\right) \cdot 1_{modes} \right]$$

we admit the following Taylor development in the tensor product space

$$V^{res}_{e^--modes} = \underbrace{\sum_{\alpha \in \mathcal{A}} F_\alpha^{(1)}\left(\vec{r}.\right) \otimes Q_\alpha}_{V^{res(1)}_{e^--modes}} + \underbrace{\sum_{\alpha,\beta \in \mathcal{A}} F_{\alpha,\beta}^{(2)}\left(\vec{r}.\right) \otimes Q_\alpha Q_\beta}_{V^{res(2)}_{e^--modes}} + \dots$$

where the coefficients are given by

$$F_\alpha^{(1)}\left(\vec{r}.\right) = \left.\frac{\partial W^{res}_{e^--modes}}{\partial Q_\alpha}\right|_{Q.=0} \quad , \qquad F_{\alpha\beta}^{(2)}\left(\vec{r}.\right) = \frac{1}{2!}\left.\frac{\partial W^{res}_{e^--modes}}{\partial Q_\alpha \partial Q_\beta}\right|_{Q.=0} \quad , \qquad \text{etc.}$$

$W^{res}_{e^--modes}$ is the restriction of the operator $V^{res}_{e^--modes}$ to the subspace $\mathcal{H}_{electrons}$ obtained when replacing the operators $\vec{R}_\mu, Q_\alpha$ by classical variables. When writing $W^{res}_{e^--modes}$, we drop all constant terms, since our interest concentrates on the derivates of $W^{res}_{e^--modes}$,

$$W^{res}_{e^--modes} = -\frac{e^2}{4\pi\varepsilon_0} \sum_{\mu=1}^{N} \sum_{v=1}^{n} \left[\frac{Z_\mu}{\left|\vec{r}_v - \vec{R}_\mu \cdot 1_{electrons}\right|} \right] - E_0\left(\vec{R}.\right) \cdot 1_{electrons}$$

The definition of two new operators

$$\mathcal{D}_\alpha \equiv \frac{\partial}{\partial Q_\alpha} = \sum_{\mu=1}^{N} \vec{X}_{\alpha\mu} \cdot \frac{\partial}{\partial \vec{R}_\mu^{(0)}}$$

$$W \equiv W^{res}_{e^--modes}\left(\vec{R}_\mu^{(0)}\right) = -\frac{e^2}{4\pi\varepsilon_0} \sum_{\mu=1}^{N} \sum_{v=1}^{n} \left[\frac{Z_\mu}{\left|\vec{r}_v - \vec{R}_\mu^{(0)} \cdot 1_{electrons}\right|} \right] - E_0\left(\vec{R}.^{(0)}\right) \cdot 1_{electrons}$$

allows simplifying the Taylor coefficients of $F\left(\vec{r}.\right)$,

$$F_\alpha^{(1)}\left(\vec{r}.\right) = \mathcal{D}_\alpha W \quad , \qquad F_{\alpha\beta}^{(2)}\left(\vec{r}.\right) = \mathcal{D}_\alpha \mathcal{D}_\beta W \quad , \qquad \text{etc.}$$

Over the following sections these coefficients are transcribed in second quantization, which leads to a compact form of the interaction term $V^{res}_{e^--modes}$.

Generalities about second quantization

Bosonic second quantization

We call $\boxed{\mathcal{H}}$ the Hilbert space appropriate to represent one boson. We consider N identical bosons, i.e. particles that behave symmetric in the exchange of one pair. To account for this symmetry we construct a Hilbert space $\mathcal{F}^N$, which only contains completely symmetric states, by writing

$$\mathcal{F}^N = \mathcal{S}\left(\mathcal{H}^{\otimes N}\right)$$

where $\mathcal{S}$ is the orthogonal projector on the symmetric subspace.

If $N = 0$, this space is identical to the complex body, in which we can fix one arbitrary normalized basis vector $|0\rangle$. This vector represents the vacuum state. To construct a basis of $\mathcal{F}^N$, $N > 0$, we start with an orthonormal basis of $\mathcal{H}$, let's say $\{|\alpha\rangle : \alpha \in \mathcal{A}\}$. A vector of $\mathcal{F}^N$ is given by

$$|\alpha_1, ..., \alpha_N\rangle \equiv \frac{1}{\sqrt{N!}} \sum_{s \in \mathcal{P}_N} |\alpha_{s(1)}\rangle \otimes ... \otimes |\alpha_{s(N)}\rangle$$

where $\mathcal{P}_N$ is the group of permutations of the set $\{1, ..., N\}$. The vectors can be shown to be orthonormal,

$$\langle \alpha_1, ..., \alpha_N | \beta_1, ..., \beta_N \rangle = \begin{cases} 1 & \text{if } \{\alpha_1, ..., \alpha_N\} = \{\beta_1, ..., \beta_N\} \\ 0 & \text{otherwise} \end{cases}$$

Further they satisfy the symmetry relation

$$|\alpha_1, ..., \alpha_N\rangle = |\alpha_{s(1)}, ..., \alpha_{s(N)}\rangle \qquad \forall s \in \mathcal{P}_N$$

This relation makes our notation very redundant. We can define a much shorter and unique notation by simply writing the number of times a certain state is occupied. If n_{α_1} bosons are in state α_1, n_{α_2} bosons in state α_2 and so on, we simply note $|n_{\alpha_1}, n_{\alpha_2}, ...\rangle$.

In this notation the exchange symmetry no longer appears. An orthonormal basis of $\mathcal{F}^N$ is given by

$$\left\{ |n_{\alpha_1}, n_{\alpha_2}, ...\rangle : n_{\alpha_i} \in \{1, 2, ...\}, \sum_i n_{\alpha_i} = N \right\}$$

The orthonormalization relations are

$$\langle n_{\alpha_1}, n_{\alpha_2}, \ldots | n'_{\alpha_1}, n'_{\alpha 2}, \ldots \rangle = \begin{cases} 1 & \text{if } n_{\alpha_i} = n'_{\alpha_i} \quad \forall i \\ 0 & \text{otherwise} \end{cases}$$

By definition we call "Fock space of bosons" the direct sum of the spaces $\mathcal{F}^N$ over all numbers of bosons,

$$\mathcal{F} \equiv \bigoplus_{N=0}^{\infty} \mathcal{F}^N = \mathcal{S}\left(\mathcal{H}^{\otimes N}\right)$$

The scalar product is defined by the scalar product over $\mathcal{F}^N$ and the condition $\mathcal{F}^N \perp \mathcal{F}^M$ if $N \neq M$. An orthonormal basis of $\mathcal{F}$ is given by

$$\left\{ \left| n_{\alpha_1}, n_{\alpha_2}, \ldots \right\rangle : n_{\alpha_i} \in \{0, 1, 2, \ldots\} \right\}$$

We define the "annihilation operator",

$$d_\alpha : \quad \mathcal{F}^N \quad \rightarrow \quad \mathcal{F}^{N-1}$$
$$\left| .., n_\alpha, .. \right\rangle \quad \mapsto \quad \sqrt{n_\alpha} \left| .., n_{\alpha-1}, .. \right\rangle$$

which destroys one boson in the state α. It can be shown that its adjoint acts like a "creation operator" of one boson in the state α,

$$d_\alpha^\dagger : \quad \mathcal{F}^N \quad \rightarrow \quad \mathcal{F}^{N+1}$$
$$\left| .., n_\alpha, .. \right\rangle \quad \mapsto \quad \sqrt{n_\alpha + 1} \left| .., n_{\alpha+1}, .. \right\rangle$$

From these definitions, we deduce the commutation relations

$$\left[d_\alpha, d_\beta^\dagger \right] = \delta_{\alpha\beta} \cdot 1 \qquad\qquad \left[d_\alpha, d_\beta \right] = 0 \qquad\qquad \left[d_\alpha^\dagger, d_\beta^\dagger \right] = 0$$

Those relations translate the completely symmetrical structure of the Fock space.

At this point, our reasoning gets a physical meaning: In section 2.1.2 (and its extension 8.1.1), the nuclei dynamics of the molecule has been decomposed in independent normal modes, which can be occupied an arbitrary number of times. The modes are called α and the energy eigenstates $\left| n_{\alpha_1}, n_{\alpha_2}, \ldots \right\rangle$. The introduced annihilation and creation operators act exactly like the ones introduced to describe a system of identical bosons. This leads us to consider the nuclei motion as composed by identical bosonic particles called "phonons", which can occupy any of the modes $\alpha \in \mathcal{A}$. The exchange symmetry of the phonons appears when we step back to the redundant notation

$$\left| \alpha_1, \ldots, \alpha_N \right\rangle \equiv \frac{1}{\sqrt{N!}} \sum_{s \in \mathcal{P}_N} \left| \alpha_{s(1)} \right\rangle \otimes \ldots \otimes \left| \alpha_{s(N)} \right\rangle$$

Fermionic second quantization

The electrons are subject to a fermionic second quantization. Up to now the set of n electrons has been treated in the Hilbert space $\mathcal{H}_{electrons}$. To keep a trace of the number of electrons let's introduce the notation

$$\mathcal{F}_{electrons}^n \equiv \mathcal{H}_{electrons} = \mathcal{A}\left\{\left(\mathcal{H}_{electron}\right)^{\otimes n}\right\}$$

Now we introduce a much larger space $\mathcal{F}_{electrons}$ containing all possible numbers of electrons. This space is called the "Fock space of electrons",

$$\mathcal{F}_{electrons} \equiv \bigoplus_{n=0}^{\infty} \mathcal{F}_{electrons}^n = \bigoplus_{n=0}^{\infty} \mathcal{A}\left\{\left(\mathcal{H}_{electron}\right)^{\otimes n}\right\}$$

To complete the definition, we define the scalar product on $\mathcal{F}_{electrons}$ as the one induced from the scalar product on $\mathcal{F}_{electrons}^n$, when choosing the subspaces to be orthogonal:

$$\mathcal{F}_{electrons}^n \perp \mathcal{F}_{electrons}^{n'} \qquad \text{if } n \neq n'$$

The antisymmetry of $\mathcal{F}_{electrons}^n$ implies that all orthogonal one-electron states can at most be occupied ones. Therefore a suitable basis of the Fock space $\mathcal{F}_{electrons}$ is given by

$$\left\{\left|n_{\tau_1}, n_{\tau_2}, \ldots\right\rangle : n_{\tau_i} \in \{0, 1\}\right\}$$

where τ_i are the energy eigenstates of $H_{electrons}^{equil, sc}$.

We define the "annihilation operator" of an electron in the state τ,

$$a_\tau : \quad \mathcal{F}_{electrons}^n \qquad\qquad \rightarrow \qquad \mathcal{F}_{electrons}^{n-1}$$
$$\left|n_{\tau_1}, n_{\tau_2}, \ldots, n_{\tau_k = \tau} = 1, \ldots\right\rangle \quad \mapsto \quad (-1)^k \left|n_{\tau_1}, n_{\tau_2}, \ldots, n_{\tau_k = \tau} = 0, \ldots\right\rangle$$

Its adjoint can be shown to act as a "creation operator" of an electron in the state τ,

$$a_\tau^\dagger : \quad \mathcal{F}_{electrons}^n \qquad\qquad \rightarrow \qquad \mathcal{F}_{electrons}^{n+1}$$
$$\left|n_{\tau_1}, n_{\tau_2}, \ldots, n_{\tau_k = \tau} = 0, \ldots\right\rangle \quad \mapsto \quad \left|n_{\tau_1}, n_{\tau_2}, \ldots, n_{\tau_k = \tau} = 1, \ldots\right\rangle$$

These definitions lead to the commutation relations

$$\left\{a_\tau, a_\tau^\dagger\right\} = 1_{electrons}$$

all the other commutators being trivial.

Using those new operators, the free electron Hamiltonian $H_{electrons}^{equil, sc}$ can be transcribed to second quantization,

$$\mathbb{H}_{electrons}^{equil, sc} = \sum_{\tau \in J} \varepsilon_\tau a_\tau^\dagger a_\tau$$

where ε_τ is the energy of the one-electron state τ and J is the set of all energy eigenstates τ. Further, we call J_0 the set of states τ, which is occupied in the electronic ground state configuration. Its complement $J_* \equiv J \setminus J_0$ contains all the excited one-electron states. Based on these notations, we define the following auxiliary operators,

$$c_\tau \equiv a_\tau^\dagger \quad \forall \tau \in J_0 \quad \text{"annihilation operator of a hole"}$$
$$b_\tau \equiv a_\tau \quad \forall \tau \in J_* \quad \text{"annihilation operator of an electron"}$$

Their adjoints are consequently given by

$$c_\tau^\dagger = a_\tau \quad \forall \tau \in J_0 \quad \text{"creation operator of a hole"}$$
$$b_\tau^\dagger = a_\tau^\dagger \quad \forall \tau \in J_* \quad \text{"creation operator of an electron"}$$

The free electron evolution expressed in these new operators yields

$$\mathbb{H}_{electrons}^{equil,sc} = \sum_{\tau \in J} \varepsilon_\tau a_\tau^\dagger a_\tau = \sum_{\tau \in J_0} \varepsilon_\tau b_\tau^\dagger b_\tau - \sum_{\tau \in J_*} \varepsilon_\tau c_\tau^\dagger c_\tau + \underbrace{\sum_{\tau_0 \in J_0} \varepsilon_{\tau_0} \cdot \mathbb{1}_{electrons}}_{constant}$$

Let's shift the zero of the energy by dropping the constant contribution,

$$\mathbb{H}_{electrons}^{equil,sc} = \sum_{\tau \in J_0} \varepsilon_\tau b_\tau^\dagger b_\tau - \sum_{\tau \in J_*} \varepsilon_\tau c_\tau^\dagger c_\tau$$

Second quantization of the interaction term

The new molecular Hilbert space is

$$\mathcal{H}_{molecule} = \mathcal{F}_{electrons} \otimes \mathcal{F}_{modes} = \left[\bigoplus_{n=0}^{\infty} \mathcal{A}\left(\mathcal{H}_{electron}^{\otimes n} \right) \right] \otimes \left[\bigoplus_{n=0}^{\infty} \mathcal{S}\left(\mathcal{H}_{mode}^{\otimes(3N-6)} \right) \right]$$

We shall transform the electron-phonon interaction term to second quantization,

$$\mathbb{V}_{e^- -modes}^{res} = \underbrace{\sum_{\alpha \in \mathcal{A}} \mathbb{F}_\alpha^{(1)}\left(\vec{r}. \right) \otimes \mathbb{Q}_\alpha}_{\mathbb{V}_{e^- -modes}^{res\,(1)}} + \underbrace{\sum_{\alpha,\beta \in \mathcal{A}} \mathbb{F}_{\alpha,\beta}^{(2)}\left(\vec{r}. \right) \otimes \mathbb{Q}_\alpha \mathbb{Q}_\beta}_{\mathbb{V}_{e^- -modes}^{res\,(2)}} + \dots$$

where the electronic terms are analogically given by

$$\mathbb{F}_\alpha^{(1)}\left(\vec{r}. \right) = \mathcal{D}_\alpha \mathbb{W} \quad , \qquad \mathbb{F}_{\alpha\beta}^{(2)}\left(\vec{r}. \right) = \mathcal{D}_\alpha \mathcal{D}_\beta \mathbb{W} \quad , \qquad \text{etc.}$$

and the phonon term by

$$\mathbb{Q}_\alpha = \sqrt{\frac{\hbar}{2\omega_\alpha}} \left(d_\alpha + d_\alpha^\dagger \right)$$

The remaining problem is to find $\mathbb{W}$ expressed in second quantization. In order to pass to this notation, we adopt the following notations

Electronic field operator:
$$\Psi\left(\vec{x}\right)=\sum_{\tau\in J}\varphi_{\tau}\left(\vec{x}\right)a_{\tau}$$

Electronic density operator:
$$\mathbb{D}\left(\vec{x}\right)=\Psi^{+}\left(\vec{x}\right)\Psi\left(\vec{x}\right)=\sum_{\tau,\tau'}\varphi_{\tau}^{*}\left(\vec{x}\right)\varphi_{\tau'}\left(\vec{x}\right)a_{\tau}^{\dagger}a_{\tau'}$$

A straightforward development yields (see appendix 8.4.2)

$$\mathbb{W}=-\int_{\mathbb{R}^3}d^3x\sum_{\mu=1}^{N}\frac{e^2Z_{\mu}}{4\pi\varepsilon_0}\frac{\mathbb{D}\left(\vec{x}\right)-\left\langle\psi_0\left|\mathbb{D}\left(\vec{x}\right)\right|\psi_0\right\rangle\cdot\mathbb{1}_{electrons}}{\left|\vec{x}-\vec{R}_{\mu}^{(0)}\cdot\mathbb{1}_{electrons}\right|}$$

We use the definition

$$w_{\tau\tau'}\equiv\sum_{\mu=1}^{N}\frac{-Z_{\mu}e^2}{4\pi\varepsilon_0}\int_{\mathbb{R}^3}d^3x\frac{\varphi_{\tau}\left(\vec{x}\right)^{*}\varphi_{\tau'}\left(\vec{x}\right)}{\left|\vec{x}-\vec{R}_{\mu}^{(0)}\right|}$$

in order to obtain a simplified expression,

$$
\begin{aligned}
\mathbb{W}\ &=\sum_{\tau,\tau'\in J}w_{\tau\tau'}\left(a_{\tau}^{\dagger}a_{\tau'}-\left\langle\psi_0\left|a_{\tau}^{\dagger}a_{\tau'}\right|\psi_0\right\rangle\cdot\mathbb{1}_{electrons}\right)\\
&=\sum_{\tau,\tau'\in J_0}w_{\tau\tau'}\left(a_{\tau}^{\dagger}a_{\tau'}-\delta_{\tau\tau'}\cdot\mathbb{1}_{electrons}\right)+\sum_{\substack{\tau\in J_*\\\tau'\in J_0}}w_{\tau\tau'}\,a_{\tau}^{\dagger}a_{\tau'}+\sum_{\substack{\tau'\in J_*\\\tau\in J_0}}w_{\tau\tau'}\,a_{\tau}^{\dagger}a_{\tau'}+\sum_{\tau,\tau'\in J_*}w_{\tau\tau'}\,a_{\tau}^{\dagger}a_{\tau'}\\
&=-\sum_{\tau,\tau'\in J_0}w_{\tau\tau'}\,a_{\tau}a_{\tau'}^{\dagger}+\sum_{\substack{\tau\in J_*\\\tau'\in J_0}}w_{\tau\tau'}\,a_{\tau}^{\dagger}a_{\tau'}+\sum_{\substack{\tau'\in J_*\\\tau\in J_0}}w_{\tau\tau'}\,a_{\tau}^{\dagger}a_{\tau'}+\sum_{\tau,\tau'\in J_*}w_{\tau\tau'}\,a_{\tau}^{\dagger}a_{\tau'}
\end{aligned}
$$

In terms of electron and hole operators,

$$\mathbb{W}=-\sum_{..}w_{\tau\tau'}\,c_{\tau}^{\dagger}c_{\tau'}+\sum_{..}w_{\tau\tau'}\,b_{\tau}^{\dagger}c_{\tau'}^{\dagger}+\sum_{..}w_{\tau\tau'}\,c_{\tau}b_{\tau'}+\sum_{..}w_{\tau\tau'}\,b_{\tau}^{\dagger}b_{\tau'}$$

Thus the terms of $\mathbb{V}_{e^--modes}^{res}$ can be written in the second quantization. For the first order term we obtain explicitly

$$
\begin{aligned}
\mathbb{V}_{e^--modes}^{res(1)}=\ &-\sum_{...}M_{\tau\tau'}^{\alpha}\,c_{\tau}^{\dagger}c_{\tau'}d_{\alpha}+\sum_{...}M_{\tau\tau'}^{\alpha}\,b_{\tau}^{\dagger}c_{\tau'}^{\dagger}d_{\alpha}+\sum_{...}M_{\tau\tau'}^{\alpha}\,c_{\tau}b_{\tau'}d_{\alpha}+\sum_{...}M_{\tau\tau'}^{\alpha}\,b_{\tau}^{\dagger}b_{\tau'}d_{\alpha}\\
&-\sum_{...}M_{\tau\tau'}^{\alpha}\,c_{\tau}^{\dagger}c_{\tau'}d_{\alpha}^{\dagger}+\sum_{...}M_{\tau\tau'}^{\alpha}\,b_{\tau}^{\dagger}c_{\tau'}^{\dagger}d_{\alpha}^{\dagger}+\sum_{...}M_{\tau\tau'}^{\alpha}\,c_{\tau}b_{\tau'}d_{\alpha}^{\dagger}+\sum_{...}M_{\tau\tau'}^{\alpha}\,b_{\tau}^{\dagger}b_{\tau'}d_{\alpha}^{\dagger}
\end{aligned}
$$

where $\quad M_{\tau\tau'}^{\alpha}=\sqrt{\dfrac{\hbar}{2\omega_{\alpha}}}\,\mathcal{D}_{\alpha}w_{\tau\tau'}=\sqrt{\dfrac{\hbar}{2\omega_{\alpha}}}\dfrac{-e^2}{4\pi\varepsilon_0}\sum_{\mu=1}^{N}Z_{\mu}\vec{X}_{\alpha\mu}\cdot\dfrac{\partial}{\partial\vec{R}_{\mu}^{(0)}}\left[\displaystyle\int_{\mathbb{R}^3}d^3x\dfrac{\varphi_{\tau}\left(\vec{x}\right)^{*}\varphi_{\tau'}\left(\vec{x}\right)}{\left|\vec{x}-\vec{R}_{\mu}^{(0)}\right|}\right]$

$\sum_{...}$ is the sum over all normal modes α and over the states τ and τ', on which the respective hole or electron operators are defined.

Note that equal electronic wave functions with different spins give two different states τ_1 and τ_2. If τ were only an index of the wave function, we had an additional sum over the two spin states in the expression of $M_{\tau\tau'}^{\alpha}$.

Discussion

(see section 2.2.2)

8.1.3 Extension of section 2.3

Introduction

First, the electron structure of the crystal is pointed out. Then, the phonon dispersion is derived and we shall see that one can choose better normal mode coordinates than the ones shown in chapter 3. Therefore, we enlarge the mathematical frame of the general method by introducing complex coordinates, without changing the underling physics. Based on the explicit electron and phonon states, the general electron-phonon interaction term is derived to first order. The chapter ends with a discussion of physical aspects and applications.

Passing from to the general molecule to the crystal we are subject to one conceptual change: The crystal electrons can be considered as either bound to specific ions or as valence electrons dispersed all over the structure. Every nucleus together with its bound electrons will be considered as one physical entity called ion. Those ions are treated as point charges. In the general theory of the molecule, the nuclei become ions and the electrons become the valence electrons. To keep a record of this conceptual change, we write $V^{res}_{e^- - nuclei} \rightarrow V^{res}_{e^- - ions}$.

Electrons in crystals

The mean electrical potential of a crystal has the periodicity of the underlying Bravais lattice. In this case the Bloch Theorem states, that the electronic energy eigenstates are of the form

$$\varphi_{\vec{k}}(\vec{r}) = u_{\vec{k}}(\vec{r}) e^{i\vec{k}\cdot\vec{r}}$$

where $u_{\vec{k}}(\vec{r})$ has the periodicity of the lattice. Further the functions $u_{\vec{k}}(\vec{r})$ can be chosen to satisfy the orthonormality relations

$$\int d^3 r \, \varphi^*_{\vec{k}'}(\vec{r}) \varphi_{\vec{k}}(\vec{r}) = \delta_{\vec{k}\vec{k}'}$$

Rigorously, every wave function $\varphi_{\vec{k}}(\vec{r})$ gives two simultaneously accessible states, with opposite spins σ . A one-electron state τ is thus entirely described by a couple $(\vec{k}, \sigma)$:

$$\tau \rightarrow (\vec{k}, \sigma)$$

For any derivation in the reduced Hilbert space without spins, it is important to remember that equal wave functions with opposite spins are orthogonal. We shall add to the index σ,

$$\varphi_{\vec{k},\sigma}\left(\vec{r}\right) = u_{\vec{k}}(\vec{r})\,e^{i\vec{k}\cdot\vec{r}}\,,$$

and use the Kronecker Delta-function to mark the orthogonality,

$$\left(\varphi_{\vec{k}',\sigma'},\varphi_{\vec{k},\sigma}\right) = \int d^3r\,\varphi_{\vec{k}',\sigma'}^*(\vec{r})\,\varphi_{\vec{k},\sigma}(\vec{r})\,\delta_{\sigma\sigma'} = \delta_{\vec{k}\vec{k}'}\,\delta_{\sigma\sigma'}$$

Phonons in crystals

The mean positions of the ions of a crystal form a periodic structure, which is usually decomposed in a Bravais lattice BL and a basis B. Each ion μ is described by two vectors $\vec{l} \in BL$ and $\vec{b} \in B$, where $\vec{l}$ indicates the position of the primitive cell and $\vec{b}$ the location of the ion within the cell. The equilibrium position of the ion is thus given by $\vec{R}_{(\vec{l},\vec{b})}^{(0)} = \vec{l} + \vec{b}$.

We first consider the ions as classical particles represented in a real phase space. The normal mode coordinates of a crystal are obtained by a suitable canonical transformation of the ionic coordinates. However, the general method, which consists in solving eigensystem

$$\left(\mathcal{M}^{-1}\mathcal{D}\right)X_\alpha = \omega_\alpha^2\,X_\alpha$$

is hard to apply and the resulting canonical transformation is laborious to deal with because it doesn't make use of the symmetries of the crystal. A more convenient canonical transformation is thus obtained by using the symmetry properties. There are two standard ways. The first results in a canonical transformation with real normal mode coordinates, which all depend on both the position and momentum variables:

$$Q_\alpha = Q_\alpha\left(Q,P\right) \in \mathbb{R} \qquad \text{and} \qquad P_\alpha = P_\alpha\left(Q,P\right) \in \mathbb{R}\,.$$

$Q \in \mathbb{R}^{3N}$ is the vector containing all the ionic displacements and $P \in \mathbb{R}^{3N}$ the vector containing the ionic moments. Such a canonical transformation is presented in ref. [44].

The second approach uses complex coordinates, which exclusively depend on the position or momentum variables:

$$Q_\alpha = Q_\alpha\left(Q\right) = X_\alpha^\dagger\,\mathcal{M}Q \in \mathbb{C} \qquad \text{and} \qquad P_\alpha = P_\alpha\left(P\right) = X_\alpha^\dagger P \in \mathbb{C}$$

This is the form of canonical transformation, which we have used to write $V^{res}_{e^--modes}$ in second quantization in chapter 2.2. Therefore, we shall use complex coordinates. First, we note that the total ionic potential has the translational symmetry of the Bravais lattice. Thus, the dynamical matrix only depends on the mutual distance of two ions but not on their absolute position,

$$\mathcal{D}_{\vec{R},\vec{R}'} = \mathcal{D}_{\vec{b},\vec{b}'}\left(\vec{l}-\vec{l}'\right) \quad \in M_{3\times3}(\mathbb{R}) \text{ for fixed } \vec{b} \text{ and } \vec{b}'$$

We define the discrete Fourier transpose of the dynamical matrix,

$$\mathcal{K}_{\vec{q},\vec{b},\vec{b}'} \equiv \sum_{\vec{R}\in\mathcal{B}} e^{-i\vec{q}\cdot\vec{R}}\, \mathcal{D}_{\vec{b},\vec{b}'}\left(\vec{R}\right) \quad \in M_{3\times3}(\mathbb{C}) \text{ for fixed } \vec{b} \text{ and } \vec{b}'$$

There are r different vectors $\vec{b}$ or $\vec{b}'$, where r is the number of ions per unit cell. The matrix $\mathcal{K}_{\vec{q}}$ obtained when varying $\vec{b}$ and $\vec{b}'$ is thus of dimension $3r \times 3r$. We solve the eigensystem

$$\mathcal{K}_{\vec{q}'}\, \vec{\epsilon}_{\vec{q},j} = \omega^2_{\vec{q},j}\, \vec{\epsilon}_{\vec{q},j}$$

where $\vec{\epsilon}_{\vec{q},j} \in \mathbb{C}^{3r}$ is called "polarization vector". The index $j = 1 \ldots 3r$. distinguishes different eigenvalues and eigenvectors of $\mathcal{K}_{\vec{q}}$. Since $\vec{\epsilon}_{\vec{q},j}$ are the eigenvectors of a hermitian matrix, they are orthogonal. Their norm is chosen in a way to satisfy the orthonormalization relations

$$\vec{\epsilon}^{\dagger}_{\vec{q},j} \cdot \vec{\epsilon}_{\vec{q}',j'} = \sum_{\vec{b},i=1,2,3} \epsilon^*_{(\vec{q},j),(\vec{b},i)}\, \epsilon_{(\vec{q}',j'),(\vec{b},i)} = \delta_{\vec{q}\vec{q}'}\, \delta_{jj'}$$

We define

$$X_{(\vec{q},j),(\vec{l},\vec{b},i)} = \frac{1}{\sqrt{NM_{\vec{b}}}} \epsilon_{(\vec{q},j),(\vec{b},i)}\, e^{i\vec{q}\cdot\vec{l}}$$

The index $i = 1, 2, 3$ indicates the three spatial components. The new vectors $X_{(\vec{q},j)}$ satisfy the generalized orthonormalization relations

$$X^{\dagger}_{(\vec{q},j)}\, M\, X_{(\vec{q}',j')} = \sum_{\vec{l},\vec{b},i} X^*_{(\vec{q},j),(\vec{l},\vec{b},i)}\, M_{\vec{b}}\, X_{(\vec{q}',j'),(\vec{l},\vec{b},i)} = \delta_{\vec{q}\vec{q}'}\, \delta_{jj'}$$

The fact that those vectors only depend on the primitive cell by a phase factor $e^{i\vec{q}\cdot\vec{l}}$ is a direct consequence of the *translational symmetry* of the Bravais lattice. As shown in ref. [45], they induce a canonical transformation

$$Q_{(\vec{q},j)} = Q_{(\vec{q},j)}(Q) = X^{\dagger}_{(\vec{q},j)}\, M\, Q\ \in \mathbb{C} \qquad \text{and} \qquad P_{(\vec{q},j)} = P_{(\vec{q},j)}(P) = X^{\dagger}_{(\vec{q},j)}\, P\ \in \mathbb{C}$$

where $Q \in \mathbb{R}^{3N}$ is the vector of the ionic displacements and $P \in \mathbb{R}^{3N}$ the vector of the ionic moments. The physical picture of the new coordinates results from the inversion of the transformation relations. It appears that each couple $\left(Q_{(\vec{q},j)}, P_{(\vec{q},j)}\right)$ describes a plane wave with spatial wave vector $\vec{q}$ and temporal angular frequency $\omega_{\vec{q},j}$. An extended discussion of the dispersion relation of particular crystals was held in the previous report [46].

The new coordinates decouple the ionic Hamiltonian as follows

$$H_{ions}^{adia,harm} = \frac{1}{2}\sum_{\vec{q},j}\left(P_{(\vec{q},j)}^{*}P_{(\vec{q},j)} + \omega_{(\vec{q},j)}^{2}Q_{(\vec{q},j)}^{*}Q_{(\vec{q},j)}\right)$$

Obviously, the real and imaginary parts of the same normal mode coordinate depend on each other. From the canonical transformation, we immediately obtain the relation

$$Q_{(\vec{q},j)}^{*} = Q_{(-\vec{q},j)}$$

Thus coupling between real an imaginary components of the normal mode coordinates represents a physical symmetry between the wave vectors $\vec{q}$ and $-\vec{q}$. In fact, those vectors are applied on each other by the *inversion symmetry* of the Bravais lattice.

We summarize: Allowing the canonical transformation to be complex, we have found a transformation, which is mathematically easy to manipulate. Furthermore, this transformation is physically reasonable as it uses the translational and inversion symmetry of the lattice.

We now step to the quantum mechanical description. In this case the complex coordinates become non-hermitian operators, which can be shown to satisfy the commutation relations

$$\left[Q_{(\vec{q},j)}, P_{(\vec{q}',j')}\right] = i\hbar\delta_{\vec{q}\vec{q}'}\delta_{jj'} \cdot \mathbb{1}_{ions}$$

The Hamiltonian becomes

$$H_{ions}^{adia,harm} = \frac{1}{2}\sum_{\vec{q},j}\left(P_{(\vec{q},j)}^{\dagger}P_{(\vec{q},j)} + \omega_{(\vec{q},j)}^{2}Q_{(\vec{q},j)}^{\dagger}Q_{(\vec{q},j)}\right)$$

Again, we can introduce annihilation and creation operators $d_{(\vec{q},j)}$ and $d_{(\vec{q},j)}^{\dagger}$, such that

$$H_{ions}^{adia,harm} = \sum_{\vec{q},j}\hbar\omega_{(\vec{q},j)}d_{(\vec{q},j)}^{\dagger}d_{(\vec{q},j)} \qquad \text{and} \qquad \left[d_{(\vec{q},j)}, d_{(\vec{q}',j')}^{\dagger}\right] = \delta_{\vec{q}\vec{q}'}\delta_{jj'} \cdot \mathbb{1}_{ions}$$

The normal mode operators $Q_{(\vec{q},j)}$ then become

$$\mathbb{Q}_{(\vec{q},j)} = \sqrt{\frac{\hbar}{2\omega_{(\vec{q},j)}}} \left(d^+_{(-\vec{q},j)} + d_{(\vec{q},j)} \right)$$

Derivation of the interaction term

To be logically coherent we shall apply the general method of chapter 2.2 to obtain the electron-phonon interaction in the scheme of second quantization. Let's remind this method:

1) write the residual interaction potential $V^{res}_{e^--ions}$, which describes the interaction between ionic and electronic excitations

2) write the operator W, which is the restriction of $V^{res}_{e^--ions}$ to the subspace $\mathcal{H}_{electrons}$ obtained when replacing the operators $\vec{R}_\mu$ by the classical equilibrium positions

3) transcribe W to its corresponding operator $\mathbb{W}$ in second quantization

4) differentiate $\mathbb{W}$ to obtain the operator $\mathbb{F}^{(1)}_{(\vec{q},j)} = \mathcal{D}_{(\vec{q},j)}\,\mathbb{W}$

5) write the first interaction term in second quantization,
$$\mathbb{V}^{res\,(1)}_{e^--modes} = \sum_{(\vec{q},j)} \mathbb{F}^{(1)}_{(\vec{q},j)}\left(\vec{r}.\right) \otimes \mathbb{Q}_{(\vec{q},j)}$$

Because of the translational symmetry of the Bravais lattice the form of the electrostatic potential of an ion only depends on its position within the unit cell but not on the absolute position in the lattice. Therefore the global potential can be written as

$$V^{res}_{e^--ions} = \sum_{(\vec{l},\vec{b}),v} U_{\vec{b}}\left(\vec{r}_v - \vec{R}_{(\vec{l},\vec{b})}\right)$$

which gives

$$W = \sum_{(\vec{l},\vec{b}),v} U_{\vec{b}}\left(\vec{r}_v - \vec{R}^{(0)}_{(\vec{l},\vec{b})}\right)$$

In second quantization this term becomes

$$\mathbb{W} = \sum_{(\vec{l},\vec{b})} \int_{\mathbb{R}^3} d^3x\, U_{\vec{b}}\left(\vec{x} - \vec{R}^{(0)}_{(\vec{l},\vec{b})}\right) \mathbb{D}\left(\vec{x}\right)$$

where $\mathbb{D}\left(\vec{x}\right)$ is the density operator,

$$\mathbb{D}\left(\vec{x}\right) = \Psi^+\left(\vec{x}\right)\Psi\left(\vec{x}\right) = \sum_{\sigma,\sigma'} \sum_{\vec{k},\vec{k'}} \delta_{\sigma\sigma'} \varphi^*_{\vec{k'},\sigma}\left(\vec{x}\right) \varphi_{\vec{k},\sigma}\left(\vec{x}\right) a^\dagger_{\vec{k'},\sigma}\, a_{\vec{k},\sigma}$$

$$= \sum_{\sigma=\pm} \sum_{\vec{k},\vec{k'}} u^*_{\vec{k'}}(\vec{x}) u_{\vec{k}}(\vec{x}) e^{i(\vec{k}-\vec{k'})\cdot\vec{x}} a^\dagger_{\vec{k'},\sigma}\, a_{\vec{k},\sigma}$$

Explicitly we obtain

$$\mathbb{W} = \sum_{(\vec{l},\vec{b}),\vec{k},\vec{k}',\sigma} \int_{\mathbb{R}^3} d^3x\, U_{\vec{b}}\left(\vec{x} - \vec{R}^{(0)}_{(\vec{l},\vec{b})}\right) u^*_{\vec{k}'}(\vec{x}) u_{\vec{k}}(\vec{x})\, e^{i(\vec{k}-\vec{k}')\cdot\vec{x}}\, a^{\dagger}_{\vec{k}',\sigma}\, a_{\vec{k},\sigma}$$

To find the first Taylor coefficient $\mathbb{F}^{(1)}_{(\vec{q}',j)}$ we make use of the formula obtained in section " Development in series" (8.1.2),

$$\mathbb{F}^{(1)}_{(\vec{q},j)} = \mathcal{D}_{(\vec{q},j)}\, \mathbb{W} = \sum_{(\vec{l},\vec{b})} \vec{X}_{(\vec{q},j),(\vec{l},\vec{b})} \frac{\partial}{\partial \vec{R}^{(0)}_{(\vec{l},\vec{b})}} \mathbb{W}$$

After substitution of $\vec{X}_{(\vec{q},j),(\vec{l},\vec{b})}$ and $\mathbb{W}$ a long but straightforward derivation yields (see appendix 8.4.3)

$$\mathbb{F}^{(1)}_{(\vec{q},j)} = -i \sqrt{\frac{N}{(2\pi)^3 M_{\vec{b}}}} \sum_{\vec{b},\vec{k},\vec{k}',\sigma} \vec{\epsilon}_{(\vec{q},j),\vec{b}} \cdot \vec{q}\, \tilde{U}(\vec{q})\, e^{-i\vec{q}\cdot\vec{b}} \left[\int_{\mathbb{R}^3} d^3x\, e^{i(\vec{q}+\vec{k}+\vec{k}')\cdot\vec{x}}\, u^*_{\vec{k}'}(\vec{x}) u_{\vec{k}}(\vec{x}) \right] a^{\dagger}_{\vec{k}',\sigma}\, a_{\vec{k},\sigma}$$

if $\vec{q} + \vec{k} - \vec{k}' \in RL$ and $\mathbb{F}^{(1)}_{(\vec{q},j)} = 0$ otherwise.

$\tilde{U}(\vec{q})$ is the Fourier Transform of the potential, $\tilde{U}(\vec{q}) = \dfrac{1}{(2\pi)^{3/2}} \int_{\mathbb{R}^3} d^3x\, U(\vec{x})\, e^{-i\vec{q}\cdot\vec{x}}$.

Using the relation $\mathbb{Q}_{(\vec{q},j)} = \sqrt{\dfrac{\hbar}{2\omega_{\vec{q}}}} \left(d^+_{(-\vec{q},j)} + d_{(\vec{q},j)} \right)$

we finally obtain

$$\mathbb{V}^{res(1)}_{e^- - ions} = \sum_{(\vec{q},j)} \mathbb{F}^{(1)}_{(\vec{q},j)}(\vec{r}.) \otimes \mathbb{Q}_{(\vec{q},j)} = \sum_{(\vec{q},j),\vec{b},\vec{k},\vec{k}',\sigma} M^{(\vec{q},j)}_{\vec{b},\vec{k},\vec{k}'}\, a^{\dagger}_{\vec{k}',\sigma}\, a_{\vec{k},\sigma} \left(d^+_{(-\vec{q},j)} + d_{(\vec{q},j)} \right)$$

with $M^{(\vec{q},j)}_{\vec{b},\vec{k},\vec{k}'} = -i \sqrt{\dfrac{N\hbar}{16\pi^3 M_{\vec{b}} \omega_{(\vec{q},j)}}} \vec{\epsilon}_{(\vec{q},j),\vec{b}} \cdot \vec{q}\, \tilde{U}(\vec{q})\, e^{-i\vec{q}\cdot\vec{b}} \left[\int_{\mathbb{R}^3} d^3x\, e^{i(\vec{q}+\vec{k}+\vec{k}')\cdot\vec{x}}\, u^*_{\vec{k}'}(\vec{x}) u_{\vec{k}}(\vec{x}) \right]$

Or in the usual notation

$$\mathbb{V}^{res(1)}_{e^- - modes} = -\sum_{\cdots} M\, c^{\dagger}_{\vec{k},\sigma} c_{\vec{k}',\sigma} d_{\vec{q},j} + \sum_{\cdots} M\, b^{\dagger}_{\vec{k},\sigma} c^{\dagger}_{\vec{k}',\sigma} d_{\vec{q},j} + \sum_{\cdots} M\, c_{\vec{k},\sigma} b_{\vec{k}',\sigma} d_{\vec{q},j} + \sum_{\cdots} M\, b^{\dagger}_{\vec{k},\sigma} b_{\vec{k}',\sigma} d_{\vec{q},j}$$

$$- \sum_{\cdots} M\, c^{\dagger}_{\vec{k},\sigma} c_{\vec{k}',\sigma} d^{\dagger}_{\vec{q},j} + \sum_{\cdots} M\, b^{\dagger}_{\vec{k},\sigma} c^{\dagger}_{\vec{k}',\sigma} d^{\dagger}_{\vec{q},j} + \sum_{\cdots} M\, c_{\vec{k},\sigma} b_{\vec{k}',\sigma} d^{\dagger}_{\vec{q},j} + \sum_{\cdots} M\, b^{\dagger}_{\vec{k},\sigma} b_{\vec{k}',\sigma} d^{\dagger}_{\vec{q},j}$$

where the sum $\sum_{\cdots}$ goes over all normal modes $(\vec{q}, j)$, over all the basis vectors $\vec{b} \in B$, and over all the states $(\vec{k}, \sigma)$ and $\boxed{(\vec{k}', \sigma)}$ on which the respective hole or excitation operators are defined.

Discussion

(see section 2.3.4)

8.2 Extended analytical discussion of the polaron dynamic

In this section we give the extended mathematical developments for results present in section 3.3.

8.2.1 Restriction to the relevant subspace

We show the existence of an orthogonal decomposition of $\mathcal{H}$ in spaces that are stable under the action of H. In particular, the decomposition yields a stable subspace $\mathcal{H}_{red}$, which contains all the polarons that couple different electron states. Furthermore, this space is showed to have a small dimension allowing numerical methods to work efficiently. Finally, $\mathcal{H}_{red}$ contains all the zero-phonon states – the states that are often taken as initial states of a relaxation process. Thus $\mathcal{H}_{red}$ is the only subspace of $\mathcal{H}$ that concerns our considerations.

First, we note that $\mathcal{H}$ can be decomposed in zero-phonon and one-phonon subspaces:

$$\mathcal{H} = \mathcal{H}_{0ph} \oplus \mathcal{H}_{1ph} = \mathcal{H}_{0ph} \oplus \left(\bigoplus_{\tau=1}^{n-g} \mathcal{H}_{1ph+\tau} \right)$$

where $\quad \mathcal{H}_{0ph} \equiv vect\left(\left\{ \left| \tau \; 0 \right\rangle : \tau = 1, ..., n \right\} \right)$

$$\mathcal{H}_{1ph+\tau} \equiv vect\left(\left\{ \left| \tau \; 1\vec{q}_i \right\rangle : i = 1, ..., N \right\} \right)$$

For any electron energy eigenstate $\tau = 1...n$ we define the orthogonal projector

$$P_{1ph+\tau} : \mathcal{H} \to \mathcal{H}_{1ph+\tau}$$

Further, we define

$$\mathcal{H}_{A,\tau} \equiv P_{1ph+\tau}\left(H\mathcal{H}_{0ph} \right) \subseteq \mathcal{H}_{1ph+\tau} \quad \text{and}$$

$$\mathcal{H}_{B,\tau} \perp \mathcal{H}_{A,\tau} \quad \text{such that} \quad \mathcal{H}_{A,\tau} \oplus \mathcal{H}_{B,\tau} = \mathcal{H}_{1ph+\tau}$$

In this way, $\mathcal{H}$ yields the orthogonal decomposition,

$$\mathcal{H} = \mathcal{H}_{0ph} \oplus \left(\mathcal{H}_{A,1} \oplus \mathcal{H}_{B,1} \right) \oplus ... \oplus \left(\mathcal{H}_{A,n-g} \oplus \mathcal{H}_{B,n-g} \right) = \mathcal{H}_{0ph} \oplus \left(\bigoplus_{\tau=1}^{n-g} \mathcal{H}_{A,\tau} \right) \oplus \left(\bigoplus_{\tau=1}^{n-g} \mathcal{H}_{B,\tau} \right)$$

Theorem (stable subspaces)

If $\mathcal{H}_{B,\tau}$ are defined as the orthogonal complements of $\mathcal{H}_{A,\tau} \equiv P_{1ph+\tau}\left(H\mathcal{H}_{0ph} \right)$ inside $\mathcal{H}_{1ph+\tau}$, then $\mathcal{H}_{B,\tau}$ are stable in time. Explicitly, $H\mathcal{H}_{B,\tau} \subseteq \mathcal{H}_{B,\tau} \quad \forall \tau$.

To prove this theorem we use the particular structure of the Fröhlich Hamiltonian and the monochromaticity of the LO-phonon spectrum (demonstration see appendix 8.4.4).

The theorem implies that the space

$$\mathcal{H}_{red} \equiv \mathcal{H}_{0\,ph} \oplus \left(\bigoplus_{\tau=1}^{n} \mathcal{H}_{A,\tau} \right) = \mathcal{H}_{0\,ph} \oplus \left(\bigoplus_{\tau=1}^{n} P_{1ph+\tau} \left(H \mathcal{H}_{0\,ph} \right) \right) \qquad \text{"reduced space"}$$

is also stable, i.e. $H\mathcal{H}_{red} \subseteq \mathcal{H}_{red}$. This is space contains $\mathcal{H}_{0\,ph}$, which contains the initial state vector of the system at zero temperature. Thus, the relaxation process will be described inside $\mathcal{H}_{red}$.

We shall now find a basis of $\mathcal{H}_{red}$. The orthogonal projector $P_{1\,ph+\tau}$ can be written as

$$P_{1\,ph+\tau} = \sum_{i=1}^{N} \left| \tau\ 1\vec{q}_i \right\rangle \left\langle \tau\ 1\vec{q}_i \right| .$$

A basis of $\mathcal{H}_{A,\tau}$ is thus given by the set of n non-orthogonal vectors

$$\left\{ \sum_{i=1}^{N} \left| \tau\ 1\vec{q}_i \right\rangle \left\langle \tau\ 1\vec{q}_i \right| H \left| v\ 0 \right\rangle \ :\ v = 1,...,n \right\}$$

A non-orthogonal basis of $\mathcal{H}_{red} \equiv \mathcal{H}_{0\,ph} \oplus \mathcal{H}_{A,1} \oplus ... \oplus \mathcal{H}_{A,n-g}$ is given by the basis vectors of its orthogonal components:

$$\left\{ \left| v\ 0 \right\rangle ,\ \left(\sum_{i=1}^{N} \left| \tau\ 1\vec{q}_i \right\rangle \left\langle \tau\ 1\vec{q}_i \right| \right) H \left| v\ 0 \right\rangle ,\ v = 1...n,\ \tau = 1...n-g \right\}$$

If those $n(n+1-g)$ vectors are linearly independent (which is almost certain to happen), then the dimension of $\mathcal{H}_{red}$ is equal to $n(n+1-g)$. An orthonormal basis of $\mathcal{H}_{red}$ is obtained by Gram-Schmidt orthonormalization.

Overview

We summarize. There is a particular decomposition of the total Hilbert space,

$$\mathcal{H} = \mathcal{H}_{red} \oplus \mathcal{H}_{B,1} \oplus ... \oplus \mathcal{H}_{B,n-g} ,$$

where all the subspaces are stable under the action of the Hamiltonian H . In particular, there is a low dimensional stable subspace $\mathcal{H}_{red}$ with four major properties:

- $\mathcal{H}_{red}$ has a small dimension that is independent of the number of normal modes, $dim\left(\mathcal{H}_{red} \right) = n\left(n - g + 1 \right)$.

- $\mathcal{H}_{red}$ is the only subspace of $\mathcal{H}$ that couples different electron states. More precisely, $\mathcal{H}_{red}$ contains all the eigenstates of the full Hamiltonian H, which involve several electron states.

- $\mathcal{H}_{red}$ is stable under the action of H, i.e. $H\mathcal{H}_{red} \subseteq \mathcal{H}_{red}$. Consequently a state vector initially contained in $\mathcal{H}_{red}$ stays inside $\mathcal{H}_{red}$ over time.

- $\mathcal{H}_{red}$ contains all the zero-phonon states, which are often considered as initial states.

A non-orthogonal basis of $\mathcal{H}_{red}$ is given by

$$\left\{ |v\ 0\rangle, \left(\sum_{i=1}^{N} |\tau\ 1\vec{q}_i\rangle\langle\tau\ 1\vec{q}_i| \right) H |v\ 0\rangle,\ v = 1...n,\ \tau = 1...n - g \right\}$$

which can be orthonormalized by the Gram-Schmidt procedure.

Other viewpoints

Up to here, the presented viewpoint was an abstract consideration of mathematical spaces. Two other viewpoints help to sharpen our understanding:

- Matrix representation:

  There is an orthonormal basis of the Hilbert space $\mathcal{H}$, in which the matrix representation of the Hamiltonian operator H is bloc-diagonal:

$$H' = \begin{pmatrix} \boxed{H_{red}} & & & \\ & \boxed{H_{B,\tau=1}} & & \\ & & \ddots & \\ & & & \boxed{H_{B,\tau=n-g}} \end{pmatrix}$$

  This matrix is obtained from the initial matrix H by a similarity transformation, which means that there is a non-singular matrix S such that $H' = S^{-1}HS$.

- Conserved physical quantity:

  The system evolution conserves a quantity x that is different from the energy. This quantity is associated with a hermitian operator X, which commutes with the Hamiltonian operator H, $[H, X] = 0$. Such an operator is easily obtained by combining all the orthogonal projectors on the different stable subspaces. For example,

$$X \equiv \sum_{\tau=1}^{n-g} \tau \cdot \left(projector\ on\ H_{B,\tau} \right)$$

In this way,

$$\left[H, X \right] = 0 \qquad and \qquad X \left| \psi \right\rangle = x \left| \psi \right\rangle \quad with \quad x = \begin{cases} 0 \ if \ \left| \psi \right\rangle \in \mathcal{H}_{red} \\ \tau \ if \ \left| \psi \right\rangle \in \mathcal{H}_{B,\tau} \end{cases}$$

8.2.2   Symmetry-degeneracies and substructure of the relevant subspace

The quantum dot system is supposed to obey a physical symmetry represented by the symmetry operator $\mathcal{P}$, which commutes with the Hamiltonian $\left[H, \mathcal{P} \right] = 0$. It follows that the eigenstates of H can be chosen to be simultaneous eigenstates of $\mathcal{P}$. The respective eigenvalues associated with $\mathcal{P}$ are noted p. Explicitly,

$$H \left| \psi \right\rangle = \varepsilon \left| \psi \right\rangle \qquad\qquad \mathcal{P} \left| \psi \right\rangle = p \left| \psi \right\rangle$$

Since $\mathcal{P}$ commutes with H, p represents a conserved physical quantity and the system evolves independently inside subspaces associated with different eigenvalues of $\mathcal{P}$. Therefore, the total Hamiltonian can be solved independently for each eigenvalue of the symmetry operator and the polaron states in different eigenspaces of $\mathcal{P}$ are independent from one another.

Our system has one spatial symmetry with respect to the x-z-plane. Thus the symmetry operator $\mathcal{P}$ inverses the y-coordinate and yields two different eigenvalues $p = \pm 1$, called "y-parity". It follows, that the Hilbert space $\mathcal{H}_{red}$ can be decomposed in two decoupled orthogonal parts associated with a different y-parity. This general result is now developed in a pedestrian way in order to get a better insight as well as to find the suitable natural basis associated the two restrictions of $\mathcal{H}_{red}$.

By virtue of the symmetry $\mathcal{P}$ the electronic envelope functions can always be chosen either even or odd in the y-coordinate. The parity along the y-axis of the envelope function ψ_ν of a given electron state $\left| \nu \right\rangle$ is noted p_ν. In the frame of the envelope function approximation, the matrix element $\left\langle \nu\ 0 \left| H \right| \tau\ 1\vec{q} \right\rangle$ between a zero-phonon state and a one-phonon state is proportional to the Fröhlich Integral

$$\int d^3x\, e^{i\vec{q}\cdot\vec{x}}\, \psi_\nu \left(\vec{x} \right) \psi_\tau \left(\vec{x} \right) = \int dx\, e^{iq_x x} \int dz\, e^{iq_z z} \int dy\, e^{iq_y y} \psi_\nu \left(\vec{x} \right) \psi_\tau \left(\vec{x} \right)\ .$$

Using the y-parity of the envelope functions, the y-integral can be written as

$$\int_0^\infty \left(e^{iq_y y} + p_\nu\, p_\tau\, e^{-iq_y y} \right) \psi_\nu \left(\vec{x} \right) \psi_\tau \left(\vec{x} \right).$$

Since

$$e^{iq_y y} + p_\nu\, p_\tau\, e^{-iq_y y} = \begin{cases} 2\cos\left(q_y y\right) & \text{if } p_\nu\, p_\tau = +1 \\ 2i\sin\left(q_y y\right) & \text{if } p_\nu\, p_\tau = -1 \end{cases}$$

we conclude that the parity of $\left\langle \nu\, 0 \middle| H \middle| \tau\, 1\vec{q}\right\rangle$ in q_y is equal to $p_\nu \cdot p_\tau$.

This symmetry consideration allows to decompose the relevant Hilbert space $\mathcal{H}_{red}$ in two decoupled orthogonal subspaces. First, the existence of two decoupled subspaces is proven and thereafter the orthogonality of those subspaces is verified.

We recall the (non-orthonormal) natural basis of $\mathcal{H}_{red}$,

$$\left\{ \left| \nu\, 0 \right\rangle,\ \sum_{i=1}^{N} \left| \tau\, 1\vec{q}_i \right\rangle \left\langle \tau\, 1\vec{q}_i \middle| H \middle| \nu\, 0 \right\rangle,\ \nu = 1...n,\ \tau = 1...n-g \right\}$$

Inside $\mathcal{H}_{red}$, the non-vanishing off-diagonal matrix elements of the Hamiltonian are either elements between a zero-phonon and a one-phonon state or elements between two one-phonon states with equal index τ. Explicitly those matrix elements are

- $\left\langle \nu\, 0 \middle| H \left(\sum_{i=1}^{N} \left| \tau\, 1\vec{q}_i \right\rangle \left\langle \tau\, 1\vec{q}_i \middle| H \middle| \mu\, 0 \right\rangle \right) = \sum_{i=1}^{N} \underbrace{\left\langle \nu\, 0 \middle| H \middle| \tau\, 1\vec{q}_i \right\rangle}_{f(\vec{q}_i)} \underbrace{\left\langle \tau\, 1\vec{q}_i \middle| H \middle| \mu\, 0 \right\rangle}_{g(\vec{q}_i)} = \sum_{i=1}^{N} f\left(\vec{q}_i\right) g\left(\vec{q}_i\right)$

- $\left(\sum_{i=1}^{N} \left\langle \nu\, 0 \middle| H \middle| \tau\, 1\vec{q}_i \right\rangle \left\langle \tau\, 1\vec{q}_i \middle| \right) H \left(\sum_{i=1}^{N} \left| \tau\, 1\vec{q}_i \right\rangle \left\langle \tau\, 1\vec{q}_i \middle| H \middle| \mu\, 0 \right\rangle \right) = \left(\varepsilon_\tau + \varepsilon_{LO} \right) \cdot \sum_{i=1}^{N} f\left(\vec{q}_i\right) g\left(\vec{q}_i\right)$

The unit difference of these two expressions is due to the fact that one-phonon states of the natural basis are not normalized. The normalization introduces another energy term.

The q_y-parity of $(f \cdot g)\left(\vec{q}_i\right)$ can be written as

$$p_{f \cdot g} = p_f \cdot p_g = \left(p_\nu \cdot p_\tau \right) \cdot \left(p_\tau \cdot p_\mu \right) = p_\nu \cdot p_\mu$$

It follows that the sum over i vanishes if $p_\nu \cdot p_\mu = -1$. In other words, if the envelope functions of two electron states $\left| \nu \right\rangle$ and $\left| \mu \right\rangle$ have different y-parity, then H has an analytically vanishing matrix element between $\left| \nu\, 0 \right\rangle$ and $\sum_{i=1}^{N} \left| \tau\, 1\vec{q}_i \right\rangle \left\langle \tau\, 1\vec{q}_i \middle| H \middle| \mu\, 0 \right\rangle$ for all $\tau = 1,...,n-g$.

We conclude that $\mathcal{H}_{red}$ can be decomposed in two decoupled subspaces, both stable under the action of the Hamiltonian H_{red},

$$\mathcal{H}_{red} = \mathcal{H}_{red}^+ \oplus \mathcal{H}_{red}^- .$$

A suitable non-orthogonal basis of those subspaces is given by,

$$\mathcal{H}_{red}^+ : \left\{ |v\ 0\rangle, \sum_{i=1}^N |\tau\ 1\vec{q}_i\rangle\langle\tau\ 1\vec{q}_i|H|v\ 0\rangle, v = 1...n, \tau = 1...n-g, p_v = +1 \right\}$$

$$\mathcal{H}_{red}^- : \left\{ |v\ 0\rangle, \sum_{i=1}^N |\tau\ 1\vec{q}_i\rangle\langle\tau\ 1\vec{q}_i|H|v\ 0\rangle, v = 1...n, \tau = 1...n-g, p_v = -1 \right\}$$

$\mathcal{H}_{red}^+$ has dimension $n_+(n-g+1)$, and $\mathcal{H}_{red}^-$ has dimension $n_-(n-g+1)$, where n_+ and n_- are the number of electron eigenstates with positive and negative parity, respectively.

It remains to verify that $\mathcal{H}_{red}^+$ and $\mathcal{H}_{red}^-$ are orthogonal. Different zero-phonon states are orthogonal and all the zero-phonon states are orthogonal to all the one-phonon states. It remains to check if two one-phonon states from $\mathcal{H}_{red}^+$ and $\mathcal{H}_{red}^-$ are orthogonal,

$$\left(\sum_{j=1}^N \langle\mu\ 0|H|\tau\ 1\vec{q}_j\rangle\langle\tau\ 1\vec{q}_j| \right)\left(\sum_{i=1}^N |\tau\ 1\vec{q}_i\rangle\langle\tau\ 1\vec{q}_i|H|v\ 0\rangle \right)$$

$$= \sum_{j=1}^N \sum_{i=1}^N \langle\mu\ 0|H|\tau\ 1\vec{q}_j\rangle\langle\tau\ 1\vec{q}_i|H|v\ 0\rangle \underbrace{\langle\tau\ 1\vec{q}_j|\tau\ 1\vec{q}_i\rangle}_{\delta_{ij}}$$

$$= \sum_{i=1}^N \langle\mu\ 0|H|\tau\ 1\vec{q}_i\rangle\langle\tau\ 1\vec{q}_i|H|v\ 0\rangle$$

As discussed before, this sum vanishes if the envelope functions ψ_μ and ψ_v have different y-parity. Therefore $\mathcal{H}_{red}^+$ and $\mathcal{H}_{red}^-$ are orthogonal.

The decomposition of $\mathcal{H}_{red}$ in two orthogonal subspaces, decoupled by H_{red}, implies that the matrix representation of the Hamiltonian H_{red} is bloc diagonal:

$$H_{red} = \begin{pmatrix} \boxed{\begin{matrix} H_{red}^+ \\ \\ {}_{n_+(n-g+1)\times n_+(n-g+1)} \end{matrix}} & \\ & \boxed{\begin{matrix} H_{red}^- \\ \\ {}_{n_-(n-g+1)\times n_-(n-g+1)} \end{matrix}} \end{pmatrix}$$

8.2.3   Zero-shift polarons

We show the existence of coupled eigenstates of H_{red} with no energy shift relative to the free evolution spectrum. Such eigenstates appear in consequence of the degeneracy of certain electron eigenstates.

We recall that the set of eigenstates of the Hamiltonian H_{red} contains all the eigenstates of the full Hamiltonian H, which superpose different electron eigenstates of H^{free}. In return, it can be shown that every eigenstate of H_{red} is a superposition of different electron eigenstates of the free Hamiltonian H^{free}. The reader's attention is called to the fact that certain eigenstates of H_{red} might be pure superpositions of different degenerate electron eigenstates of the free Hamiltonian. Such eigenstates of H_{red} are also eigenstates of the free Hamiltonian H^{free}, although they couple different electron states. In the following, we agree on calling those states "zero-shift eigenstates".

In the present quantum dot system, the electron energy eigenstates are at most twice degenerate due to one spatial symmetry with respect to the x-z-plane (spin degeneracy is neglected). We consider two degenerate electron states $|\tau_+\rangle$ and $|\tau_-\rangle$, where the sign refers to the wave function's parity along the y-coordinate. The corresponding zero-phonon states $|\tau_+\ 0\rangle$ and $|\tau_-\ 0\rangle$ belong to different orthogonal subspaces $\mathcal{H}_{red}^+$ and $\mathcal{H}_{red}^-$, respectively. Therefore, an eigenstate of the Hamiltonian H_{red} can never be a superposition of $|\tau_+\ 0\rangle$ and $|\tau_-\ 0\rangle$. However, the one phonon states $|\tau_+\ 1\vec{q}\rangle$ and $|\tau_-\ 1\vec{q}\rangle$ appear both in any of the states $\mathcal{H}_{red}^+$ and $\mathcal{H}_{red}^-$. Inside $\mathcal{H}_{red}^+$, for example, we find natural basis states of the form

$$\sum_{i=1}^{N}|\tau_+\ 1\vec{q}_i\rangle\langle\tau_+\ 1\vec{q}_i|H|\nu\ 0\rangle \text{ and } \sum_{i=1}^{N}|\tau_-\ 1\vec{q}_i\rangle\langle\tau_-\ 1\vec{q}_i|H|\nu\ 0\rangle ,$$

where ν ranges over all the electron states with an even envelope function in the y-coordinate. Eigenstates of H_{red}^+ that are pure superpositions of such basis states have an energy equal to $\varepsilon_{\tau_+}+\varepsilon_{LO}\equiv\varepsilon_{\tau_-}+\varepsilon_{LO}\equiv\varepsilon_{\tau}+\varepsilon_{LO}$. In other words, those polarons have zero energy shifts relative to the spectrum of the free Hamiltonian, although they couple different electron states.

For simplicity, we shall consider a fixed y-parity $p=+1$ or $p=-1$. Then, every zero-shift eigenstate of H_{red}^p associated with the electron level τ has the form

$$|\psi_0\rangle = \sum_{\nu}\left[a_\nu\sum_{i=1}^{N}|\tau_+\ 1\vec{q}_i\rangle\langle\tau_+\ 1\vec{q}_i|H|\nu\ 0\rangle + b_\nu\sum_{i=1}^{N}|\tau_-\ 1\vec{q}_i\rangle\langle\tau_-\ 1\vec{q}_i|H|\nu\ 0\rangle\right],$$

where ν ranges over the n_p electron states with y-parity $p_\nu = p$.

It will now be investigated if and how many such eigenstates exist. A necessary and sufficient condition for $|\psi_0\rangle$ being an eigenstate of H^p_{red} is that $H^p_{red}|\psi_0\rangle$ has zero projection on all the basis vectors of $\mathcal{H}^p_{red}$, which are orthogonal to $|\psi_0\rangle$. Those basis vectors are explicitly:

$$\left\{ |\nu\ 0\rangle, \sum_{i=1}^{N} |\mu\ 1\vec{q}_i\rangle\langle\mu\ 1\vec{q}_i|H|\nu\ 0\rangle,\ \nu = 1...n, p_\nu = p, \mu = 1...n - g, \mu \neq \tau_+, \mu \neq \tau_- \right\}$$

The projection of $H^p_{red}|\psi_0\rangle$ on any one-phonon state $|\mu\ 1\vec{q}_i\rangle$, $\mu \neq \tau_+$, $\mu \neq \tau_-$, vanishes, since H^p_{red} has zero matrix elements between different one-phonon states. Thus, the necessary and sufficient condition for $|\psi_0\rangle$ being a zero-shift eigenstate of H^p_{red} is that $H^p_{red}|\psi_0\rangle$ has zero projection on the n_p vectors $|\nu\ 0\rangle$ with parity p. Explicitly, we require

$$\langle\nu\ 0|H^p_{red}|\psi_0\rangle = 0 \quad \forall\ \nu\ such\ that\ p_\nu = p.$$

These are n_p linearly independent equations for the $2n_p$ coefficients a_ν and b_ν. Thus there are $2n_p - n_p = n_p$ linearly independent solutions of a_ν and b_ν.

We conclude: Every degenerate and not fully excited electron energy ε_τ gives rise to n_p linearly independent eigenvectors of H^p_{red} with zero energy shifts with respect to spectrum of the free Hamiltonian. For the total reduced Hamiltonian H_{red} it follows the existence of $n\ (= n_+ + n_-)$ linearly independent zero-shift eigenvectors with energies equal to $\varepsilon_\tau + \varepsilon_{LO}$. If d is the number of degenerate and not fully excited electron energies, then the total number of strictly non-shifted states adds up to $n \cdot d$.

We emphasize that the choice of zero-shift eigenvectors is not unique. Since the zero-shift eigenvectors associated with one degenerate level τ have an identical energy $\varepsilon_\tau + \varepsilon_{LO}$, they span an eigenspace $\mathcal{H}^{zero,\tau}_{red}$. As there are n linear independent zero-shift eigenstates, the energy $\varepsilon_\tau + \varepsilon_{LO}$ is n-times degenerated and $\mathcal{H}^{zero,\tau}_{red}$ has dimension n. Every superposition of zero-shift eigenstates inside $\mathcal{H}^{zero,\tau}_{red}$ is again a zero-shift eigenstate of H_{red}. Furthermore, the full Hilbert space $\mathcal{H}$ contains many more eigenstates with energy $\varepsilon_\tau + \varepsilon_{LO}$. Those states are elements of the subspaces $\mathcal{H}_{B,\tau+}$ and $\mathcal{H}_{B,\tau-}$. The latter were defined as the spaces spanned by eigenvectors of H of the form $\sum_{i=1}^{N} c_i |\tau_+\ 1\vec{q}_i\rangle$ and $\sum_{i=1}^{N} c_i |\tau_-\ 1\vec{q}_i\rangle$, respectively. All those superpositions have

the energy $\varepsilon_\tau + \varepsilon_{LO}$ equal to the energy of the zero-shift subspace $\mathcal{H}_{red}^{zero,\tau}$. Thus $\mathcal{H}_{B,\tau+} \oplus \mathcal{H}_{B,\tau-} \oplus \mathcal{H}_{red}^{zero,\tau}$ is the complete eigenspaces of the full Hamiltonian H with energy $\varepsilon_\tau + \varepsilon_{LO}$. Any superposition of zero-shift eigenstates of $\mathcal{H}_{red}^{zero,\tau}$ and states from $\mathcal{H}_{B,\tau+}$ and $\mathcal{H}_{B,\tau-}$ is again an eigenstate of H. The crucial point, however, is that a zero-shift eigenvector of H_{red} can never be expressed as a superposition of vectors from the uncoupled subspaces $\mathcal{H}_{B,\tau+}$ and $\mathcal{H}_{B,\tau-}$ since they are both orthogonal to $\mathcal{H}_{red}$. Thus, the zero-shift eigenstates are indeed a particular category of coupled eigenstates.

Finally, an additional important property is developed, which will be used in the next section. The demonstration above yields that H_{red} possesses $n \cdot d$ eigenstates, such that $\langle v\ 0 | H_{red} | \psi \rangle = 0 \ \ \forall\ v$.

On the other hand, the total number of eigenstates of H_{red} is $n(n - g + 1)$. Thus, the total number with non-vanishing contribution of the zero-phonon states adds up to

$n(n - g + 1) - n \cdot d = n(n - g - d + 1)$.

This conclusion will be used in the following section.

8.2.4   Strong coupling substructure

In this section the strength of the matrix elements of the Hamiltonian are investigated in detail. These considerations allow to identify strong coupling subspaces of $\mathcal{H}_{red}$ with weak mutual coupling. We emphasize, however, that our procedure consists in a justifying argumentation and not an analytically strict development.

We recall the (non-orthonormal) natural basis of $\mathcal{H}_{red}$,

$$\left\{ |v\ 0\rangle ,\ \sum_{i=1}^{N} |\tau\ 1\vec{q}_i\rangle \langle \tau\ 1\vec{q}_i | H | v\ 0\rangle ,\ v = 1...n,\ \tau = 1...n - g \right\}$$

Inside $\mathcal{H}_{red}$, the non-vanishing off-diagonal matrix elements of the Hamiltonian are either elements between a zero-phonon and a one-phonon state or elements between two one-phonon states with equal index τ. Explicitly those matrix elements write

- $\left\langle v\ 0 \middle| H \left(\sum_{i=1}^{N} |\tau\ 1\vec{q}_i\rangle \langle \tau\ 1\vec{q}_i | H | \mu\ 0\rangle \right) \right\rangle = \sum_{i=1}^{N} \underbrace{\langle v\ 0 | H | \tau\ 1\vec{q}_i\rangle}_{f(\vec{q}_i)} \underbrace{\langle \tau\ 1\vec{q}_i | H | \mu\ 0\rangle}_{g(\vec{q}_i)} = \sum_{i=1}^{N} f(\vec{q}_i) g(\vec{q}_i)$

- $\left(\sum_{i=1}^{N} \langle v\ 0 | H | \tau\ 1\vec{q}_i\rangle \langle \tau\ 1\vec{q}_i | \right) H \left(\sum_{i=1}^{N} |\tau\ 1\vec{q}_i\rangle \langle \tau\ 1\vec{q}_i | H | \mu\ 0\rangle \right) = (\varepsilon_\tau + \varepsilon_{LO}) \cdot \sum_{i=1}^{N} f(\vec{q}_i) g(\vec{q}_i)$

The reader bothered by the unit difference of these two expressions, is recalled that the one-phonon states of the natural basis are not normalized. Their normalization leads to another energy unit.

These matrix elements are large if the overlap of the functions $f(\vec{q})$ and $g(\vec{q})$ is large. In particular, this overlap becomes eminent if the two functions are equal. $f(\vec{q})$ and $g(\vec{q})$ are equal if an only if the underlying state indices are equal, $\mu = \nu$. Thus, one can expect that the Hamiltonian couples mainly the states of the set

$$\left\{ |\nu\; 0\rangle, \; \sum_{i=1}^{N} |\tau\; 1\vec{q}_i\rangle \langle \tau\; 1\vec{q}_i| H |\nu\; 0\rangle, \; \tau = 1...n-g \right\}$$

for a given ν. In other words, the vectors inside the subspace,

$$\mathcal{H}_{red}^{\nu} \equiv vect \left\{ |\nu\; 0\rangle, \; \sum_{i=1}^{N} |\tau\; 1\vec{q}_i\rangle \langle \tau\; 1\vec{q}_i| H |\nu\; 0\rangle, \; \tau = 1...n-g \right\}$$

are strongly coupled. On the other hand, the coupling between different subspaces $\mathcal{H}_{red}^{\nu}$ and $\mathcal{H}_{red}^{\mu}$ is relatively weak. Thus, we shall call the spaces $\mathcal{H}_{red}^{\nu}$ "strong coupling subspaces".

The weak coupling argument based on a small overlap of the functions $f(\vec{q})$ and $g(\vec{q})$ fails in the case of zero-shift superpositions. The justification is that such superpositions have by their nature vanishing contribution of zero-phonon states $|\nu\; 0\rangle$. Therefore, weak coupling terms between one-phonon basis states become important. In the previous section (8.2.3) it was shown that H_{red} yields nd zero-shift eigenstates, where d is the number of degenerate and not fully excited electron levels. Inside one subspace $\mathcal{H}_{red}^{\nu}$ of dimension $n-g+1$ and the remaining number of strongly coupled states can thus be shown to sum up to $n-g-d+1$.

We summarize: Every subspace $\mathcal{H}_{red}^{\nu}$ with orthogonal (!) basis

$$\left\{ |\nu\; 0\rangle, \; \sum_{i=1}^{N} |\tau\; 1\vec{q}_i\rangle \langle \tau\; 1\vec{q}_i| H |\nu\; 0\rangle, \; \tau = 1...n-g \right\}$$

contains $n-g-d+1$ orthogonal vectors with strong mutual coupling by the Hamiltonian. In return, those vectors are very weakly coupled to all the other subspaces $\mathcal{H}_{red}^{\mu}$, $\mu \neq \nu$.

This has crucial consequences for the diagonalization of H_{red}: There are $n-g-d+1$ eigenvectors of H_{red} with strong contribution of $\mathcal{H}_{red}^{\nu}$ and quasi vanishing contribution

of all the other subspaces $\mathcal{H}_{red}^{\mu}$, $\mu \neq \nu$. A good approximation of these eigenvectors is obtained by diagonalizing H_{red}^{ν}, defined as the restriction of H_{red} to $\mathcal{H}_{red}^{\nu}$. All together, there are n subspaces $\mathcal{H}_{red}^{\nu}$. Thus, H_{red} has $n(n-g-d+1)$ eigenvectors, which are nearly contained in one of the subspaces $\mathcal{H}_{red}^{\nu}$, exclusively.

8.2.5   Similar subspaces

We justify the affirmation that strong coupling subspaces $\mathcal{H}_{red}^{\nu+}$ and $\mathcal{H}_{red}^{\nu-}$ of two degenerate electron states $|v_+\rangle$ and $|v_-\rangle$ yield a similar restriction of the Hamiltonian H_{red}. Therefore, those subspaces have similar eigenvectors and eigenvalues.

The basis of $\mathcal{H}_{red}^{\nu}$ developed in the previous section is

$$\left\{ |v\ 0\rangle,\ \sum_{i=1}^{N} |\tau\ 1\vec{q}_i\rangle \langle \tau\ 1\vec{q}_i |H|v\ 0\rangle,\ \tau = 1...n-g \right\}.$$

This basis is orthogonal but non-orthonormal because the one-phonon states are not normalized. For the following considerations, it is useful to use the orthonormalized basis

$$\left\{ |v\ 0\rangle,\ \chi_{\tau,v} \sum_{i=1}^{N} |\tau\ 1\vec{q}_i\rangle \langle \tau\ 1\vec{q}_i |H|v\ 0\rangle,\ \tau = 1...n-g \right\},$$

where the normalization factor $\chi_{\tau,v}$ is given by

$$\chi_{\tau,v} = \left[\sum_{i=1}^{N} \left| \langle \tau\ 1\vec{q}_i |H|v\ 0\rangle \right|^2 \right]^{-1/2}.$$

Now the case of two degenerate electron states $|v_+\rangle$ and $|v_-\rangle$ is considered, where the sign refers to the y-parity of the envelope functions. Their respective strong coupling subspaces are

$$\mathcal{H}_{red}^{\nu+} = \left\{ |v_+\ 0\rangle,\ \chi_{\tau,v+} \sum_{i=1}^{N} |\tau\ 1\vec{q}_i\rangle \langle \tau\ 1\vec{q}_i |H|v_+\ 0\rangle,\ \tau = 1...n-g \right\} \quad \text{and}$$

$$\mathcal{H}_{red}^{\nu-} = \left\{ |v_-\ 0\rangle,\ \chi_{\tau,v-} \sum_{i=1}^{N} |\tau\ 1\vec{q}_i\rangle \langle \tau\ 1\vec{q}_i |H|v_-\ 0\rangle,\ \tau = 1...n-g \right\}$$

We show that the restrictions of the Hamiltonian H_{red} (or H) to $\mathcal{H}_{red}^{\nu+}$ and $\mathcal{H}_{red}^{\nu-}$ are nearly equal. First, the diagonal elements of H in the bases of $\mathcal{H}_{red}^{\nu+}$ and $\mathcal{H}_{red}^{\nu-}$ are shown to be strictly equal.

For elements between two zero-phonon states the independence on the y-parity is an immediate consequence of the electron degeneracy,

$$\langle v_+ \; 0|H|v_+ \; 0\rangle = \varepsilon_v \text{ and } \langle v_- \; 0|H|v_- \; 0\rangle = \varepsilon_v \quad \Rightarrow \quad \langle v_+ \; 0|H|v_+ \; 0\rangle = \langle v_- \; 0|H|v_- \; 0\rangle$$

The matrix elements between two one-phonon states write

$$\left(\chi_{\tau,v_\pm} \sum_{j=1}^{N} \langle v_\pm \; 0|H|\tau \; 1\vec{q}_j\rangle\langle\tau \; 1\vec{q}_j| \right) H \left(\chi_{\tau',v_\pm} \sum_{i=1}^{N} |\tau \; 1\vec{q}_i\rangle\langle\tau \; 1\vec{q}_i|H|v_\pm \; 0\rangle \right)$$

Regrouping and orthonormality yield

$$\chi_{\tau,v_\pm}{}^2 \sum_{j=1}^{N}\sum_{i=1}^{N} \langle v_\pm \; 0|H|\tau' \; 1\vec{q}_j\rangle \underbrace{\langle\tau' \; 1\vec{q}_j|H|\tau \; 1\vec{q}_i\rangle}_{\varepsilon_{\tau+LO}\,\delta_{i,j}}\langle\tau \; 1\vec{q}_i|H|v_\pm \; 0\rangle$$

$$= \chi_{\tau,v_\pm}{}^2 \sum_{i=1}^{N} \langle v_\pm \; 0|H|\tau \; 1\vec{q}_i\rangle\langle\tau \; 1\vec{q}_i|H|v_\pm \; 0\rangle\,\varepsilon_{\tau+LO}$$

$$= \chi_{\tau,v_\pm}{}^2 \sum_{i=1}^{N} \left|\langle\tau \; 1\vec{q}_i|H|v_\pm \; 0\rangle\right|^2 \varepsilon_{\tau+LO} = \chi_{\tau,v} = \frac{\sum_{i=1}^{N}\left|\langle\tau \; 1\vec{q}_i|H|v_\pm \; 0\rangle\right|^2}{\sum_{i=1}^{N}\left|\langle\tau \; 1\vec{q}_i|H|v \; 0\rangle\right|^2}\,\varepsilon_{\tau+LO} = \varepsilon_{\tau+LO}$$

This quantity is again independent of the y-parity. Thus, the diagonal elements of the restriction of H to the subspaces $\mathcal{H}_{red}^{v+}$ and $\mathcal{H}_{red}^{v-}$ are equal. Since the diagonal matrix elements are highly predominant, the similarity of the two strong coupling subspaces $\mathcal{H}_{red}^{v+}$ and $\mathcal{H}_{red}^{v-}$ is obvious.

8.3   Numerical implementation

We give insight in sophisticated numerical tools used to perform the computation of the polaron states in the pyramidal quantum dot. In particular, we present a personalized method using an irregular adaptive discretization of the reciprocal space (8.3.2). For this method to be applicable, we have transcribed the Fröhlich Hamiltonian to an irregular discretization (8.3.3).

Further, we summarize some notions of finite element method used for the integration of Fröhlich integrals (8.3.1) and give relations between discrete space discretization and reciprocal space discretization (8.3.4).

8.3.1   Direct space discretization

Generalities

A finite element method with a mesh of trilateral prism is used (see Fig. 20) is used to represent the pyramidal quantum dot in direct space.
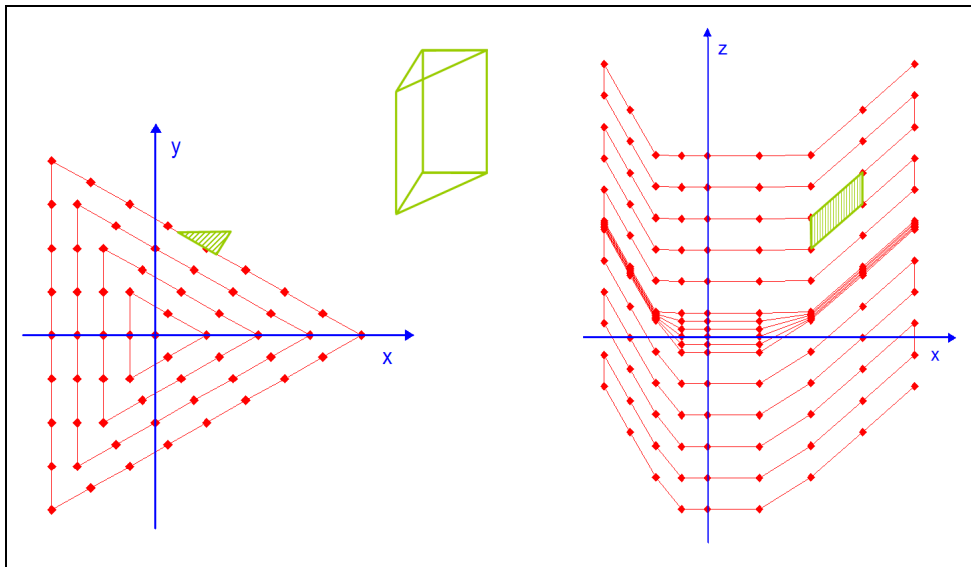
Fig. 20:   Finites elements covering the pyramidal heterostructure, F. Michelini [1, 2]

In opposition to finite difference methods, the finite element method presents the special feature of interpolating the values of the modelized functions by the mean of interpolation functions attached to each element. Those interpolation functions h derive from universal functions initially defined with respect a master element.
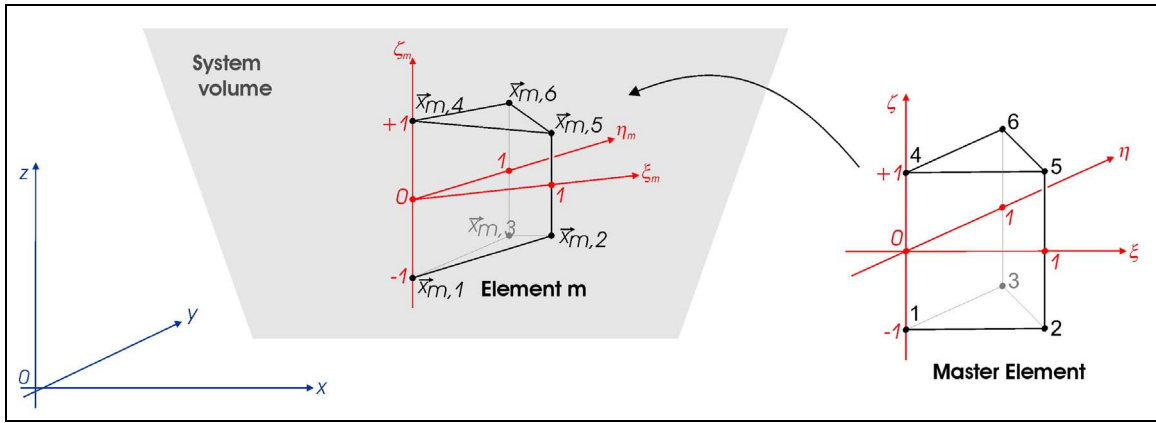
Fig. 21: Prismic finite elements

One finite element m inside a large mesh is shown in Fig. 21. The respective element corners are referred to as "nodes" and distinguished by an index i. Each element is endowed with a set of intrinsic coordinates (ξ_m, η_m, ζ_m), that are the images of the coordinates of the master element.

A three-dimensional function ψ is interpolated as

$$\psi(\vec{r}) = \sum_{i=1}^{6} \psi_{m,i}\, h_i(\xi, \eta, \zeta),$$

where m is the element containing the vector $\vec{r}$ and $\psi_{m,i}$ is the "exact" value of the function ψ at the node i of the element m. The interpolation functions are chosen as linear functions and defined with respect to the coordinates of the mater element,

$$
\begin{aligned}
h_1 &= \tfrac{1}{2}(1-\xi-\eta)(1-\zeta) & h_4 &= \tfrac{1}{2}(1-\xi-\eta)(1+\zeta) \\
h_2 &= \tfrac{1}{2}\xi(1-\zeta) & h_5 &= \tfrac{1}{2}\xi(1+\zeta) \\
h_3 &= \tfrac{1}{2}\eta(1-\zeta) & h_6 &= \tfrac{1}{2}\eta(1+\zeta)
\end{aligned}
$$

The transformation between the coordinates (ξ_m, η_m, ζ_m) and the absolute coordinates (x, y, z) is obtained by the particular interpolation functions

$$x = \sum_{i=1}^{6} x_i\, h_i(\xi, \eta, \zeta) \qquad y = \sum_{i=1}^{6} y_i\, h_i(\xi, \eta, \zeta) \qquad z = \sum_{i=1}^{6} z_i\, h_i(\xi, \eta, \zeta)$$

In the present modelization the mesh nodes are such that

$$
\begin{aligned}
x_1 &= x_4 & y_1 &= y_4 \\
x_2 &= x_5 & y_2 &= y_5 \\
x_3 &= x_6 & y_3 &= y_6
\end{aligned}
$$

Thus, the Jaccobian between (x, y, z) and (ξ_m, η_m, ζ_m) is shown to write

$$J_m \equiv \begin{vmatrix} \dfrac{\partial x}{\partial \xi_m} & \dfrac{\partial x}{\partial \eta_m} & \dfrac{\partial x}{\partial \zeta_m} \\[2mm] \dfrac{\partial y}{\partial \xi_m} & \dfrac{\partial y}{\partial \eta_m} & \dfrac{\partial y}{\partial \zeta_m} \\[2mm] \dfrac{\partial z}{\partial \xi_m} & \dfrac{\partial z}{\partial \eta_m} & \dfrac{\partial z}{\partial \zeta_m} \end{vmatrix} = \begin{array}{l} \tfrac{1}{2}\left(z_{m,4}\left(1 - \xi_m - \eta_m\right) + z_{m,5}\xi_m + z_{m,6}\eta_m - z_{m,1}\left(1 - \xi_m - \eta_m\right) - z_{m,2}\xi_m - z_{m,3}\eta_m \right) \\[2mm] \times \left[\left(x_{m,2} - x_{m,1}\right)\left(y_{m,3} - y_{m,1}\right) - \left(x_{m,3} - x_{m,1}\right)\left(y_{m,2} - y_{m,1}\right) \right] \end{array}$$

This Jaccobian allows to perform numerical integrations in direct space. The two cases of interest are the integration of the norm of an electronic envelope function and the integration of a Fröhlich matrix element.

Norm integration

$$\langle \psi | \psi \rangle = \int\limits_{crystal} d^3r \; \psi^*\!\left(\vec{r}\right)\psi\!\left(\vec{r}\right)$$

$$= \sum_m \int\limits_{element\,m} d^3r \left(\sum_{i=1}^{6} \psi^*_{m,i}\,\varphi_i\!\left(\xi_m\!\left(\vec{r}\right),\eta_m\!\left(\vec{r}\right),\zeta_m\!\left(\vec{r}\right)\right) \right)\!\left(\sum_{j=1}^{6} \psi_{m,j}\,\varphi_j\!\left(\xi_m\!\left(\vec{r}\right),\eta_m\!\left(\vec{r}\right),\zeta_m\!\left(\vec{r}\right)\right) \right)$$

$$= \sum_m \int\limits_0^1 d\xi \int\limits_0^{1-\xi} d\eta \int\limits_{-1}^1 d\zeta \; J_m\left(\xi,\eta,\zeta\right)\!\left(\sum_{i=1}^{6} \psi^*_{m,i}\,\varphi_i\left(\xi,\eta,\zeta\right) \right)\!\left(\sum_{j=1}^{6} \psi_{m,j}\,\varphi_j\left(\xi,\eta,\zeta\right) \right)$$

$$= \sum_m \sum_{i=1}^{6} \sum_{j=1}^{6} A_{m,i,j}\, \psi^*_{m,i}\, \psi_{m,j}$$

where $\quad A_{m,i,j} = \int\limits_0^1 d\xi \int\limits_0^{1-\xi} d\eta \int\limits_{-1}^1 d\zeta \; J_m\left(\xi,\eta,\zeta\right)\varphi_i\left(\xi,\eta,\zeta\right)\varphi_j\left(\xi,\eta,\zeta\right)$

The integration is laborious but straightforward. We find

$$A_{m,i,j} = \vec{c}_m \cdot \vec{d}_{(i,j)}$$

with

$$\vec{c}_m = -\tfrac{1}{720}\left[\left(x_{m,2} - x_{m,1}\right)\left(y_{m,3} - y_{m,1}\right) - \left(x_{m,3} - x_{m,1}\right)\left(y_{m,2} - y_{m,1}\right) \right]\left(z_1 - z_4, z_2 - z_5, z_3 - z_6\right)$$

$$\vec{d}_{(i,j)} = \begin{pmatrix} (12,4,4) & (4,4,2) & (4,2,4) & (6,2,2) & (2,2,1) & (2,1,2) \\ (4,4,2) & (4,12,4) & (2,4,4) & (2,2,1) & (2,6,2) & (1,2,2) \\ (4,2,4) & (2,4,4) & (4,4,12) & (2,1,2) & (1,2,2) & (2,2,6) \\ (6,2,2) & (2,2,1) & (2,2,1) & (12,4,4) & (4,4,2) & (4,2,4) \\ (2,2,1) & (2,6,2) & (1,2,2) & (4,4,2) & (4,12,4) & (2,4,4) \\ (2,1,2) & (1,2,2) & (2,2,6) & (4,2,4) & (2,4,4) & (4,4,12) \end{pmatrix}$$

Integration of a Fröhlich matrix element

The Fröhlich integral is developed as follows:

$$\int\limits_{crystal} d^3r\, e^{i\vec{q}\cdot\vec{r}}\, \psi_\tau^*\left(\vec{r}\right)\psi_{\tau'}\left(\vec{r}\right)$$

$$=\sum_m \int\limits_{element\,m} d^3r\; e^{i\vec{q}\cdot\vec{r}}\left(\sum_{i=1}^{6}\psi_{\tau,m,i}^*\,\varphi_i\left(\xi_m\left(\vec{r}\right),\eta_m\left(\vec{r}\right),\zeta_m\left(\vec{r}\right)\right)\right)\left(\sum_{j=1}^{6}\psi_{\tau',m,j}\,\varphi_j\left(\xi_m\left(\vec{r}\right),\eta_m\left(\vec{r}\right),\zeta_m\left(\vec{r}\right)\right)\right)$$

$$=\sum_m\sum_{i=1}^{6}\sum_{j=1}^{6}\psi_{\tau,m,i}^*\,\psi_{\tau',m,j}\int\limits_{element\,m} d^3r\; e^{i\vec{q}\cdot\vec{r}}\,\varphi_i\left(\xi_m\left(\vec{r}\right),\eta_m\left(\vec{r}\right),\zeta_m\left(\vec{r}\right)\right)\varphi_j\left(\xi_m\left(\vec{r}\right),\eta_m\left(\vec{r}\right),\zeta_m\left(\vec{r}\right)\right)$$

$$=\sum_m\sum_{i=1}^{6}\sum_{j=1}^{6}\psi_{\tau,m,i}^*\,\psi_{\tau',m,j}\int_0^1 d\xi\int_0^{1-\xi} d\eta\int_{-1}^{1} d\zeta\, J_m\left(\xi,\eta,\zeta\right)e^{i\vec{q}\cdot\vec{r}(\xi,\eta,\zeta)}\,\varphi_i\left(\xi,\eta,\zeta\right)\varphi_j\left(\xi,\eta,\zeta\right)$$

The remaining integral,

$$\int_0^1 d\xi\int_0^{1-\xi} d\eta\int_{-1}^{1} d\zeta\, J_m\left(\xi,\eta,\zeta\right)e^{i\vec{q}\cdot\vec{r}(\xi,\eta,\zeta)}\,\varphi_i\left(\xi,\eta,\zeta\right)\varphi_j\left(\xi,\eta,\zeta\right),$$

can be computed in different ways:

1) Analytical: possible, but slow and complicated (about 100 exponentials)

2) Numerical: possible, but slow

3) Approximated: relatively fast

$$\int_0^1 d\xi\int_0^{1-\xi} d\eta\int_{-1}^{1} d\zeta\, J_m\left(\xi,\eta,\zeta\right)e^{i\vec{q}\cdot\vec{r}_m(\xi,\eta,\zeta)}\,\varphi_i\left(\xi,\eta,\zeta\right)\varphi_j\left(\xi,\eta,\zeta\right)$$

$$\approx e^{i\vec{q}\cdot\vec{r}_m}\int_0^1 d\xi\int_0^{1-\xi} d\eta\int_{-1}^{1} d\zeta\, J_m\left(\xi,\eta,\zeta\right)\,\varphi_i\left(\xi,\eta,\zeta\right)\varphi_j\left(\xi,\eta,\zeta\right)=e^{i\vec{q}\cdot\vec{r}_m}\,A_{m,i,j}$$

In our problem, the third method has been used, which is well justified by the slow variation of the exponential compared to the mesh density. In deed, the maximal relevant wavevector yields a magnitude smaller than $q_{max}\sim 0.5nm^{-1}$, whereas the node step in the relevant zones is in the order of $d_{min}\sim 0.05nm$. The error induced by the third approximation can thus be shown to be smaller than 1%.

8.3.2 Reciprocal space discretization

The underlying Bravais lattice of GaAs is a face-centered cubic lattice with conventional cubic cell has side $a\simeq 0.565\text{Å}$. Its reciprocal lattice is a body-centered cubic lattice with conventional cubic cell of side $s=4\pi/a\simeq 22.24nm^{-1}$. The normal mode wavevectors $\vec{q}$ are confined to a primitive cell of the reciprocal lattice, usually taken as the first Brillouin zone. The latter is a truncated octahedron with large radius $s/2\simeq 11.12nm^{-1}$ and small radius $s\sqrt{3}/4\simeq 9.63nm^{-1}$ (see Fig. 22).
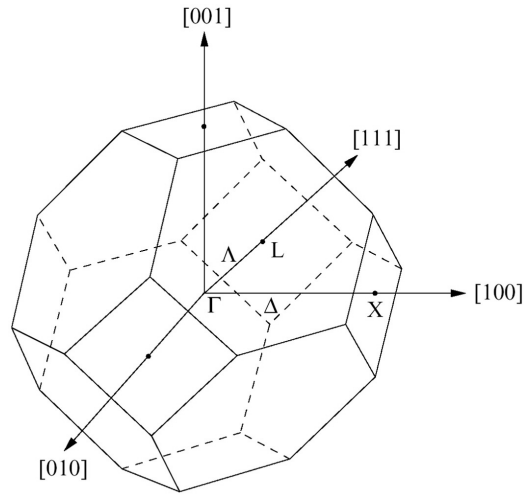
Fig. 22: First Brillouin zone of the body-centered cubic lattice

The Fröhlich matrix elements are subject to strong variation with wavevector $\vec{q}$. A good discretization accounts for this dependence by a varying point density. The latter is achieved by an *irregular discretization*, which is *adaptively* refined in the regions of strong variation of the Fröhlich elements.

In an irregular discretization the volume Ω_i surrounding a given wave vector $\vec{q}_i$ enters the calculation of the Fröhlich elements (see 8.3.3). Therefore, each vector $\vec{q}_i$ is assigned a volume Ω_i, taken as the volume of its Wigner-Seitz-cell. This cell is defined as the region of all the points $\vec{q}$ that are closer to $\vec{q}_i$ than to any other vector $\vec{q}_i$, $j \neq i$.

How does the refinement work? To generate the well adapted irregular mesh, a regular initial mesh with a small number of points is created. Then, the Wigner-Seitz-volume of each mesh node is computed. Simultaneously, each node is associated a neighbor-list, containing all the neighbors with touching Wigner-Seitz-cells. Thereafter, the Fröhlich matrix element associated with each mesh node is evaluated and polaron spectrum of the given mesh is computed. For each pair of neighbors the fluctuation of the Fröhlich matrix element is evaluated. The neighbors with the highest fluctuation are added a new node in between. The same procedure is repeated until convergence of the polaron spectrum is obtained. The convergence is reached if the maximal variation of all the polaron energies between two successive steps is smaller than a preset threshold.

Fig. 23 shows a two-dimensional example of the meshing in two successive steps. Starting with a regular mesh in q-space (black), the Fröhlich elements of each node are evaluated. The neighbors with the highest fluctuation are chosen for further refinement (blue). The resulting new mesh is less regular and admits more sophisticated Wigner-Seitz volumes (red)
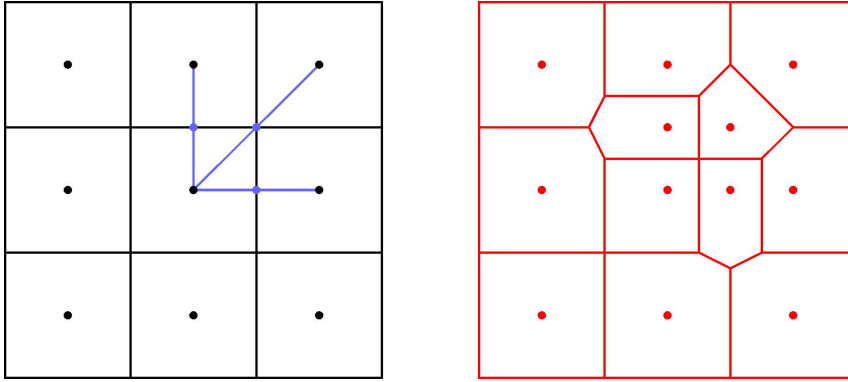
Fig. 23: Two-dimensional visualization of adaptive refinement. Black: initial discretization, red: first refinement, blue: neighbors with highest fluctuation.

A more realistic, three-dimensional visualization of the adaptive irregular meshing of the first Brillouin zone is given in Fig. 24.
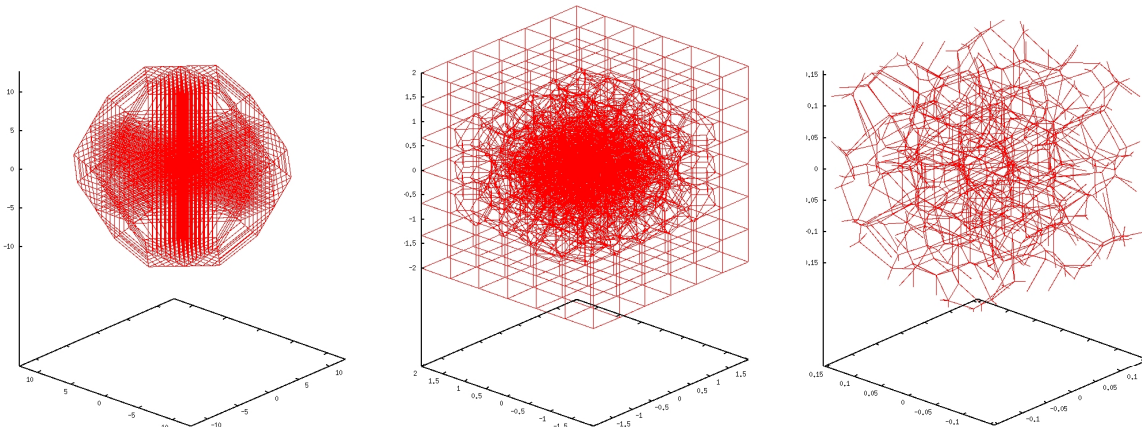
Fig. 24: Adaptive discretization of the first Brillouin zone. Only the Wigner-Seitz-cells are drawn. Left: total zone, middle: zoomed to center by a factor 10, right: zoomed to center by a factor 100.

This adaptive construction of an irregular discretization with simultaneous evaluation of the Wigner-Seitz volume defines a complex computational problem that demands sophisticated programming structures. The effort seems nevertheless well justified by considering the following advantages:

- The polaron spectrum computed based on an adaptive irregular mesh is shown to converge with *500* wavevectors $\vec{q}_i$, whereas an optimized regular mesh requires more than *100'000* wavevectors to achieve the same precision. (convergence threshold = *$1\mu eV$*)

- The mesh adapts itself to any arbitrary set of envelope functions. Thus, the method can be used without modifications to investigate other dot structures.

- The structure of the adaptively created mesh, carefully visualized, gives itself an insight in the physics.

8.3.3   Derivation of the Fröhlich Hamiltonian with irregular discretization

Regular infinitesimal discretization

This section prepares the transcription of the Fröhlich Hamiltonian to an irregular finite discretization. The Fröhlich Hamiltonian is given by (see section 3.2.2)

$$H^{Fr\ddot{o}hlich} = \sum_{i=1}^{N} \sum_{\nu\mu} \left(M_{\nu\mu}^{\vec{q}_i} a_\nu^\dagger a_\mu d_{\vec{q}_i} + M_{\nu\mu}^{\vec{q}_i *} a_\mu^\dagger a_\nu d_{\vec{q}_i}^\dagger \right)$$

with $M_{\nu\mu}^{\vec{q}_i} = \dfrac{\lambda}{q_i\sqrt{V}} \displaystyle\int_{\mathbb{R}^3} d^3x \; e^{i\vec{q}_i \cdot \vec{x}} \psi_\nu^*(\vec{x}) \psi_\mu(\vec{x})$, where λ is a complex constant

The cubic quantization volume V, supposed to become infinitely large, implies a regular discretization of the reciprocal space, since the wavevectors $\vec{q}$ satisfy the periodic boundary conditions of this volume. Explicitly, if v_x, v_y and v_z design the sides of the volume V, then every $\vec{q} = (q_x, q_y, q_z)$ satisfies

$$e^{iq_x v_x} = 1 \qquad \Leftrightarrow \qquad q_x \in \frac{2\pi}{v_x}\mathbb{Z} \qquad \Rightarrow \qquad \Delta q_x = \frac{2\pi}{v_x}$$

In the same way

$$\Delta q_y = \frac{2\pi}{v_y} \quad \text{and} \quad \Delta q_z = \frac{2\pi}{v_z}.$$

Thus, the volume ω associated with each wavevector is given by

$$\omega = \Delta q_x \Delta q_y \Delta q_z = \frac{(2\pi)^3}{v_x v_y v_z} = \frac{8\pi^3}{V}$$

This volume becomes infinitesimal as V becomes infinite. In the Fröhlich Hamiltonian V is replaced by ω,

$$M_{\nu\mu}^{\vec{q}_i} = \frac{\lambda\sqrt{\omega}}{8\pi^3 q_i} \int_{\mathbb{R}^3} d^3x \; e^{i\vec{q}_i \cdot \vec{x}} \psi_\nu^*(\vec{x}) \psi_\mu(\vec{x})$$

For further use we introduce

$$\vartheta_{\nu\mu}^{\vec{q}_i} = \frac{\lambda}{8\pi^3} \int_{\mathbb{R}^3} d^3x \; e^{i\vec{q}_i \cdot \vec{x}} \psi_\nu^*(\vec{x}) \psi_\mu(\vec{x}) \quad \text{such that} \quad M_{\nu\mu}^{\vec{q}_i} = \frac{\sqrt{\omega}}{q_i} \vartheta_{\nu\mu}^{\vec{q}_i}$$

The non-vanishing matrix elements of the Hamiltonian in the natural basis write

- $\langle \nu\, 0 | H | \mu\, 0 \rangle = \delta_{\nu\mu} \varepsilon_\nu$

- $\left\langle \nu\, 0 \left| H \left(\sum_{i=1}^{N} | \tau\, 1\vec{q}_i \rangle \langle \tau\, 1\vec{q}_i | H | \mu\, 0 \right) \right. \right\rangle = \sum_{i=1}^{N} \langle \nu\, 0 | H | \tau\, 1\vec{q}_i \rangle \langle \tau\, 1\vec{q}_i | H | \mu\, 0 \rangle = \sum_{i=1}^{N} M_{\nu\tau}^{\vec{q}_i} M_{\tau\mu}^{\vec{q}_i}$

$$\bullet \quad \left(\sum_{i=1}^{N} \langle v \; 0 | H | \tau \; 1\vec{q}_i \rangle \langle \tau \; 1\vec{q}_i | \right) H \left(\sum_{i=1}^{N} | \tau \; 1\vec{q}_i \rangle \langle \tau \; 1\vec{q}_i | H | \mu \; 0 \rangle \right)$$

$$= \varepsilon_{\tau + LO} \sum_{i=1}^{N} \langle v \; 0 | H | \tau \; 1\vec{q}_i \rangle \langle \tau \; 1\vec{q}_i | H | \mu \; 0 \rangle = \varepsilon_{\tau + LO} \sum_{i=1}^{N} M_{v\tau}^{\vec{q}_i} M_{\tau\mu}^{\vec{q}_i}$$

We conclude that the matrix elements of the reduced Hamiltonian, whose dimension does not depend on the number of normal modes N, depend on the original Fröhlich elements through the sums

$$\sum_{i=1}^{N} M_{v\tau}^{\vec{q}_i} M_{\tau\mu}^{\vec{q}_i} = \sum_{i=1}^{N} \frac{g_{v\tau}^{\vec{q}_i} \sqrt{\omega}}{q_i} \frac{g_{\tau\mu}^{\vec{q}_i} \sqrt{\omega}}{q_i}$$

This feature will be used in the irregular discretization.

Irregular finite discretization

We consider now an irregular finite partition of the first Brillouin zone in M volumes Ω_j, $j = 1, ..., M$, much larger than ω and inside each of which the Fröhlich integral is approximated by a constant. f defines the application, which associates to each wavevector index i the index j of its surrounding volume Ω_j. Each Ω_j is ascribed a vector $\vec{Q}_j$ indicating a point inside Ω_j, usually taken as the bar center. The invariance of the Fröhlich integral inside each volume Ω_j translates to

$$g_{\tau\tau'}^{\vec{q}_i} = g_{\tau\tau'}^{\vec{q}_k} \equiv g_{\tau\tau'}^{\vec{Q}_j} \quad \text{if } f(i) = f(k).$$

The sum above writes

$$\sum_{i=1}^{N} M_{v\tau}^{\vec{q}_i} M_{\tau\mu}^{\vec{q}_i} = \sum_{i=1}^{N} \frac{g_{v\tau}^{\vec{q}_i} \sqrt{\omega}}{q_i} \frac{g_{\tau\mu}^{\vec{q}_i} \sqrt{\omega}}{q_i} = \sum_{j=1}^{M} g_{v\tau}^{\vec{Q}_j} g_{\tau\mu}^{\vec{Q}_j} \omega \sum_{f(i)=j} \frac{1}{q_i^2}$$

The second sum goes over Ω_j / ω terms. If the volumes ω become infinitesimal, the sum can be written as a continuous average, i.e.

$$\sum_{f(i)=j} \frac{1}{q_i^2} = \frac{\Omega_j}{\omega} \left\langle \frac{1}{q^2} \right\rangle_{\Omega_j}$$

Thus

$$\sum_{i=1}^{N} M_{v\tau}^{\vec{q}_i} M_{\tau\mu}^{\vec{q}_i} = \sum_{j=1}^{M} g_{v\tau}^{\vec{Q}_j} g_{\tau\mu}^{\vec{Q}_j} \Omega_j \left\langle \frac{1}{q^2} \right\rangle_{\Omega_j} = \sum_{j=1}^{M} \left(g_{v\tau}^{\vec{Q}_j} \sqrt{\Omega_j} \sqrt{\left\langle \frac{1}{q^2} \right\rangle_{\Omega_j}} \right) \left(g_{\tau\mu}^{\vec{Q}_j} \sqrt{\Omega_j} \sqrt{\left\langle \frac{1}{q^2} \right\rangle_{\Omega_j}} \right)$$

We merely recognize the terms

$$M_{v\mu}^{irreg \; \vec{Q}_j} = g_{v\tau}^{\vec{Q}_j} \sqrt{\Omega_j} \sqrt{\left\langle \frac{1}{q^2} \right\rangle_{\Omega_j}}$$

as the suitable substitutions of the terms

$$M_{\nu\mu}^{\vec{q}_i} = \frac{\sqrt{\omega}}{q_i} \, \vartheta_{\nu\mu}^{\vec{q}_i} \, .$$

We conclude that the transcription to an irregular finite discretization is achieved by replacing two replacements:

- replace constant volumes ω with the variable volumes Ω_j

- replace $\dfrac{1}{q_i}$ with $\sqrt{\left\langle \dfrac{1}{q^2} \right\rangle_{\Omega_j}}$

The first replacement is ascribed to the passage from a regular to an irregular discretization and the second replacement rises from the passage from infinitesimal to finite elements. The description of the irregular finite discretization comprehends, of course, finite regular discretizations. The latter require only the second replacement.

The following table summarizes the mathematical transcription between a regular infinitesimal discretization and an irregular finite discretization.

	Regular infinitesimal discretization $\Leftrightarrow$ Irregular finite discretization	
Wavevectors	$\vec{q}_i$, $i = 1, ..., N$ (regular)	$\Leftrightarrow$ $\vec{Q}_j$, $j = 1, ..., M$ (irregular)
Reciprocal space volumes	$\omega = \dfrac{8\pi^3}{V}$ (constant)	$\Leftrightarrow$ Ω_j (variable)
Fröhlich matrix elements	$M_{\nu\mu}^{\vec{q}_i} = \dfrac{\sqrt{\omega}}{q_i} \vartheta_{\nu\mu}^{\vec{q}_i}$	$\Leftrightarrow$ $M_{\nu\mu}^{irreg\,\vec{Q}_j} = \vartheta_{\nu\tau}^{\vec{Q}_j} \sqrt{\Omega_j} \sqrt{\left\langle \dfrac{1}{q^2} \right\rangle_{\Omega_j}}$
Fröhlich Hamiltonian	$\displaystyle\sum_{i=1}^{N} \sum_{\nu\mu} M_{\nu\mu}^{\vec{q}_i} a_\nu^\dagger a_\mu d_{\vec{q}_i} + h.c.$	$\Leftrightarrow$ $\displaystyle\sum_{j=1}^{M} \sum_{\nu\mu} M_{\nu\mu}^{irreg\,\vec{Q}_j} a_\nu^\dagger a_\mu d_{\vec{Q}_j} + h.c.$

Tab. 10: Transcription of the Fröhlich Hamiltonian to an irregular finite discretization

We recall that

$$\vartheta_{\nu\mu}^{\vec{q}_i} = \frac{\lambda}{8\pi^3} \int_{\mathbb{R}^3} d^3x \; e^{i\vec{q}_i \cdot \vec{x}} \psi_\nu^*(\vec{x}) \psi_\mu(\vec{x})$$

$$\lambda = \sqrt{\frac{\hbar\omega_{LO} e^2}{2\varepsilon_0 V q_i^2} \left(\frac{1}{\varepsilon_\infty} - \frac{1}{\varepsilon_r} \right)} \approx 3.444 \cdot 10^{-25} \, J \, m^{1/2} = 6.797 \cdot 10^{-2} \, eV \, nm^{1/2} \qquad \text{(GaAs)}$$

The numerical values of the physical parameters were taken from [21]:

$$\hbar\omega_{LO} = 35.9 \, meV \, , \; \varepsilon_\infty = 10.9 \, , \; \varepsilon_r = 12.9 \; \lambda \approx 3.444 \cdot 10^{-25} \, J \, m^{1/2} = 6.797 \cdot 10^{-2} \, eV \, nm^{1/2}$$

8.3.4   Relations between direct and reciprocal space discretization

The reciprocal space contains the normal mode wavevectors $\vec{q}$. They are used to evaluate the Fröhlich integral

$$\int\limits_{crystal} d^3r\, e^{i\vec{q}\cdot\vec{r}}\, \psi_\tau^*\left(\vec{r}\right)\psi_{\tau'}\left(\vec{r}\right),$$

which is represents spatial frequency analysis of the function $f\left(\vec{r}\right)=\psi_\tau^*\left(\vec{r}\right)\psi_{\tau'}\left(\vec{r}\right)$.

Fourier's theory of frequency analysis yields limiting relationships between direct and reciprocal space discretization: A one-dimensional function, that is known on an interval $\left[0,X\right]$ in discrete points separated by Δx, can be spectrally analyzed on the interval $\left[0,1/2\Delta x\right]$ with a maximal resolution of $\Delta v_{min}=1/2X$.

In the present context, the mesh of the three-dimensional direct space is considered as given. It has a maximal diameter d_{max} and a minimum separation between neighboring nodes of d_{min}. Analogically to the one-dimensional case, those parameters set an upper limit for the reciprocal space radius and lower limit for the element volumes.

The highest frequency resolution is obtained in the direction of the maximal diameter and corresponds to $\Delta v_{min}=1/2d_{max}$. There is no use for two wavevectors to be separated less than Δv_{min}. This is the order of the smallest element size, which should be considered. Further refinement does not alter the computation result, but generates useless operations.

The highest frequency that can be accounted for is given by the smallest direct space step,

$$q\leq q_{max}=\frac{1}{2d_{min}}\,.$$

The present mesh (created by F. Michelini to compute the envelope functions [1, 2]) works with minimal node distance in the relevant zone of $d_{min}\approx 0.05nm$, leading to $q_{max}\approx 10nm^{-1}$. This is coherent with the size of the first Brillouin zone.

8.4   Mathematical extensions and demonstrations

8.4.1   Eigensystem of the dynamical matrix

In this section we that the non-symmetrical matrix $\left(\mathcal{M}^{-1}\mathcal{D}\right)$ has a positive non-degenerate spectrum with eigenvectors X_α that can be orthonormalized in the sense

$$X_\alpha^T \mathcal{M} X_\beta = \delta_{\alpha\beta} \, .$$

First note that a symmetrical matrix S, which is multiplied at left and right with a diagonal matrix D is again a symmetrical matrix. Demonstration:

$$\left(DSD\right)^T = D^T S^T D^T = DSD$$

Thus the matrix $\left(\sqrt{\mathcal{M}^{-1}}\,\mathcal{D}\sqrt{\mathcal{M}^{-1}}\right)$ is symmetrical and positive. It can be diagonalized, the eigenvectors being orthogonal and the eigenvalues being positive.

$$\sqrt{\mathcal{M}^{-1}}\,\mathcal{D}\sqrt{\mathcal{M}^{-1}}\,Y_\alpha = \omega_\alpha^2\,Y_\alpha$$

The positivity of the eigenvalues is expressed in their form of squared real numbers. The orthogonality of the eigenvectors and the choice of unitary norms give the orthonormalization relations

$$Y_\alpha^T\,Y_\beta = \delta_{\alpha\beta}$$

Multiplying the eigensystem at left with $\sqrt{\mathcal{M}^{-1}}$ yields

$$\mathcal{M}^{-1}\mathcal{D}\left(\sqrt{\mathcal{M}^{-1}}\,Y\right)_\alpha = \omega_\alpha^2\left(\sqrt{\mathcal{M}^{-1}}\,Y_\alpha\right)$$

We can thus substitute $X_\alpha \equiv \sqrt{\mathcal{M}^{-1}}\,Y_\alpha$, which gives

$$\left(\mathcal{M}^{-1}\mathcal{D}\right)X_\alpha = \omega_\alpha^2\,X_\alpha$$

By inversing the substitution, $Y_\alpha = \sqrt{\mathcal{M}}\,X_\alpha$, the orthonormality relations become

$$X_\alpha^T \mathcal{M} X_\beta = \delta_{\alpha\beta}$$

which concludes the demonstration.

8.4.2   Second quantization method

All 1-body functions of the electronic position operators can be written in second quantization by the relation

$$\sum_{v=1}^{n} f\left(\vec{r}_v\right) = \int_{\mathbb{R}^3} d^3x\, f\left(\vec{x}\right) \cdot \mathbb{D}\left(\vec{x}\right)$$

We apply this relation to the operator $W^{(0)}$:

$$W^{(0)} = W_{e^- - modes}^{res}\left(\vec{R}.^{(0)}\right) = -\frac{e^2}{4\pi\varepsilon_0} \sum_{\mu=1}^{N} \sum_{v=1}^{n} \left[\frac{Z_\mu}{\left|\vec{r}_v - \vec{R}_\mu^{(0)} \cdot \mathbb{1}_{electrons}\right|} \right] - E_0\left(\vec{R}.^{(0)}\right) \cdot \mathbb{1}_{electrons} \ .$$

The first term transforms to second quantization as follows:

$$\sum_{v=1}^{n} \frac{Z_\mu}{\left|\vec{r}_v - \vec{R}_\mu \cdot \mathbb{1}_{electrons}\right|} = \int_{\mathbb{R}^3} d^3x\, \frac{Z_\mu \cdot \mathbb{D}\left(\vec{x}\right)}{\left|\vec{x} - \vec{R}_\mu \cdot \mathbb{1}_{electrons}\right|}$$

For the second term inside the brackets, we use the following relation, which imme-diately derives from the definition of $E_0\left(\vec{R}.\right)$:

$$E_0\left(\vec{R}.\right) = \left\langle \psi_0 \left| \left\{ \sum_{v=1}^{n} \frac{\vec{p}_v^2}{2m_e} + \frac{e^2}{8\pi\varepsilon_0} \sum_{v\neq v'} \frac{1}{\left|\vec{r}_v - \vec{r}_{v'}\right|} - \frac{e^2}{4\pi\varepsilon_0} \sum_{\mu=1}^{N} \sum_{v=1}^{n} \frac{Z_\mu}{\left|\vec{r}_v - \vec{R}_\mu \cdot \mathbb{1}_{electrons}\right|} \right\} \right| \psi_0 \right\rangle$$

Since we are only interested in the derivates of $W^{(0)}$ with respect to the ionic coordi-nates, we can merely neglect the first to terms of $E_0\left(\vec{R}.\right)$.:

$$E_0\left(\vec{R}.^{(0)}\right) \rightarrow \left\langle \psi_0 \left| \left\{ -\frac{e^2}{4\pi\varepsilon_0} \sum_{\mu=1}^{N} \sum_{v=1}^{n} \frac{Z_\mu}{\left|\vec{r}_v - \vec{R}_\mu^{(0)} \cdot \mathbb{1}_{electrons}\right|} \right\} \right| \psi_0 \right\rangle = -\frac{e^2}{4\pi\varepsilon_0} \sum_{\mu=1}^{N} \int_{\mathbb{R}^3} d^3x\, \frac{Z_\mu \cdot \left\langle \psi_0 \left| \mathbb{D}\left(\vec{x}\right) \right| \psi_0 \right\rangle}{\left|\vec{x} - \vec{R}_\mu^{(0)} \cdot \mathbb{1}_{electrons}\right|}$$

Replacing those expressions yields

$$W^{(0)} \rightarrow \ \mathbb{W}^{(0)} = -\int_{\mathbb{R}^3} d^3x \sum_{\mu=1}^{N} \frac{e^2 Z_\mu}{4\pi\varepsilon_0} \frac{\mathbb{D}\left(\vec{x}\right) - \left\langle \psi_0 \left| \mathbb{D}\left(\vec{x}\right) \right| \psi_0 \right\rangle \cdot \mathbb{1}_{electrons}}{\left|\vec{x} - \vec{R}_\mu^{(0)} \cdot \mathbb{1}_{electrons}\right|}$$

8.4.3 Second quantization of the crystal

$$\mathbb{W} = \sum_{(\vec{l},\vec{b}),\vec{k},\vec{k}',\sigma} \int_{\mathbb{R}^3} d^3x\, U_{\vec{b}}\left(\vec{x} - \vec{R}_{(\vec{l},\vec{b})}^{(0)}\right) u_{\vec{k}'}^*\left(\vec{x}\right) u_{\vec{k}}\left(\vec{x}\right) e^{i\left(\vec{k}-\vec{k}'\right)\cdot\vec{x}} a_{\vec{k}',\sigma}^{\dagger} a_{\vec{k},\sigma}$$

$$\mathbb{F}_{(\vec{q},j)}^{(1)} = \mathcal{D}_{(\vec{q},j)} \mathbb{W}$$

$$= \sum_{(\vec{l}',\vec{b}')} \vec{X}_{(\vec{q},j),(\vec{l}',\vec{b}')} \frac{\partial}{\partial\vec{R}_{(\vec{l}',\vec{b}')}^{(0)}} \sum_{(\vec{l},\vec{b}),\vec{k},\vec{k}',\sigma} \int_{\mathbb{R}^3} d^3x\, U_{\vec{b}}\left(\vec{x} - \vec{R}_{(\vec{l},\vec{b})}^{(0)}\right) u_{\vec{k}'}^*\left(\vec{x}\right) u_{\vec{k}}\left(\vec{x}\right) e^{i\left(\vec{k}-\vec{k}'\right)\cdot\vec{x}} a_{\vec{k}',\sigma}^{\dagger} a_{\vec{k},\sigma}$$

$$= \sum_{(\vec{l},\vec{b}),\vec{k},\vec{k}',\sigma} \vec{X}_{(\vec{q},j),(\vec{l}',\vec{b}')} \int_{\mathbb{R}^3} d^3x\, \left[\frac{\partial}{\partial\vec{R}_{(\vec{l},\vec{b})}^{(0)}} U_{\vec{b}}\left(\vec{x} - \vec{R}_{(\vec{l},\vec{b})}^{(0)}\right) \right] u_{\vec{k}'}^*\left(\vec{x}\right) u_{\vec{k}}\left(\vec{x}\right) e^{i\left(\vec{k}-\vec{k}'\right)\cdot\vec{x}} a_{\vec{k}',\sigma}^{\dagger} a_{\vec{k},\sigma}$$

$$\tilde{U}(\vec{K}) = \frac{1}{(2\pi)^{3/2}} \int_{\mathbb{R}^3} d^3x \, U(\vec{x}) e^{-i\vec{K}\cdot\vec{x}} \qquad \leftrightarrow \qquad U(\vec{x}) = \frac{1}{(2\pi)^{3/2}} \int_{\mathbb{R}^3} d^3K \, \tilde{U}(\vec{K}) e^{i\vec{K}\cdot\vec{x}}$$

$$\mathbb{F}_{(\vec{q},j)}^{(1)} = \frac{1}{(2\pi)^{3/2}} \sum_{(\vec{l},\vec{b}),\vec{k},\vec{k}',\sigma} \vec{X}_{(\vec{q},j),(\vec{l},\vec{b}')} \int_{\mathbb{R}^3} d^3x \left[\frac{\partial}{\partial \vec{R}_{(\vec{l},\vec{b})}^{(0)}} \int_{\mathbb{R}^3} d^3K \, \tilde{U}(\vec{K}) e^{i\vec{K}\cdot\left(\vec{x}-\vec{R}_{(\vec{l},\vec{b})}^{(0)}\right)} \right] u_{\vec{k}'}^*(\vec{x}) u_{\vec{k}}(\vec{x}) e^{i(\vec{k}-\vec{k}')\cdot\vec{x}} a_{\vec{k}',\sigma}^\dagger a_{\vec{k},\sigma}$$

$$= -\frac{i}{(2\pi)^{3/2}} \sum_{(\vec{l},\vec{b}),\vec{k},\vec{k}',\sigma} \vec{X}_{(\vec{q},j),(\vec{l},\vec{b}')} \int_{\mathbb{R}^3} d^3x \int_{\mathbb{R}^3} d^3K \, \vec{K} \, \tilde{U}(\vec{K}) e^{i\vec{K}\cdot\left(\vec{x}-\vec{R}_{(\vec{l},\vec{b})}^{(0)}\right)} u_{\vec{k}'}^*(\vec{x}) u_{\vec{k}}(\vec{x}) e^{i(\vec{k}-\vec{k}')\cdot\vec{x}} a_{\vec{k}',\sigma}^\dagger a_{\vec{k},\sigma}$$

$$= -\frac{i}{(2\pi)^{3/2}} \sum_{(\vec{l},\vec{b}),\vec{k},\vec{k}',\sigma} \vec{X}_{(\vec{q},j),(\vec{l},\vec{b}')} \int_{\mathbb{R}^3} d^3K \, \vec{K} \, \tilde{U}(\vec{K}) e^{-i\vec{K}\cdot\vec{R}_{(\vec{l},\vec{b})}^{(0)}} \left[\int_{\mathbb{R}^3} d^3x \, e^{i(\vec{K}+\vec{k}-\vec{k}')\cdot\vec{x}} u_{\vec{k}'}^*(\vec{x}) u_{\vec{k}}(\vec{x}) \right] a_{\vec{k}',\sigma}^\dagger a_{\vec{k},\sigma}$$

Since $u_{\vec{k}'}^*(\vec{x}) u_{\vec{k}}(\vec{x})$ has the periodicity of the Bravais lattice, the integral over x can only be different from zero if the exponential also has the periodicity of the Bravais lattice. Therefore $(\vec{K} + \vec{k} - \vec{k}')$ has to be an element of the reciprocal lattice, i.e.

$$\vec{K} + \vec{k} - \vec{k}' = \vec{G} \in RL$$

$$\mathbb{F}_{(\vec{q},j)}^{(1)} = -\frac{i}{(2\pi)^{3/2}} \sum_{(\vec{l},\vec{b}),\vec{k},\vec{k}',\sigma,\vec{G}} \vec{X}_{(\vec{q},j),(\vec{l},\vec{b}')} \left(\vec{G} - \vec{k} + \vec{k}'\right) \tilde{U}\left(\vec{G} - \vec{k} + \vec{k}'\right) e^{-i\left(\vec{G}-\vec{k}+\vec{k}'\right)\cdot\vec{R}_{(\vec{l},\vec{b})}^{(0)}}$$

$$\times \left[\int_{\mathbb{R}^3} d^3x \, e^{i\vec{G}\cdot\vec{x}} u_{\vec{k}'}^*(\vec{x}) u_{\vec{k}}(\vec{x}) \right] a_{\vec{k}',\sigma}^\dagger a_{\vec{k},\sigma}$$

$$= -\frac{i}{(2\pi)^{3/2} \sqrt{NM_{\vec{b}}}} \sum_{(\vec{l},\vec{b}),\vec{k},\vec{k}',\sigma,\vec{G}} \vec{\epsilon}_{(\vec{q},j),\vec{b}} \, e^{i\vec{q}\cdot\vec{l}} \left(\vec{G} - \vec{k} + \vec{k}'\right) \tilde{U}\left(\vec{G} - \vec{k} + \vec{k}'\right) e^{-i\left(\vec{G}-\vec{k}+\vec{k}'\right)\cdot\left(\vec{l}+\vec{b}\right)}$$

$$\times \left[\int_{\mathbb{R}^3} d^3x \, e^{i\vec{G}\cdot\vec{x}} u_{\vec{k}'}^*(\vec{x}) u_{\vec{k}}(\vec{x}) \right] a_{\vec{k}',\sigma}^\dagger a_{\vec{k},\sigma}$$

$$= -\frac{i}{(2\pi)^{3/2} \sqrt{NM_{\vec{b}}}} \sum_{\vec{b},\vec{k},\vec{k}',\sigma,\vec{G}} \vec{\epsilon}_{(\vec{q},j),\vec{b}} \left[\sum_{\vec{l}} e^{i\left(\vec{q}-\vec{G}+\vec{k}-\vec{k}'\right)\cdot\vec{l}} \right] \left(\vec{G} - \vec{k} + \vec{k}'\right) \tilde{U}\left(\vec{G} - \vec{k} + \vec{k}'\right) e^{-i\left(\vec{G}-\vec{k}+\vec{k}'\right)\cdot\vec{b}}$$

$$\times \left[\int_{\mathbb{R}^3} d^3x \, e^{i\vec{G}\cdot\vec{x}} u_{\vec{k}'}^*(\vec{x}) u_{\vec{k}}(\vec{x}) \right] a_{\vec{k}',\sigma}^\dagger a_{\vec{k},\sigma}$$

Since there is a very large number of ions N,

$$\sum_{\vec{l}} e^{i\left(\vec{q}-\vec{G}+\vec{k}-\vec{k}'\right)\cdot\vec{l}} = \begin{cases} N & \text{if } \vec{q} - \vec{G} + \vec{k} - \vec{k}' = 0 \\ 0 & \text{otherwise} \end{cases}$$

Thus

$$\mathbb{F}_{(\vec{q},j)}^{(1)} = -i \sqrt{\frac{N}{(2\pi)^3 M_{\vec{b}}}} \sum_{\vec{b},\vec{k},\vec{k}',\sigma} \vec{\epsilon}_{(\vec{q},j),\vec{b}} \cdot \vec{q} \, \tilde{U}(\vec{q}) e^{-i\vec{q}\cdot\vec{b}} \left[\int_{\mathbb{R}^3} d^3x \, e^{i\left(\vec{q}+\vec{k}+\vec{k}'\right)\cdot\vec{x}} u_{\vec{k}'}^*(\vec{x}) u_{\vec{k}}(\vec{x}) \right] a_{\vec{k}',\sigma}^\dagger a_{\vec{k},\sigma}$$

if $\vec{q} + \vec{k} - \vec{k}' \in RL$ and $\mathbb{F}_{(\vec{q},j)}^{(1)} = 0$ otherwise.

8.4.4   Theorem (stable subspaces)

Consider the decomposition

$$\mathcal{H} = \mathcal{H}_{0ph} \oplus \left(\mathcal{H}_{A,1} \oplus \mathcal{H}_{B,1} \right) \oplus \ldots \oplus \left(\mathcal{H}_{A,n-g} \oplus \mathcal{H}_{B,n-g} \right)$$

with

$$\mathcal{H}_{A,\tau} \equiv P_{1ph+\tau} \left(H \mathcal{H}_{0ph} \right) \subseteq \mathcal{H}_{1ph+\tau} \quad \text{and}$$

$$\mathcal{H}_{B,\tau} \perp \mathcal{H}_{A,\tau} \quad \text{such that} \quad \mathcal{H}_{A,\tau} \oplus \mathcal{H}_{B,\tau} = \mathcal{H}_{1ph+\tau}$$

To prove that the spaces $\mathcal{H}_{B,\tau}$ are stable with respect to the Hamiltonian operator H, it is necessary and sufficient to show that

(1) $\mathcal{H}_{B,\tau}$ has zero projection on $H\mathcal{H}_{0\,ph}$

(2) $\mathcal{H}_{B,\tau}$ has zero projection on $H\mathcal{H}_{B,\nu}$ for $\nu \neq \tau$

(3) $\mathcal{H}_{B,\tau}$ has zero projection on $H\mathcal{H}_{A,\nu}$ for all ν

Before proving those properties, it is helpful to introduce a basis $\left\{ \left| \alpha^{(\tau)} \right\rangle \right\}$ of $\mathcal{H}_{A,\tau}$ and a basis $\left\{ \left| \beta^{(\tau)} \right\rangle \right\}$ of $\mathcal{H}_{B,\tau}$:

$$\left| \alpha^{(\tau)} \right\rangle \equiv \sum_{i=1}^{N} \left| \tau \; 1\vec{q}_i \right\rangle \left\langle \tau \; 1\vec{q}_i \left| H \right| \alpha \; 0 \right\rangle$$

$$\left| \beta^{(\tau)} \right\rangle \equiv \sum_{j=1}^{N} \lambda_j^{(\tau,\beta)} \left| \tau \; 1\vec{q}_j \right\rangle$$

The coefficients $\lambda_j^{(\tau,\beta)}$ are such that the orthogonality condition $\left\langle \alpha^{(\tau)} \left| \beta^{(\tau)} \right\rangle = 0 \right.$ is satisfied. Explicitly,

$$\left\langle \alpha^{(\tau)} \left| \beta^{(\tau)} \right\rangle = \sum_{i=1}^{N} \sum_{j=1}^{N} \lambda_j^{(\tau,\beta)} \left\langle \alpha \; 0 \left| H \right| \tau \; 1\vec{q}_i \right\rangle \left\langle \tau \; 1\vec{q}_i \left| \tau \; 1\vec{q}_j \right\rangle \right. = \sum_{i=1}^{N} \lambda_i^{(\tau,\beta)} \left\langle \alpha \; 0 \left| H \right| \tau \; 1\vec{q}_i \right\rangle$$

$$\sum_{i=1}^{N} \lambda_i^{(\tau,\beta)} \left\langle \alpha \; 0 \left| H \right| \tau \; 1\vec{q}_i \right\rangle = 0 \qquad \forall \alpha = 1\ldots n, \; \beta = 1\ldots n, \; \tau = 1\ldots n-g \qquad (*)$$

▪ Property (1) follows immediately from this relation. In deed,

$$\left\langle \nu \; 0 \left| H \right| \beta^{(\tau)} \right\rangle \equiv \left\langle \nu \; 0 \left| H \left(\sum_{i=1}^{N} \lambda_i^{(\tau,\beta)} \left| \tau \; 1\vec{q}_j \right\rangle \right) \right. = \sum_{i=1}^{N} \lambda_i^{(\tau,\beta)} \left\langle \nu \; 0 \left| H \right| \tau \; 1\vec{q}_i \right\rangle = 0$$

⇨ $\mathcal{H}_{B,\tau}$ has zero projection on $H\mathcal{H}_{0\,ph}$

▪ To show property (2), the particular structure of the Hamiltonian is used. The Fröhlich Hamiltonian has vanishing matrix elements between two states of identi-

cal phonon number. The free Hamiltonian is diagonal in the chosen basis. It follows the total Hamiltonian has vanishing matrix elements between two one-phonon states unless the two states are identical,

$$\left\langle \tau \, 1\vec{q}_i \left| H \right| \nu \, 1\vec{q}_j \right\rangle = \delta_{\tau\nu}\delta_{ij} \left\langle \tau \, 1\vec{q}_i \left| H \right| \tau \, 1\vec{q}_i \right\rangle$$

Since $\mathcal{H}_{B,\tau}$ and $\mathcal{H}_{B,\nu}$ ($\nu \neq \tau$) are distinct one-phonon spaces, $\mathcal{H}_{B,\tau}$ has zero projection on $H\mathcal{H}_{B,\nu}$. This testifies property (2).

- For property (3), it has to be shown that $\left\langle \alpha^{(\nu)} \left| H \right| \beta^{(\tau)} \right\rangle = 0$ for any choice of the states $\left| \alpha^{(\nu)} \right\rangle$ and $\left| \beta^{(\tau)} \right\rangle$. We start inserting the unity operator of the one-phonon subspace,

$$\left\langle \alpha^{(\nu)} \left| H \right| \beta^{(\tau)} \right\rangle = \left\langle \alpha^{(\nu)} \left| \left(\sum_{\mu=1}^{n} \sum_{s=1}^{N} \left| \mu \, 1\vec{q}_s \right\rangle \left\langle \mu \, 1\vec{q}_s \right| \right) H \right| \beta^{(\tau)} \right\rangle$$

Then, replace $\left| \alpha^{(\nu)} \right\rangle$ and $\left| \beta^{(\tau)} \right\rangle$ by their definition and reorder:

$$\left\langle \alpha^{(\nu)} \left| H \right| \beta^{(\tau)} \right\rangle = \left(\sum_{i=1}^{N} \left\langle \alpha \, 0 \left| H \right| \nu \, 1\vec{q}_i \right\rangle \left\langle \nu \, 1\vec{q}_i \right| \right) \left(\sum_{\mu=1}^{n} \sum_{s=1}^{N} \left| \mu \, 1\vec{q}_s \right\rangle \left\langle \mu \, 1\vec{q}_s \right| \right) H \left(\sum_{j=1}^{N} \lambda_j^{(\tau,\beta)} \left| \tau \, 1\vec{q}_j \right\rangle \right)$$

$$= \sum_{\mu=1}^{n} \sum_{s=1}^{N} \sum_{i=1}^{N} \sum_{j=1}^{N} \lambda_j^{(\tau,\beta)} \left\langle \alpha \, 0 \left| H \right| \nu \, 1\vec{q}_i \right\rangle \left\langle \nu \, 1\vec{q}_i \right| \mu \, 1\vec{q}_s \right\rangle \left\langle \mu \, 1\vec{q}_s \left| H \right| \tau \, 1\vec{q}_j \right\rangle$$

Use the orthogonality,

$$\left\langle \alpha^{(\nu)} \left| H \right| \beta^{(\tau)} \right\rangle = \sum_{\mu=1}^{n} \sum_{s=1}^{N} \sum_{i=1}^{N} \sum_{j=1}^{N} \lambda_j^{(\tau,\beta)} \left\langle \alpha \, 0 \left| H \right| \nu \, 1\vec{q}_i \right\rangle \delta_{\nu\mu}\delta_{is} \left\langle \mu \, 1\vec{q}_s \left| H \right| \tau \, 1\vec{q}_j \right\rangle$$

$$= \sum_{i=1}^{N} \sum_{j=1}^{N} \lambda_j^{(\tau,\beta)} \left\langle \alpha \, 0 \left| H \right| \nu \, 1\vec{q}_i \right\rangle \left\langle \nu \, 1\vec{q}_i \left| H \right| \tau \, 1\vec{q}_j \right\rangle$$

Here the particular structure of the Hamiltonian operator is used, which was mentioned above: $\left\langle \nu \, 1\vec{q}_i \left| H \right| \tau \, 1\vec{q}_j \right\rangle = \delta_{\nu\tau}\delta_{ij} \left\langle \tau \, 1\vec{q}_i \left| H \right| \tau \, 1\vec{q}_i \right\rangle$. Thus,

$$\left\langle \alpha^{(\nu)} \left| H \right| \beta^{(\tau)} \right\rangle = \sum_{i=1}^{N} \sum_{j=1}^{N} \lambda_j^{(\tau,\beta)} \left\langle \alpha \, 0 \left| H \right| \nu \, 1\vec{q}_i \right\rangle \delta_{\nu\tau}\delta_{ij} \left\langle \tau \, 1\vec{q}_i \left| H \right| \tau \, 1\vec{q}_i \right\rangle$$

$$= \sum_{i=1}^{N} \lambda_i^{(\tau,\beta)} \left\langle \alpha \, 0 \left| H \right| \nu \, 1\vec{q}_i \right\rangle \left\langle \tau \, 1\vec{q}_i \left| H \right| \tau \, 1\vec{q}_i \right\rangle \delta_{\tau\nu}$$

This expression vanishes if $\tau \neq \nu$. It remains to show that this is true if $\tau = \nu$. In this case,

$$\left\langle \alpha^{(\tau)} \left| H \right| \beta^{(\tau)} \right\rangle = \sum_{i=1}^{N} \lambda_i^{(\tau,\beta)} \left\langle \alpha \, 0 \left| H \right| \tau \, 1\vec{q}_i \right\rangle \left\langle \tau \, 1\vec{q}_i \left| H \right| \tau \, 1\vec{q}_i \right\rangle$$

For this expression to vanish, the monochromaticity of the phonon spectrum is considered. Explicitly,

$$\langle \tau \; 1\vec{q}_i | H | \tau \; 1\vec{q}_i \rangle = \varepsilon_\tau + \varepsilon_{LO} \quad \forall \, i = 1, \dots, N$$

This relation allows to factorize,

$$\langle \alpha^{(\tau)} | H | \beta^{(\tau)} \rangle = (\varepsilon_\tau + \varepsilon_{LO}) \sum_{i=1}^N \lambda_i^{(\tau,\beta)} \langle \alpha \; 0 | H | \tau \; 1\vec{q}_i \rangle$$

The sum on the right is equal to zero as stated in property $(*)$. We conclude that

$\langle \alpha^{(\nu)} | H | \beta^{(\tau)} \rangle = 0$ for any choice of the states $|\alpha^{(\nu)}\rangle$ and $|\beta^{(\tau)}\rangle$.

This concludes the demonstration.

8.5 Computational implementation

Our program is written in Fortran 90 using the LAPACK library for matrix operations.

8.5.1 Listing of the modules, subroutines and functions

The total code contains 3424 command lines. In some versions of this document, it has been submitted on the CD attached at the end. The following list contains all the modules, subroutines and functions. The left column indicates the unit's type and name and the right column yields a short explanation.

program MAIN (97 lines)	main program
internal subroutine SIMULATION_START	writes the simulation title and measures the initial time
internal subroutine SIMULATION_END	write the simulation end and total computation time
module MODULE_GLOBAL_VARIABLES (223 lines)	contains the global program variables
module subroutine INITIATE_GLOBAL_VARIABLES	sets certain user defined variables
internal function STRING	integer to string conversion
module MODULE_GLOBAL_FUNCTIONS (399 lines)	contains the global functions
module function NORM	norm of a three dimensional double complex vector
module function DOT_PROD	dot product of a three dimensional double complex vect
module subroutine CROSS_PROD	cross product of a three dimensional double complex vect
module function CROSS_PROD_2D	cross product of a two dimensional double complex vect
module function DISTANCE_LINE_LINE	finds the distance between two straight lines in 3D
module subroutine INTERSECT_LINE_PLANE	finds the intersection of a line with a plane in 3D
module function TETRAHEDRON_VOLUME	computes a tetrahedron volume
module subroutine MIDDLE_PLANE	computes the orthogonal middle plane between two points
module function DISTANCE_LINE_POINT_2D	computes the distance between a line and a point in 2D
module subroutine MATRIX_DIAGONALIZATION	diagonalizes a hermitian double complex matrix
module subroutine MATRIX_INVERSION	inverts a hermitian double complex matrix
module function COMPLEX_NORM	computes the magnitude of a double complex number
module function SGN	standard sgn function
module subroutine POLYNOM1	computes a first degree interpolation polynomial
module subroutine POLYNOM3	computes a third degree interpolation polynomial
module subroutine ORDER_VECTOR	orders the elements of a vector with increasing value

module subroutine ORDER_VECTOR2	orders the elements of a two vectors with increasing values
module function STRING	integer to string conversion
module MODULE_WIGNER_SEITZ (681 lines)	**contains functions to compute a wigner-seitz volume**
module subroutine WIGNER_SEITZ_VOLUME	computes a wigner-seitz volume
internal subroutine FIND_TRUE_NEIGHBORS	finds the wigner-seitz neighbors of a given point
internal subroutine TRANSLATE_CENTER_TO_ORIGIN	shifts all relevant vectors
internal subroutine PREPARE_NEIGHBORS	computes the distance to all the neighbor points
internal subroutine FIND_MAX_CELL_RADIUS	computes the outer sphere radius of a wigner-seitz cell
internal subroutine MULTIPLE_MIDPLANE_INTERSECT	cuts an initial volume with a set of planes
module subroutine ACTUALIZE_CELL_TRIANGLES	covers a polyhedron surface with triangles
module subroutine CORRECT_CELL_CORNERS	corrects wrongly placed cell corners
module subroutine ACTUALIZE_CELL_EDGES	computes all the edges of a polyhedron
module subroutine SAVE_CELL_EDGES	saves the edges of a polyhedron
module subroutine SAVE_CELL_EDGES_SHORT	saves the edges of a polyhedron for code verification
module subroutine SAVE_CELL_TRIANGLES	saves the surface triangles of a polyhedron
module subroutine INITIALIZE_WIGNER_SEITZ	sets variables used to compute a wigner-seitz volume
module function TEST_TRIANGLE_COMPLANARITY	checks whether two triangles are coplanar
module function TEST_TRIANGLE_OVERLAP	checks whether two coplanar triangles overlap
module function TEST_INTERSECT_SEG_SEG_2D	computes the intersection of two straight lines in 2D
module MODULE_OUTPUT_ROUTINES (784 lines)	**contains subroutines to visualize simulation results**
module subroutine PRINT_POLARON_STATES_ORTHO	lists all the polaron vectors in the tensor product basis
module subroutine PRINT_POLARON_STATES_NATURAL	lists all the polaron vectors in the natural basis
module subroutine SAVE_QVECTORS	saves all the normal mode vectors used for the computation
module subroutine SAVE_ALL_POLARONIC_QSPECTRA1D	saves all the phonon density function along a straight line
module subroutine SAVE_ALL_POLARONIC_QSPECTRA3D	saves all the phonon density function in 3D
module subroutine SAVE_ALL_POLARONIC_FTSPECTRA3D	saves all the vibrational density function in 3D
module subroutine SAVE_ALL_FROEHLICH_QSPECTRA1D	saves all the Fröhlich coupling integral along a straight line
module subroutine SAVE_ALL_FROEHLICH_QSPECTRA3D	saves all the Fröhlich coupling integral in 3D
module subroutine SAVE_POLARONIC_QSPECTRUM1D	saves one phonon density function along a straight line
module subroutine SAVE_POLARONIC_QSPECTRUM3D	saves one phonon density function in 3D
module subroutine SAVE_POLARONIC_FTSPECTRUM3D	saves one vibrational density function in 3D
module subroutine SAVE_FROEHLICH_QSPECTRUM1D	saves one Fröhlich coupling integral along a straight line
module subroutine SAVE_FROEHLICH_QSPECTRUM3D	saves one Fröhlich coupling integral in 3D
module subroutine SAVE_QFUNCTION_1D	interpolates, smoothes and saves a 1D function in q-space
module subroutine SAVE_QFUNCTION_3D	interpolates, smoothes and saves a 3D function in q-space
module subroutine SAVE_FTFUNCTION_3D	interpolates, smoothes and saves the FT of a 3D q-function
module subroutine SAVE_ENVELOPE_GRAPHS	saves all the electronic envelope functions in 1D
internal subroutine SAVE_ENVELOPE_GRAPH	saves one electronic envelope function in 1D
module subroutine OPEN_RESULT	loads the results of a previous computation
module subroutine SAVE_RESULT	saves the results of the running computation
module subroutine WRITE_VECTOR	writes a formats double real vector
module subroutine WRITE_COMPLEX_MATRIX	writes a formats double complex matrix
module MODULE_READ_DATA (68 lines)	**contains subroutines to read the initial simulation data**
module subroutine READ_DATA	reads all the initial simulation data
module subroutine READ_ENVELOP_FUNCTIONS	reads the electronic envelope functions
module subroutine READ_ENERGIES	reads the electronic energies
module subroutine READ_MESH_COORDINATES	reads the direct space mesh nodes
module subroutine READ_MESH_ELEMENT_POINTS	reads the direct space mesh connections
module MODULE_PREPARE_DATA (248 lines)	**contains subroutines to prepare the initial simulation**

	data
module subroutine PREPARE_DATA	prepares all the simulation data
module subroutine SET_POTENTIAL_WELL_FUNCTIONS	creates envelope test-functions of an infinite potential well
internal function S	creates S-function of an infinite potential well
internal function P	creates P-function of an infinite potential well
module subroutine SET_GAUSSIAN_FUNCTIONS	creates envelope test-functions with Gaussian shape
module subroutine EVALUATE_ELEMENT_VOLUME	computes the volumes of the directs space mesh elements
module subroutine EVALUATE_NODE_VOLUME	computes the volumes associated with each mesh node
module subroutine EVALUATE_MESH_EXTENTION	computes the global dimension of the mesh
module subroutine EVALUATE_RELEVANT_MESH_NODES	evaluates the mesh nodes with important contribution
module subroutine NORMALIZE_ENVELOPE_FUNCTIONS	normalizes the envelope functions (for test-functions)
internal function NORM	integrates the norm of an envelope function
module MODULE_RELEVANT_POLARON_STATES (180 lines)	**contains subroutines to analyze the full Hamiltonian**
module subroutine RELEVANT_POLARON_STATES	finds all the polaron states and en. of the reduces subspace
module subroutine EVALUATE_RELEVANT_BASISVECTORS	evaluates the natural basis vectors (normalized)
module subroutine GRAM_SCHMIDT_ORTHONORMALIZATION	computes an orthonormal basis out of the natural basis
module subroutine EVALUATE_REDUCED_HAMILTONIAN	evaluates the reduced Hamiltonian
module function REDUCED_MATRIX_ELEMENT	evaluates a single matrix element of the reduced Hamiltonian
module subroutine EVALUATE_POLARON_STATES	evaluates the polaron states in the tensor product basis
module MODULE_DYNAMIC_POLARON_EVAL (744) lines	**contains subroutines to compute the polarons adaptively**
module subroutine DYNAMIC_POLARON_EVALUATION	computes all the polarons using an adaptive q-meshing
module subroutine ACTUALIZE_MEMORY_VARIABLES	saves the result of a given simulation step
module function EXIT_CHECK	checks exit criteria such as spectrum convergence
module subroutine QGRID_REFINEMENT	refines the q-meshing in function the fluctuations
module subroutine EVALUATE_UNNORMALIZED_FROEHLICH	computes the Fröhlich matrix elements without $1/q/\sqrt{V}$
module subroutine EVALUATE_NORMALIZED_FROEHLICH	computes the true Fröhlich matrix elements
module subroutine EVALUATE_QVOLUMES	computes the Wigner-Seitz volume around a q-vector
module subroutine GENERATE_INITIAL_QVECTORS	generates the initial mesh in q-spaces
module subroutine GENERATE_FULL_HAMILTONIAN	generates the full Hamiltonian in the tensor product basis
module subroutine INITIATE	sets the harmonic functions "exponential", "sinus", "cosinus"
module function FROEHLICH	integrates a single Fröhlich coupling term
module subroutine SAVE_CALCULATION	saves the intermediate result of the running simulation
module subroutine OPEN_LAST_CALCULATION	loads the intermediate result of a previous simulation
module subroutine SAVE_MEMORY_VARIABLES	saves all the simulation outputs of previous simulation steps

8.5.2   Visualization tools

The following two frames show some helpful commands that were used to generate most of the graphical data presented in this report.

GNU PLOT

```
2D Graphs                          set pm3d
plot 'file.dat'                    set palette rgb 9,9,2
plot 'file.dat' with lines         unset colorbox
3D Graphs                          set xrange [-20:40]
splot 'file.dat'                   set yrange [-35:35]
splot 'file.dat' with lines        set zrange [0:0.05]
Opitions                           set dgrid3d 30,30
set xlabel "X axis"                set style data lines
set ylabel "Y axis"                splot 'graph.dat'
set zlabel "Z axis"
set multiplot
.
.
.
unset multiplot
```

MATLAB

This self-explaining code was used with MATLAB (6.1.0.450) to plot all the isosurfaces shown in this report.

```
n       = 50;                                     nb of points along a cube side
radius  = 20;                                     half length of the cube side
axe     = 20;                                     half length of the drawn cube side

x(1:n)  = -radius:((radius*2)/(n-1)):radius+0.000001;
y(1:n)  = -radius:((radius*2)/(n-1)):radius+0.000001;
z(1:n)  = -radius:((radius*2)/(n-1)):radius+0.000001;
[X,Y,Z] = meshgrid(x,y,z); V(1:n,1:n,1:n) = 0;

V(1:n^3) = import_file(1:n^3);                    is replaced with the actual file name

p = patch(isosurface(x,y,z,V,sum(sum(sum(V)))/n^3*2));
xlabel('x [nm]'); ylabel('y [nm]'); zlabel('z [nm]');
isonormals(X,Y,Z,V,p);
set(p,'FaceColor','red','EdgeColor','none');
daspect([1 1 1]);
view(3);
axis tight;
camlight;
lighting gouraud;
view(-50, 30);
axis([-axe axe -axe axe -axe axe])
```

8.6 Additional computational results

8.6.1 Quantum dot with two electron levels

Tab. 11 and Tab. 12 show the energies and polaron state vectors in the normalized natural basis for the dot sizes 7.5nm and 5nm. For explications about the signification of these tables the reader is referred to 5.1.2.

2 level system size = 7.5nm	Energy [meV]	State Vector					
		Subspace A		Subspace B+		Subspace B-	
		|A 0>	|A 1q> (|A 0>)	|B+ 0>	|A 1q> (|B+ 0>)	|B- 0>	|A 1q> (|B- 0>)
polaron state 1	50.011	0.9786	0.2057	0.0001	0.0007	0.0000	0.0000
polaron state 4	89.229	0.2056	0.9785	0.0087	0.0165	0.0000	0.0000
polaron state 2	81.307	0.0003	0.0004	0.8752	0.4837	0.0000	0.0000
polaron state 6	89.484	0.0041	0.0169	0.4837	0.8751	0.0000	0.0000
polaron state 3	81.350	0.0000	0.0000	0.0000	0.0000	0.8768	0.4808
polaron state 5	89.440	0.0000	0.0000	0.0000	0.0000	0.4808	0.8768

Tab. 11: Polaron eigenvectors of the two-level system expressed in the normalized natural basis, 7.5nm dot

2 level system size = 5nm	Energy [meV]	State Vector					
		Subspace A		Subspace B+		Subspace B-	
		|A 0>	|A 1q> (|A 0>)	|B+ 0>	|A 1q> (|B+ 0>)	|B- 0>	|A 1q> (|B- 0>)
polaron state 1	61.556	0.9769	0.2137	0.0001	0.0011	0.0000	0.0000
polaron state 3	94.563	0.2137	0.9769	0.0037	0.0038	0.0000	0.0000
polaron state 4	101.064	0.0003	0.0006	0.8036	0.5952	0.0000	0.0000
polaron state 5	101.837	0.0016	0.0053	0.5952	0.8036	0.0000	0.0000
polaron state 2	94.551	0.0000	0.0000	0.0000	0.0000	0.8033	0.5956
polaron state 6	101.849	0.0000	0.0000	0.0000	0.0000	0.5956	0.8033

Tab. 12: Polaron eigenvectors of the two-level system expressed in the normalized natural basis, 5nm dot

Tab. 13 and Tab. 14 show the polaron state vectors in the tensor product basis for the dot sizes 7.5nm and 5nm. The respective "normal mode distribution functions" and "vibrational density functions" are shown in Fig. 25 to Fig. 28. Again, further explications and the 10nm dot results are shown in 5.1.2.

2 level system size = 7.5nm	Energy [meV]	State Vector			
		|A 0>	|B+ 0>	|B- 0>	all |A 1q>
polaron state 1	50.011	0.9786	0.0001	0.0000	0.2057
polaron state 4	89.229	0.2056	0.0087	0.0000	0.9786
polaron state 2	81.307	0.0003	0.8752	0.0000	0.4837
polaron state 6	89.484	0.0041	0.4837	0.0000	0.8752
polaron state 3	81.350	0.0000	0.0000	0.8768	0.4808
polaron state 5	89.440	0.0000	0.0000	0.4808	0.8768

Tab. 13: Polaron eigenvectors of the two-level system expressed in the tensor product basis, 7.5nm dot

2 level system size = 5nm	Energy [meV]	State Vector			
		|A 0>	|B+ 0>	|B- 0>	all |A 1q>
polaron state 1	61.556	0.9769	0.0001	0.0000	0.2137
polaron state 3	94.563	0.2137	0.0037	0.0000	0.9769
polaron state 4	101.064	0.0003	0.8036	0.0000	0.5952
polaron state 5	101.837	0.0016	0.5952	0.0000	0.8036
polaron state 2	94.551	0.0000	0.0000	0.8033	0.5956
polaron state 6	101.849	0.0000	0.0000	0.5956	0.8033

Tab. 14: **Polaron eigenvectors of the two-level system expressed in the tensor product basis, 7.5nm dot**
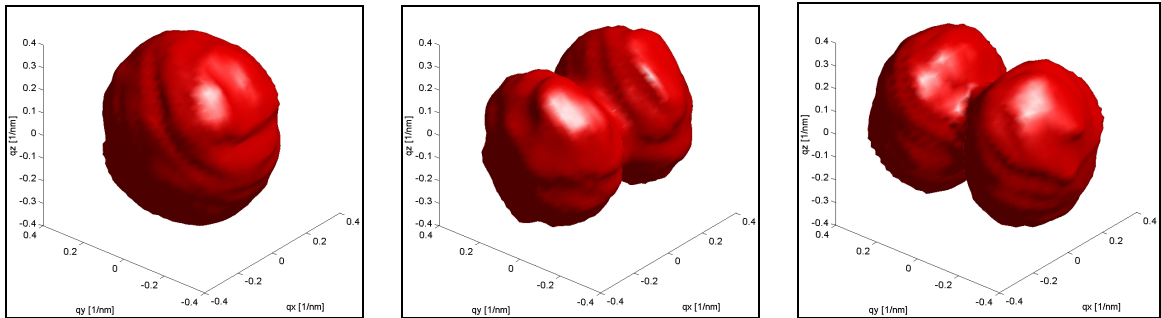
Fig. 25: **Isosurfaces of the phonon density functions associated with the subspaces A, B_+, B_- , 7.5nm dot**
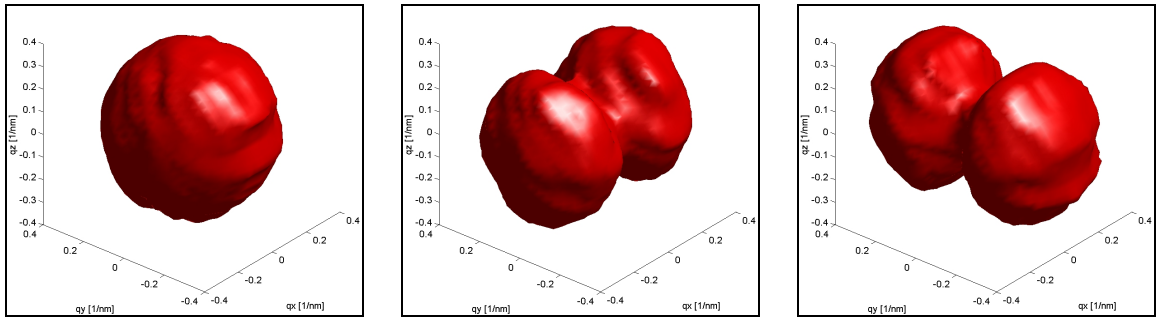
Fig. 26: **Isosurfaces of the phonon density functions associated with the subspaces A, B_+, B_- , 5nm dot**
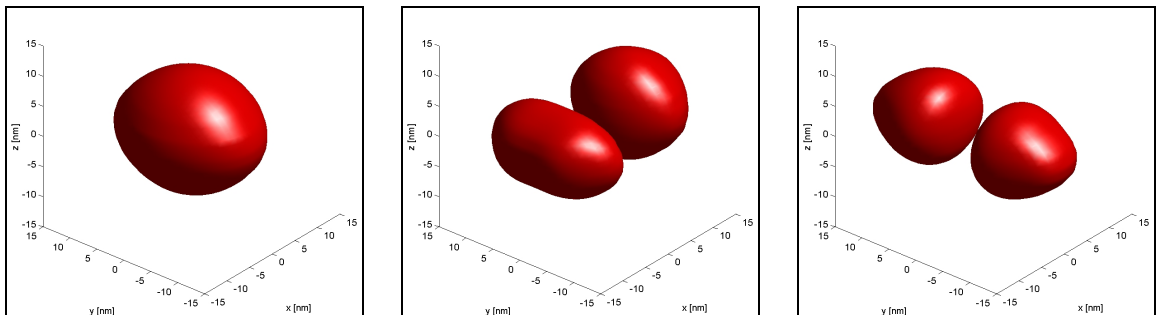
Fig. 27: **Isosurfaces of the vibrational density functions associated with the electron states A, B_+, B_- (= Fourier transforms of Fig. 25). 7.5nm dot**
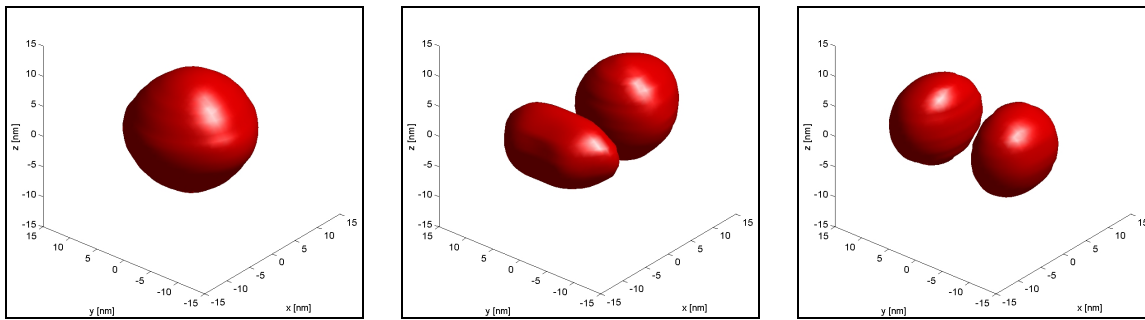
Fig. 28: **Isosurfaces of the vibrational density functions associated with the electron states A, B$_+$, B$_-$ (= Fourier transforms of Fig. 26). 7.5nm dot**

8.6.2 Quantum dot with three electron levels
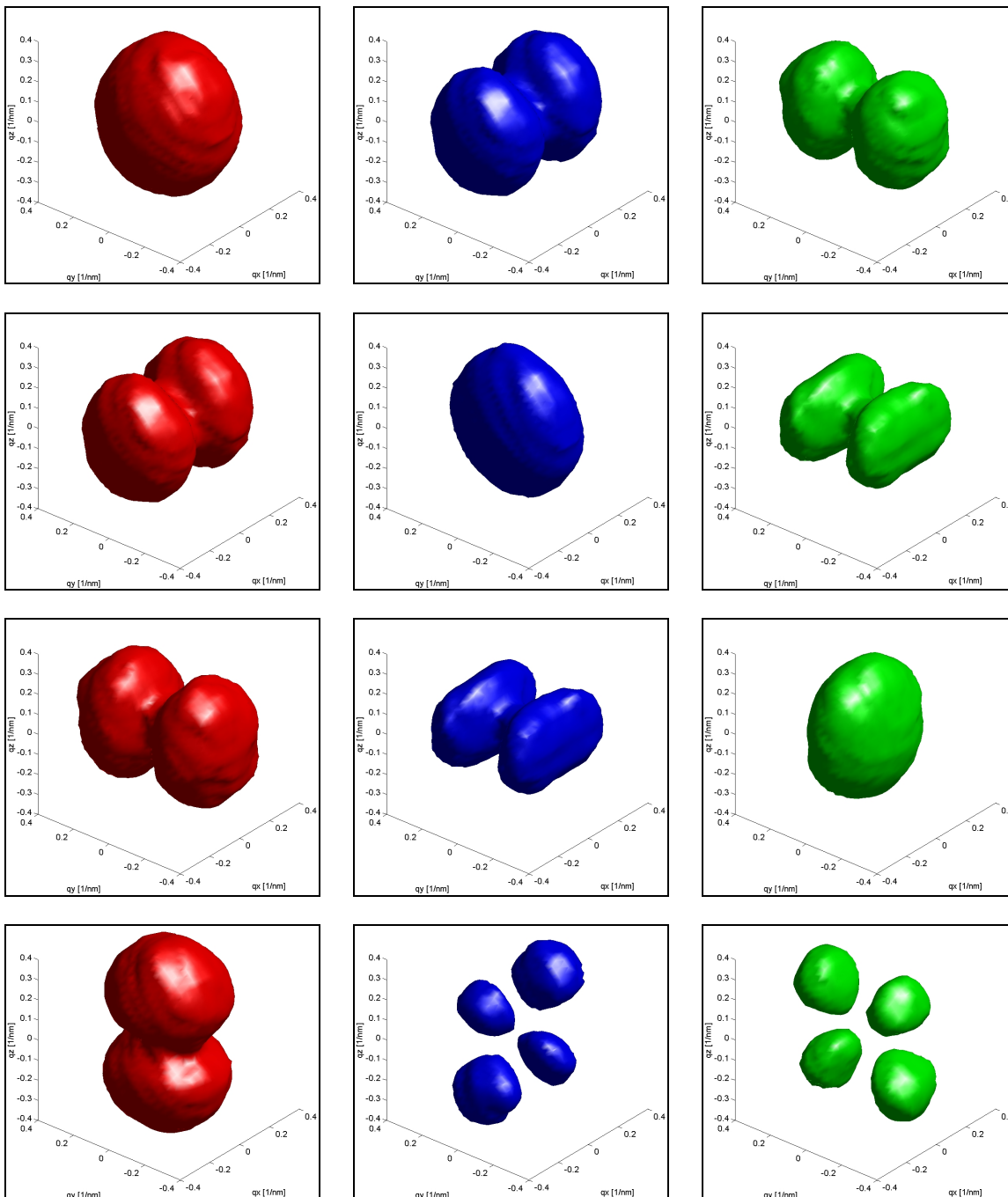
The Fourier transforms of these 12 functions, representing the "vibrational density" of the crystal, are shown in section 5.2.2.

The coefficients $\eta(\vec{q}_i)$, $\zeta(\vec{q}_i)$ of the zero-shift state inside the subspace B– $\left(\equiv \mathcal{H}_{red}^{B-}\right)$ are proportional to the other coefficients inside the same subspace (see third row of the 12 images above). $\xi(\vec{q}_i)$ vanishes.

For the other three zero-shift states, the choice of the coefficients $\eta(\vec{q}_i)$, $\zeta(\vec{q}_i)$ is not unique. One linearly independent choice is represented by the following isosurfaces

$$\eta(\vec{q}_i) \qquad\qquad \zeta(\vec{q}_i)$$
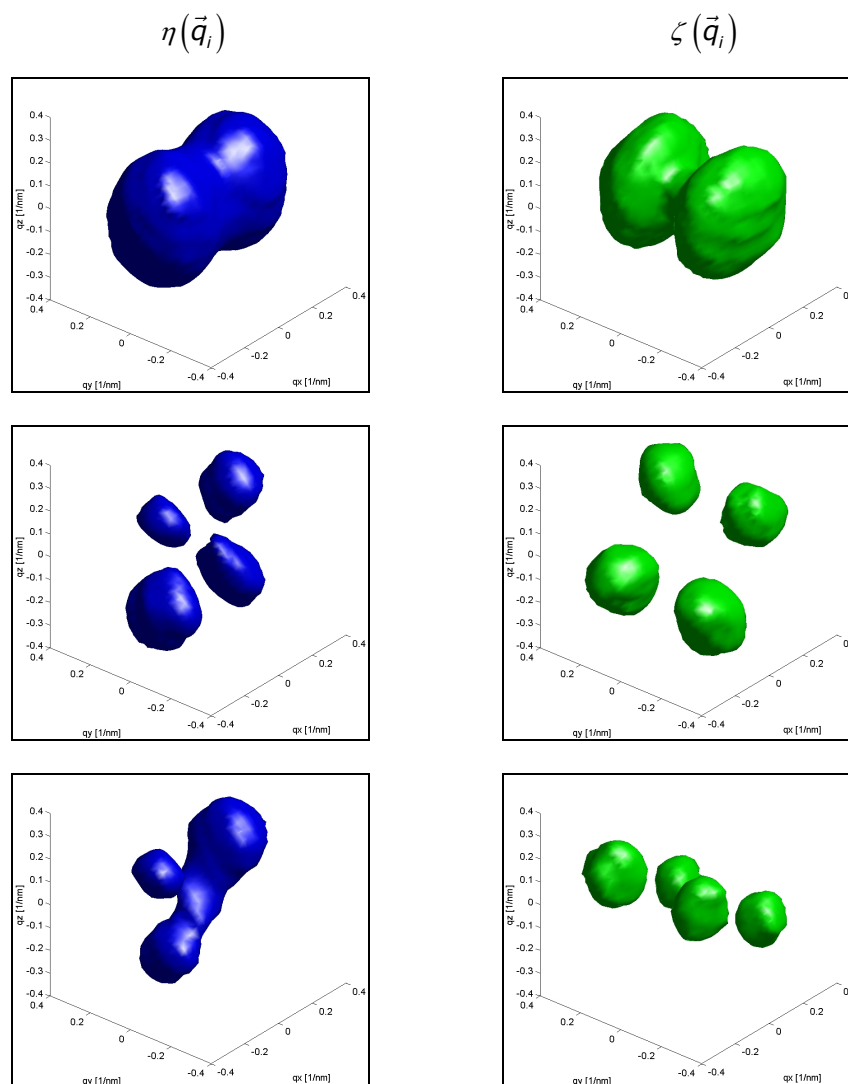
The Fourier transforms of these 6 functions, representing the "vibrational density" of the crystal, are shown in section 5.2.2.

8.7   A long time ago

8.7.1   History of the "phonon", "polaron" and "Fröhlich interaction"

We shall briefly present the historical origins of three concepts, which lie among others at the basis of present-day research on quantum dots.

In the twenties, the Indian physicist Raman discovered that monochromatic light could change its frequency when being diffracted in a medium – an effect that was later referred to as the "Raman effect". It seemed that the diffraction of light could be explained based on inelastic scattering of microscopic particles; a scattering between particles of light and particles of molecular vibration or between photons and phonons as we shall say later. Today, the Raman-spectroscopy is one of the commonly used methods to determine the phonon energies of crystals.

On the theoretical level, the Russian physicist Tamm found in 1930 that the motion of a solid lattice is built up on discrete quanta of kinetic energy approximately associated with harmonic normal modes. He called them "quanta of sound". In 1932, Jakow Frenkel (Fig. 29) writes that those quanta of sound behave in many aspects as if they were independent particles. Therefore, he suggests calling them "phonons" in analogy with the "photons", the quanta of electromagnetic vibration [47]. The respective extract of Frenkel's original text is printed in appendix 8.7.1.

Fig. 29: JAKOW I. FRENKEL among the fathers of the "phonon"
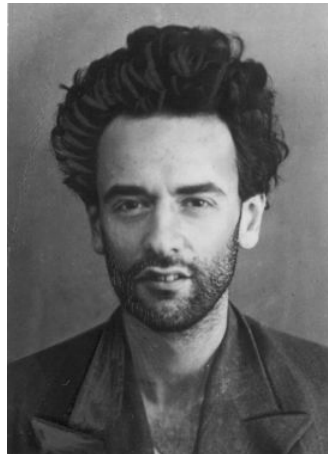
Fig. 30: LEW LANDAU among the fathers of the "polaron"

Fig. 31: HERBERT FRÖHLICH father of the "Fröhlich interaction"

Ever since Raman, Tamm and Frenkel the concept of phonons has been very successful. Its first achievement was the explanation of the Raman effect in terms of inelastic photon-phonon scattering. Later, many other interactions involving phonons were developed, one of which is the interaction between electrons and phonons. A particular type of these interactions is the "Fröhlich interaction", which we widely apply within this report. It was introduced in 1949 by Herbert Fröhlich (Fig. 31) [40]. The

abstract of the respective original document is printed in appendix 8.7.4. The ideas of the derivation and an extended physical interpretation of the Fröhlich interaction is presented in section 2.4. Nowadays, phonons are considered as one possible set of basis states in the Hilbert space associated with the crystal system. They are *quantum mechanical forms* that behave in their mathematical structure like *bosonic particles*. They are part of a large amount of quasi-particles, which are all quantized excitations of many-particle-systems. Another example of such quasi-particles is the "polaron", a coupled electron-phonon state. To the best of our knowledge, its physical content was first outlined by Lew Landau (Fig. 30) in 1933 [48]. An extract of his original document, composed in German, is shown in appendix 8.7.3.

8.7.2   Frenkel's introduction of the "phonon", 1932

The text below is a copy of Frenkel's original text, in which he introduces the term "phonon" [49]. The crucial sentence is highlighted in yellow.

If the electrons are strongly bound to the individual atoms their 'lattice states' of motion will form, as we know, narrow bands separated by wide gaps, which correspond to selective reflection. Under these conditions the conductivity will be very small whatever the number of the corresponding electrons, because of the smallness of the transition probability from one atom to the next one. It is interesting to note that it must reach a maximum value when the number of electrons corresponding to the whole band of lattice states is equal to just one-half of the number of these states. If the whole band is filled the electrons will be unable to pass to states lying higher up in the phase-space skyscraper—at least under the influence of moderate electric fields—for these states are separated from the original ones by a long range of floors corresponding to forbidden motion (selective reflection).

This explains why the inner electrons, though able in principle just as the outer ones to pass from one atom to the next (although with an extremely small probability) do not play any role whatever in the conduction of electricity in a metallic body. It serves also to explain the power of many non-metallic bodies to become conductive under the influence of light (inner photo-electric effect) or heat (semi-conductors). In both cases some of the electrons are thrown from a state in a narrow band—filled or unfilled—into a state lying much higher up and corresponding to a relatively rapid motion through the lattice, i.e. described by a wave function $\psi = C(\mathbf{r})e^{i\mathbf{\gamma}\cdot\mathbf{r}}$ with but a slightly variable periodicity factor $C(\mathbf{r})$.

We shall not pause here to undertake a quantitative development of this 'collectivistic' theory of the motion of the electrons in a solid body. This rather complicated theory which has been worked out by F. Bloch and by R. Peierls will be examined later on. An important part of this theory is concerned with giving an adequate description of the heat motion of the atoms in a solid body and of the interaction of this motion and that of the electrons, in terms of the exchange of momentum and energy between the electrons and the elastic or sound waves representing the heat motion in a solid according to Debye's theory. It is possible to give a very simple and vivid interpretation of the corresponding results, using the 'individualistic' description of the motion of the electrons, as we have done before, and introducing the fictitious but sometimes very convenient conception of 'phonons', i.e. sound or heat quanta associated with the elastic (or acoustical) waves which serve for the description of heat motion in a solid body.

3595.4   M m

132

8.7.3   Landau's early vision of the "polaron", 1933

The copy below shows an original text of Lew Landau written on the subject of electrons surrounded by a field of crystal deformation, a physical picture of the "polaron".

Briefe, vorläufige Mitteilungen und Diskussionen

ÜBER DIE BEWEGUNG DER ELEKTRONEN IM KRISTALL-GITTER.

Von. L. Landau.

(Eingegangen am 14. Mai 1933).

Es ist bekannt, dass ein Elektron im periodischen Felde sich ohne Widerstand bewegen kann. Verzerren wir das Gitter leicht an einer Stelle, so führt das zunächst nur zu einer Streuung der Elektronen an der betreffenden Stelle. Dabei entsteht aber noch keineswegs die Möglichkeit, dem Elektron an der betreffenden Stelle zu haften. Dies wäre nach einem bekannten Satz der Wellenmechanik nur dann möglich, wenn das verzerrte Gitter ausser kontinuierlichen noch diskrete Eigenwerte besitzen würde. Das ist aber bei schwachen Verzerrungen nicht der Fall.

Betrachten wir zunächst ein freies Elektron, auf welchen in einem bestimmten Gebiet ein schwaches Feld wirkt. Dann können wir im Einklang mit Peierls[1] beweisen, dass schon die Lösung der Schrödinger-Gleichung bei $E = 0$ bei schwachen Feldern knotenlos ist, also dem tiefst möglichen Eigenwert entspricht. Suchen wir nämlich die Lösung der Schrödinger-Gleichung

$$\Delta\psi = \frac{2mU}{h'^2}\,\psi \qquad (1)$$

bei kleinem U in der Form

$$\psi = 1 + \chi \qquad (2)$$

wo χ auch klein ist, so ergibt sich

$$\Delta\chi = \frac{2mU}{h'^2} \qquad (3)$$

---

[1] ZS. f. Phys. **58**, 59, 1929.

Fällt U im Unendlichen rascher als $1/r^2$ ab, so besitzt diese Gleichung eine überall endliche Lösung, deren Werte denen von U proportional sind. Bei genügend kleinen U ist also $|\chi| < 1$, also $1 + \chi$ nirgends 0. (Bezeichnen wir die Dimension des Gebietes, wo U won 0 verschieden ist mit a, so sehen wir, dass ein diskreter Eigenwert nur dann bestehen kann, wenn $\frac{mUa^2}{h'^2}$ von der Grössenordnung 1 ist).

Ganz analog lässt sich der Beweis für ein periodisches Gitter erbringen, indem wir als Ausgangspunkt die dem tiefsten Eigenwert entsprechende und folglich bei streng periodischem Felde knotenlose Lösung nehmen, und das „verzerrte" ψ in der Form $\psi = \psi_0 + \chi$ schreiben.

Eine kleine Verzerrung führt also noch zu keiner Möglichkeit, das Elektron festzuhalten. Eine solche entsteht erst nur bei grossen Verzerrungen. Wir können nun zwei wesentlich verschiedene Fälle unterscheiden. Der energetisch günstigste Zustand des Gesamtsystems kann nämlich entsprechen erstens dem unverzerrten Gitter und dem „freien" sich bewegenden Elektron und zweitens dem an einer stark verzerrten Stelle haftenden Elektron. Im ersten Falle kann das Elektron überhaupt vom Gitter nicht eingefangen werden. Dieser Sachverhalt scheint sich bei Diamant zu verwirklichen. Im zweiten Falle kann aber das Einfangen des Elektrons nur bei Überschreitung einer Energieschwelle zustande kommen. Bei einer kleinen Verzerrung ändern sich ja die Eigenwerte des Elektrons, wie bereits bestimmt wurde, nicht. Die Energieänderung des Gesamtsystems besteht somit allein in der Verzerrungsenergie, ist also wesentlich positiv. Wir haben also zu erwarten, dass das Einfangen des Elektrons Aktivierungserscheinungen aufweist. Dem entspricht der Sachverhalt bei NaCl, das bei tiefen Temperaturen durch Röntgenstrahlen nicht verfärbt werden kann. Es wäre interessant, in dieser Erscheinung das $e^{-\frac{A}{kT}}$ Gesetz nachzuprüfen und die Grösse der Aktivierungsenergie A zu bestimmen.

Ukrainisches Physikalisch - Technisches Institut, Charkow.

8.7.4   Fröhlich's derivation of his interaction, 1949

The following copy shows the abstract of Fröhlich's original document about interactions between electrons and longitudinal polarization waves.

XX. *Properties of Slow Electrons in Polar Materials**.

By H. FRÖHLICH, H. PELZER† and S. ZIENAU,
Department of Theoretical Physics, The University, Liverpool‡.

[Received November 25, 1949.]

SUMMARY.

Using a variational method we have investigated the properties of the lowest energy levels in a range $\hbar\omega$ above the ground level of the system consisting of an electron and a continuous dielectric medium. The latter is supposed to have a single vibrational frequency $\omega/2\pi$ for long longitudinal polarization waves. The interaction between the electron and the medium then depends on three parameters, the static dielectric constant ϵ, the optical refractive index $\epsilon_\infty^{\frac{1}{2}}$, and ω. The replacement of a crystalline lattice by a continuum is a good approximation if the length $b=(\hbar/2m\omega)^{\frac{1}{2}}$ is large compared with the lattice distance, a condition which is usually fulfilled.

We find that the energy of the ground level may be considerably (compared with $\hbar\omega$) below the energy which the system would have in the absence of interaction. The electron can be found with equal probability at any point in the medium. The average polarization of the medium therefore vanishes at any point. This does not hold, however, for the average polarization at a given distance from the electron. This quantity varies at large distances as the polarization of a point charge, but shows deviations below distances of the order b. The energy of interaction depends very little on the average velocity of the electron. Slow electrons, therefore, behave very similarly to free electrons (§ 4). It follows then that self trapping in the lattice—a suggestion which has often been discussed—does not exist (§ 5).

Modified forms of previous formulæ of the mean free path of electrons are given in § 6. It is shown, however, that the validity of the whole method used at present to calculate mean free paths requires further investigation.

9 Bibliography

[1] Michelini F, Dupertuis MA, Kapon E. "Effects of the one-dimensional quantum barriers in pyramidal quantum dots". Applied Physics Letters 84 (20): 4086-4088 May 17 2004

[2] Michelini F. "Electronic and optical properties of pyramidal quantum dots", to be published, Journal of Applied Physics

[3] M. A. Nielsen, I. L. Chuang. "Quantum Computation and Quantum Information". Cambridge University Press; 2000

[4] D. P. DiVincenzo. "The physical implementation of quantum computation". Fortschritte der Physik 48, 771; 2000

[5] Brown KR, Lidar DA, Whaley KB. "Quantum computing with quantum dots on quantum linear supports". Phys Rev A 65 (1): Art. No. 012307 Jan 2002

[6] Thompson RM, Stevenson RM, Shields AJ, Farrer I, Lobo CJ, Ritchie DA, Leadbeater ML, Pepper M. "Single-photon emission from exciton complexes in individual quantum dots". Phys. Rev. B 64 (20): Art. No. 201302 Nov 15 2001.

[7] Becher C, Kiraz A, Michler P, Schoenfeld WV, Petroff PM, Zhang LD, Hu E, Imamoglu A. " A quantum dot single-photon source". Physica E-Low-Dimensional Systems & Nanostructures 13 (2-4): 412-417 Mar 2002

[8] Sebald K, Michler P, Passow T, Hommel D, Bacher G, Forchel A. Single-photon emission of CdSe quantum dots at temperatures up to 200 K". Appl. Phys. Lett. 81 (16): 2920-2922 Oct 14 2002

[9] Thompson RM, Stevenson RM, Shields AJ, Farrer I, Lobo CJ, Ritchie DA, Leadbeater ML, Pepper M. "Single photon emission from few particle states in InAs quantum dots". Compound Semiconductors 2001 Institute of Physics Conference Series (170)501-506 2002

[10] Hours J, Varoutsis S, Gallart M, Bloch J, Robert-Philip I, Cavanna A, Abram I, Laruelle F, Gerard JM. "Single photon emission from individual GaAs quantum dots". Appl. Phys. Lett. 82 (14): 2206-2208 Apr 7 2003

[11] Baier MH, Pelucchi E, Kapon E, Varoutsis S, Gallart M, Robert-Philip I, Abram I. "Single photon emission from site-controlled pyramidal quantum dots". Appl. Phys. Lett. 84 (5): 648-650 Feb 2 2004

[12] Kapon E, Pelucchi E, Watanabe S, Malko A, Baier MH, Leifer K, Dwir B, Michelini F, Dupertuis MA. "Site- and energy-controlled pyramidal quantum dot heterostructures". Physica E-Low-Dimensional Systems & Nanostructures 25 (2-3): 288-297 Nov 2004

[13] U. Bockelmann and G. Bastard, Phys. Rev. B 42, 8947 (1990).

[14] Arakawa Y, Sakaki H. Appl. Phys. lett. 24, 195 (1982).

[15] Benisty H, Sotomayor-Torres C M, Weisbuch C. Phys. Rev. B 44, 10 945 (1991)

[16] Brunner K, Bockelmann U, Abstreiter G, Walther M, Böhm G, Tränkle G, Weimann G. Phys. Rev. Lett. 69, 3216 (1992).

[17] Bockelmann U. Phys Rev B 48, 17 637 (1993)

[18] Lipsanen H, Sopanen M, Ahopelto J. Phys Rev B 51, 13 868 (1995)

[19] Notomi M, Naganuma M, Nishida T, TamamuraT, Iwamura H, Nojima S, Okamoto M. Appl. Phy Lett 58, 720 (1991).

[20] Raymond S, Fafard S, Charbonneau S, Leon R, Leonard D, Petroff PM, Merz JL. " Photocarrier recombination in AlyIn1-yAs/AlxGa1-x as self-assembled quantum dots". Physical Review B 52 (24): 17238-17242 DEC 15 1995

[21] Inoshita T, Sakaki H. "Electron relaxation in a quantum dot: Significance of multiphonon processes". Phys. Rev. B 46 (11), 7260 (1992)

[22] Ferreira R, Bastard G. "Phonon-assisted capture and intradot Auger relaxation in quantum dots". Appl. Phys. Lett. Vol. 74, N. 19, 2818 (1999)

[23] Verzelen O, Bastard G, Ferreira R. "Energy relaxation in quantum dots". Phys Rev B 66, 081308(R) (2002)

[24] Ferreira R, Verzelen O, Bastard G. "Optical properties of excitonic polarons in semiconductor quantum dots". Physica E: Low-dimensional Systems and Nanostructures, Volume 21, Issues 2-4, March 2004, Pages 164-170.

[25] Lemaitre A, Ashmore AD, Finley JJ, Mowbray DJ, Skolnick MS, Hopkinson M, Krauss TF. "Enhanced phonon-assisted absorption in single InAs/GaAs quantum dots". Physical Review B 63 (16): Art. No. 161309 APR 15 2001

[26] Lemaitre A, Ashmore AD, Finley JJ, Mowbray DJ, Skolnick MS, Hopkinson M, Krauss TF. "Enhanced phonon-assisted absorption in single InAs/GaAs quantum dots". Physical Review B 63 (16): Art. No. 161309 APR 15 2001

[27] R. Heitz et al., Phys. Rev. B 64, 241305 (2001).

[28] J. Urayama et al., Phys. Rev. Lett. 86, 4930 (2001).

[29] Dalessi S, Numerical computation of the electronic envelope functions in a vertical quantum wire. unpublished, EPFL, 2004.

[30] Inoshita T, Sakaki H. "Density of states and phonon-induced relaxation of electrons in semiconductor quantum dots". Physical Review B 56 (8): R4355-R4358 Aug 15 1997.

[31] Hameau S, Guldner Y, Verzelen O, Ferreira R, Bastard G, Zeman J, Lemaitre A, Gerard JM. "Strong electron-phonon coupling regime in quantum dots: Evidence for everlasting resonant polarons". Physical Review Letters 83 (20): 4152-4155 Nov 15 1999

[32] Kral K, Khas Z. "Electron self-energy in quantum dots". Physical Review B 57 (4): R2061-R2064 Jan 15 1998.

[33] Verzelen O, Ferreira R, Bastard G. "Polaron lifetime and energy relaxation in semiconductor quantum dots". Physical Review B, Vol 62, No 8, pp 4809. Auguste 15 2000.

[34] Reuse F. "Introduction à l'Electrodynamique et à l'Optique Quantiques". Polycopié EPFL 2004. Chapitre 9.

[35] Mila F. "Physique du solide avancée I et II". ITP EPFL. Chapter 4.

[36] Evrard R, Devreese J T. "Polarons in Ionic Crystals and Polar Semiconductors". North-Holland Publishing Company, 1971. Chapter 2.

[37] Devreese J T. "Polarons". Encyclopedia of Applied Physics, Vol. 14, p. 383-395.

[38]   Evrard R, Devreese J T. "Polarons in Ionic Crystals and Polar Semiconductors". North-Holland Publishing Company, 1971. page 39.

[39]   Evrard R, Devreese J T. "Polarons in Ionic Crystals and Polar Semiconductors". North-Holland Publishing Company, 1971. Chapter 2.

[40]   Fröhlich H, Pelzer H, Zienau S. "Properties of Slow Electrons in Polar Materials" in "The London, Edinburgh, and Dublin philosophical magazine", Vol 41., pp. 7416, 1950.

[41]   Obreschkow D. "Electron-phonon interaction in molecules and crystals". EPFL, 2004.

[42]   Ferreira R, Verzelen O, Bastard G. "Excitonic polarons in semiconductor quantum dots". physica status solidi (b). Volume 238, Issue 3, Date: August 2003, Pages: 575-580

[43]   Ferreira R, Verzelen O, Bastard G. "Excitonic polarons in semiconductor quantum dots". physica status solidi (b). Volume 238, Issue 3, Date: August 2003, Pages: 575-580

[44]   Reuse F, Chapitre 3.10.

[45]   Mila F., Chapitre 4.2.

[46]   Obreschkow D. "Phonon states in GaAs/Ga$_{1-x}$Al$_x$As heterostructures". EPFL, 2004.

[47]   J. Frenkel. "Wave Mechanics Elementary Theory", 1st edition. Oxford; 1932. p. 265

[48]   Laundau L. "Über die Bewegung der Elektronen im Kristallgitter". Briefe, vorläufige Mitteilungen und Diskussionen (1933)

[49]   Frenkel J. "Wave Mechanics Elementary Theory", 1st edition. Oxford; 1932. p. 265